Genome-wide response patterns in stressed hepatocytes

ZUR ERLANGUNG DES AKADEMISCHEN GRADES DES DOKTORS

DER NATURWISSENSCHAFTEN (DR. RER. NAT.)

DER CHEMISCHEN FALKULTÄT

DER TECHNISCHEN UNIVERSITÄT DORTMUND

VORGELEGT VON Gisela Lorena Campos Melo

AUS Concepción, Chile

DORTMUND, GERMANY 2013

1. Gutachter: Prof. Dr. J.G. Hengstler

2. Gutachter: Prof. Dr. Frank Wehner

Ich versichere hiermit, dass ich die vorliegende Dissertation selbstständig und ohne unzulässige fremde Hilfe erbracht habe. Ich habe keine anderen als die angegebenen Quellen und Hilfsmittel benutzt, sowie wörtliche und sinngemäße Zitate kenntlich gemacht.

_____ _____

Ort, Datum Unterschrift

Summary

The liver is the major detoxifying organs of the body. These functions are performed mainly by hepatocytes, the major cellular component of the liver parenchyma. These cells express high levels of phase I (e.g. P450 enzymes) and phase II metabolic enzymes, which catalyze the chemical reactions necessary for detoxification. Phase-I reactions have long been regarded as the major determinant for hepatotoxicity. However, recent reports suggest that upon exposure to toxic compounds, complex signaling and transcriptional mechanisms are triggered in hepatocytes, which are fundamental for the progression to cell death and also for the proper activation of the regenerative response.

In this thesis, I used gene array analysis to obtain an unbiased overview over the most important transcriptional regulatory networks in different models of hepatocyte stress in vivo and in vitro, namely carbon tetrachloride induced acute liver damage, partial hepatectomy or lipopolysaccharide exposure (in vivo) and hepatocyte isolation and cultivation in vitro. These analyses identified common gene expression signatures in all models, with induction of inflammation, repression of metabolism and induction of proliferation as predominant features. Time-resolved analysis of CCl_4-induced transcriptional responses revealed a strong and highly dynamic gene expression response upon CCl_4 administration, with 1452 genes deregulated ($\geq$2-fold, $p<0.05$, FDR adjusted), including well-known (e.g. fos, CEBP/δ) and also novel transcription factors (e.g. Klf6, SOX4) strongly upregulated as early as 2h after intoxication. Histological analyses indicated that these transcription factors were induced in hepatocytes. Further bioinformatics analysis revealed gene motifs associated to endoplasmic reticulum stress response as early as 2h after intoxication. A similar but not complete ER-stress signature was also observed in isolated hepatocytes and in partial hepatectomy, indicating that ER-stress is also a common response in different models of hepatocyte stress. The response after CCl_4 in vivo included splicing of Xbp1, eIF2α phosphorylation and induction of the transcription factor CHOP, which were validated by PCR, qRT-PCR and western blot. Histological analysis indicated that the ER-stress response was activated in hepatocytes, because CHOP was located in the nuclei of pericentral hepatocytes. Also, genes associated with ER-stress induced apoptosis such as GADD34, Ero1L and Trb3 were strongly induced during the first 24h of CCl_4 administration, suggesting a potential role of ER-stress in the cell death mechanisms induced by CCl_4. These genes have been previously described to

be dependent on CHOP expression. To assess the contribution of ER-stress to CCl_4-induced liver damage, we used well established CHOP knockout mice. Surprisingly, CHOP knockout mice were not protected, but rather more sensitive than wild type counterparts to CCl_4-induced hepatotoxicity, as determined by plasma transaminases and quantification of dead cell areas. These results were observed at various time points and different doses of CCl_4, indicating that CHOP does not play a critical role in cell death in this model of hepatotoxicity. Of the previously established CHOP-dependent genes, only Trb3 was significantly reduced in CHOP knockout mice, whereas Ero1L, GADD34 and Bim were induced to similar levels as in wild type mice, indicating that other transcriptional regulatory networks can compensate for the lack of CHOP.

In conclusion, my work identified common features in the transcriptional response to different types of hepatocyte stress in vivo and in vitro, including induction of inflammation and repression of metabolic functions. Time-resolved analysis upon CCl_4-intoxication revealed a complex transcriptional regulatory network activated in hepatocytes, which included well known and novel transcription factors. Among these, a strong ER-stress response was activated in hepatocytes, which included expression of gene clusters associated to cell death, including CHOP and its downstream pro-apoptotic genes. Surprisingly, CHOP knockout mice were not protected, but rather more sensitive to CCl_4-hepatotoxicity, indicating that CHOP does not play a critical role in this model of hepatotoxicity. The basic blueprint of the transcriptional regulatory networks identified in this thesis will serve as a good basis to unveil the precise contribution of further signaling and transcriptional responses induced in response to hepatotoxic compounds.

Zusammenfassung

Die Leber ist das wichtigste entgiftende Organ des Körpers. Diese Funktion wird überwiegend von Hepatozyten ausgeübt, welche das größte zelluläre Kompartiment der Leber darstellen. Hepatozyten exprimieren in hohem Maße Phase I (z.B. Cytochrom P450 Enzyme) und Phase II metabolisierende Enzyme, welche die Entgiftungsreaktionen katalysieren. Phasen-I-Reaktionen wurden lange als wichtigste Einflussgröße der Hepatotoxizität angesehen. Allerdings zeigen neuere Befunde, dass Hepatozyten nach Exposition gegenüber toxischen Substanzen komplexe Signaltransduktion- und transkriptionelle Mechanismen aktivieren können. Diese sind entscheidend für die Verursachung des Zelltods, aber auch der erforderlichen Regeneration.

In dieser Arbeit habe ich Gene Array Analysen eingesetzt, um zunächst einen vollständigen Überblick über die Veränderungen auf der Ebene der RNA zu erhalten. Hierfür habe ich verschiedene in vitro als auch in vivo Modelle eingesetzt, bei welchen Stress in Hepatozyten ausgelöst wird: Induktion von akute Hepatotoxizität durch Tetrachlorkohlenstoff (CCl_4), partielle Hepatektomie, Induktion einer Leberentzündung durch LPS, als auch die Isolierung und Kultivierung von Hepatozyten. Diese Untersuchungen haben gezeigt, dass Hepatozyten mit einem stereotypen Muster auf diese unterschiedlichen Arten von Zellstress reagieren: vorherrschende Muster sind die Induktion von Entzündungsgenen, Repression der Expression von Genen, welche metabolische Funktionen ausüben, als auch die Induktion der Expression von Genen, welche eine Rolle bei Proliferation spielen. Zeitaufgelöste Untersuchungen der durch CCl_4 verursachten transkriptionellen Antwort zeigten eine starke Genexpressionsantwort mit 1452 hochregulierten Genen ($\geq$ zweifach, $p< 0.05$, FDR adjustiert), einschließlich gut bekannten (z.B. fos, CEBP/δ) und neuer Transkriptionsfaktoren (Klf6, SOX4). Diese waren schon zwei Stunden nach Intoxikation hochreguliert. Histologische Untersuchungen zeigten, dass diese Transkriptionsfaktoren in Hepatozyten induziert waren. Weitere biostatistische Untersuchungen führten zur Aufdeckung von Genexpressionsveränderungen, welche den Mechanismus des „endoplasmatischen Retikulum Stress“ (ER-Stress) anzeigten. Eine ähnliche ER-Stress Antwort wurde auch in isolierten Hepatozyten und nach partieller Hepatektomie beobachtet. Dies zeigt, dass ER-Stress eine relativ allgemeine Antwort auf unterschiedliche Arten von Zellstress darstellt. Weiterhin umfasste die Antwort auf CCl_4- Intoxikation das spleisen von Xbp1, eIf2α- Phosphorylierung

und die transkriptionelle Induktion des Transkriptionsfaktors CHOP. Dies konnte durch PCR, qRT-PCR und Western Blot Analysen nachgewiesen werden. Histologische Untersuchungen zeigten, dass die ER-Stress Antwort in Hepatozyten aktiviert wurde, weil CHOP in den Kernen der perizentralen Hepatozyten lokalisiert war. Weitere Gene, welche mit ER-Stress induzierter Apoptose assoziiert sind, wurden während der ersten 24h nach CCl_4 Intoxikation induziert: GADD34, Ero1L und Trb3. Kürzlich wurde veröffentlichet, dass diese Gene vom Transkriptionsfaktor CHOP abhängen. Um diesen Zusammenhang zu untersuchen, habe ich CHOP knockout Mäuse eingesetzt. Überraschenderweise waren CHOP knockout Mäuse nicht vor CCl_4 induzierter Hepatotoxizität geschützt. Vielmehr erwiesen sie sich als susceptibler. Dies konnte durch den Nachweis von Plasmatransaminasen (und der Quantifizierung der Nekroseregion) belegt werden. Diese Befunde wurden bei unterschiedlichen CCl_4-Dosen und Untersuchungszeitpunkten reproduziert. Sie zeigen, dass CHOP in diesem Modell der Hepatotoxizität keine ausschlaggebende Rolle spielt. Von den kürzlich als CHOP- abhängig beschriebenen Genen war nur Trb3 in den CHOP knockout Mäusen signifikant reduziert. Hingegen zeigten Ero1L, GADD34 und Bim eine ähnliche Expression in Wildtyp und knockout Mäusen. Daher scheinen andere regulatorische Mechanismen den Verlust von CHOP in Hepatozyten zu kompensieren.

Zusammenfassend kann festgestellt werden, dass in dieser Arbeit allgemeine, stereotype Reaktionsmuster von Hepatozyten auf unterschiedliche Arten von Zellstress identifiziert wurden. Diese umfassen die Induktion von Entzündungsgenen und die Unterdrückung von Genen, welche in Stoffwechselfunktionen involviert sind. Zeitaufgelöste Genexpressionsanalysen nach CCl_4- Vergiftung haben ein komplexes transkriptionell regulatorisches Netzwerk in Hepatozyten aufgedeckt. Darunter wurde eine starke ER-Stress Antwort in Hepatozyten beobachtet. Dazu gehörte der ER-Stress assoziierte Transkriptionsfaktor CHOP und durch CHOP kontrollierte pro-apoptotische Gene. Überraschenderweise waren jedoch CHOP knockout nicht vor CCl_4- induzierter Hepatotoxizität geschützt, sondern tendenziell sogar empfindlicher. Daher scheint CHOP in dem CCl_4-Modell der Hepatotoxizität keine kritische Rolle zu spielen. Die in dieser Arbeit geleistete Aufdeckung der transkriptionellen regulatorischen Netzwerke gestresster Hepatozyten stellt eine Basis für die weitere Entschlüsselung hepatotoxischer Mechanismen dar.

Contents

Figures

Tables

1 Introduction

1.1 Liver structure

The liver is located in the right upper quadrant of the abdominal cavity (Fig 1). Due to its major role in metabolism, it is a highly vascularized organ. About 25% of its blood supply comes from the hepatic artery, which provides oxygenated blood from the aorta. The remaining 75% blood supply comes from the portal vein, which collects nutrients from the intestine, spleen and stomach. Once oxygen and nutrients are consumed from arterial and portal circulation, the blood exits the liver via the hepatic vein which drains into the inferior vena cava [1]. Due to this particular vascularization, xenobiotics, drugs or chemicals ingested via the gastrointestinal tract directly access the liver via the entero-hepatic circulation (i.e. portal vein).

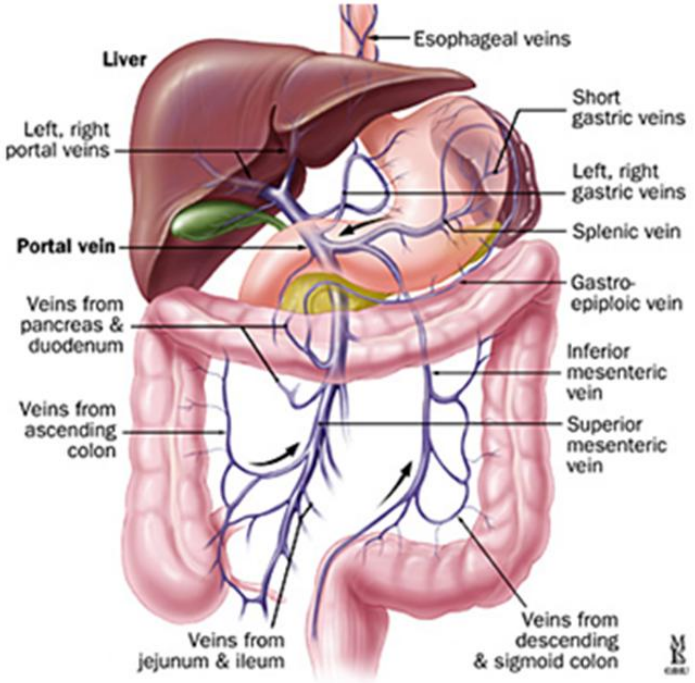

Figure 1: Liver Entero-Hepatic Circulation. The liver blood supplies come 75% from the portal vein and 25% through the hepatic artery. The blood flow from the portal vein is rich in nutrients since it carries blood that passes through the stomach, spleen and intestines. Therefore if xenobiotics are taken up they will pass the liver through the portal vein to be metabolized. (Figure from http://www.Hopkins-gi.org)

Liver cells are organized in well-defined histological units called lobule (Fig 2). A lobule has a hexagonal shape and consists of hepatocytes, which represent the largest cell population of the liver and non-parenchymal cells such as Kupffer cells, stellate cells, and liver sinusoidal endothelial cells [2]. Hepatocytes form plates (aka cords), which radiate from the central vein. Neighboring hepatocytes are joined by tight junctions. In their interface they form bile canaliculi, which represent their apical pole. The bile canaliculi form a network that directs bile flow into bile ducts, which are located at the edge of the lobule. On the basolateral side, hepatocytes face blood capillaries called sinusoids, which arise from branches of the hepatic artery and portal vein located around the lobule. Histologically, branches of the hepatic arteries, portal veins, and the bile ducts form the so-called "portal triad" (Fig 2).

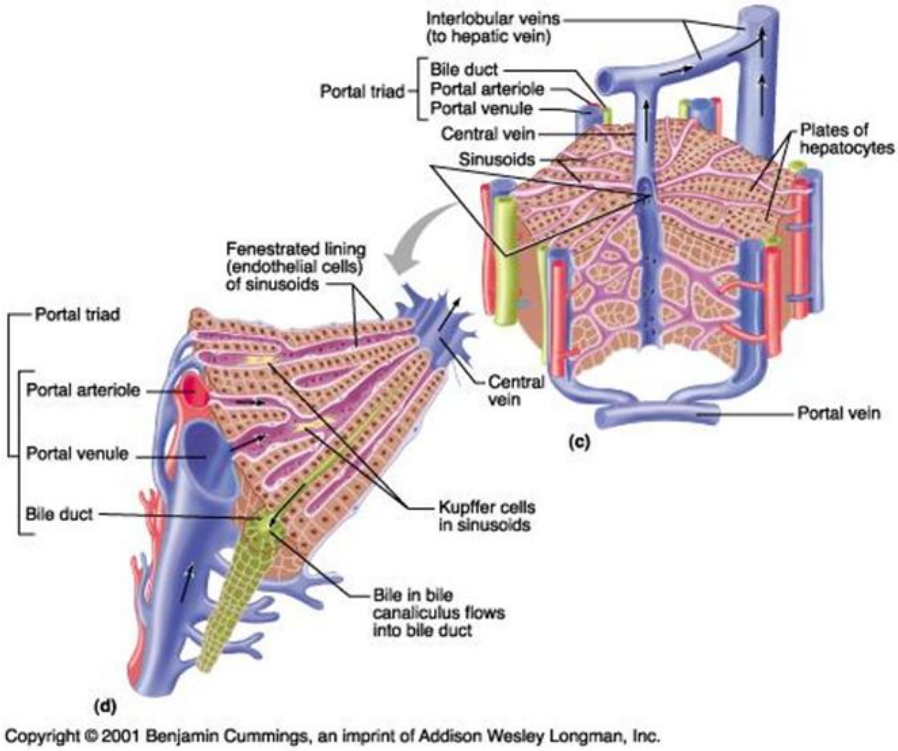

Figure 2: Liver lobules and Portal Triad. In the liver it is possible to distinguish microscopically liver lobules, which are multicellular anatomical units formed by a Central Vein, the Portal triad (composed by the portal vein, bile duct and hepatic artery) and liver sinusoids. The later are formed by liver epithelial cells and hepatocytes. Non parenchymal cells (short NPC) such as stellate cells and Kupffer cells are located in the space of Disse between liver epithelial cells and hepatocytes. (Figure from http://www.easynotecards.com)

1.2 **Liver zonation**

Hepatocytes are histologically indistinguishable; however, they present a high degree of specialization in different areas of the liver lobule. Extensive studies have demonstrated that three zones can be clearly defined in the lobule, based on the expression of specific proteins on hepatocytes, such as glutamine synthetase (GS) or Pepck1 [3].This zonation is important for the proper metabolism of glucose and ammonia, but also of drugs and xenobiotics [4]. Based on this zonation, hepatocytes near central veins are described as "perivenous" and hepatocytes near portal triads are designated "periportal" (Fig 3).

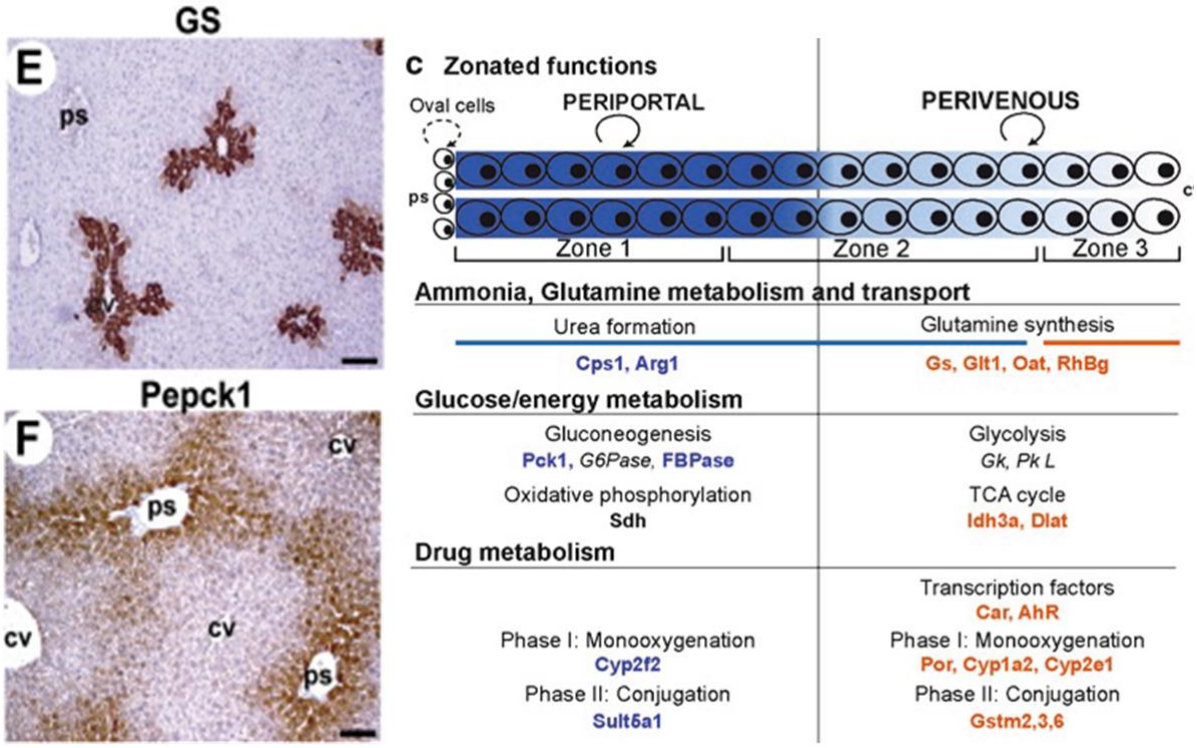

Figure 3: The metabolic functions of the liver show a zonal lobular pattern. Hepatocytes that are located in the periportal area are in charge of ammonia detoxification and gluconeogenesis among others. Phosphoenolpyruvate carboxykinase (Pepck1) an enzyme used in gluconeogenesis is shown. Pericentral hepatocytes perform glycolysis, glutamine synthesis (GS- glutamine synthetase) and cytochrome P450 reactions. (Adapted from Benhamouche et al 2006, and Colnot et al 2011)

One of the best understood mechanisms controlling liver zonation is the Wnt/β-catenin pathway. Wnt ligands (possibly secreted by endothelial cells in the central vein) activate the β-catenin pathway in perivenous (PV) hepatocytes, while in periportal hepatocytes (PP) the high expression of APC, the inhibitor of β-catenin, keeps this pathway inactive [3, 4] (Fig 4). This hypothesis was well demonstrated by transgenic mice with hepatocyte-specific β-catenin knockout mice which presented a uniform periportal-like pattern, while targeted hepatocyte deletion of APC, which renders all hepatocytes in a perivenous-like state [3, 4]. Moreover, the importance of the Wnt//β-catenin pathway in metabolism was highlighted by deletion of β–catenin in the liver. These mice were insensitive to CCl_4 intoxication, probably due to the lack of Cyp2E1 expression [4].

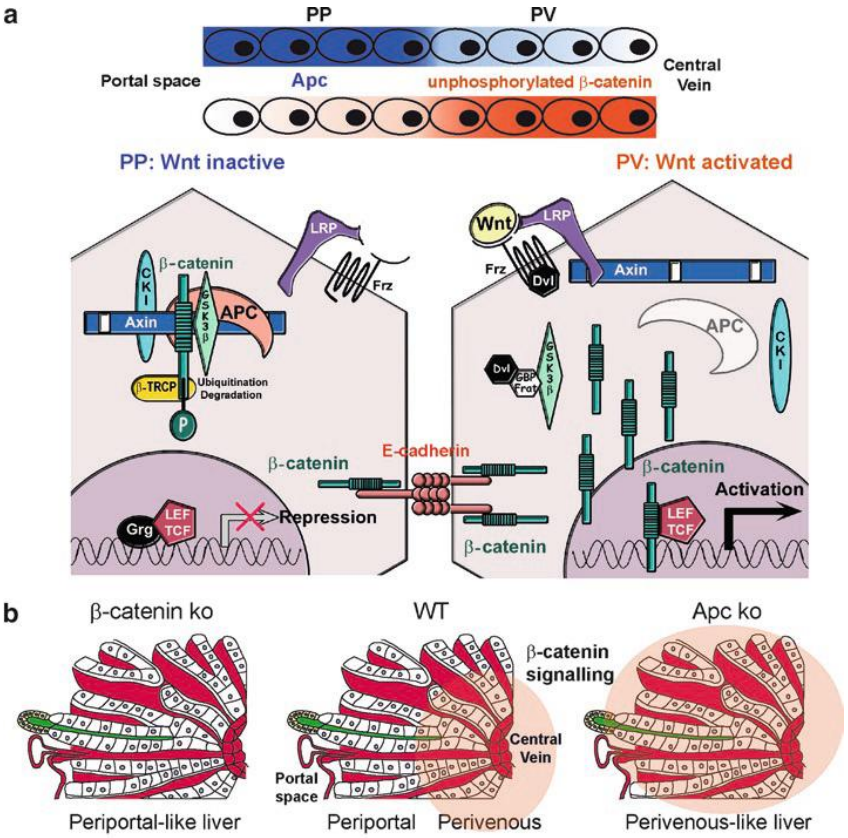

Figure 4: Wnt/β-Catenin pathway in liver zonation. A. Perivenous hepatocytes express β-catenin which can translocate into the nucleus to activate the transcription of genes related to metabolism such as glutamine synthetase and Cytochrome P450 expression. Periportal hepatocyte expresses higher levels of APC, the inhibitor of β-catenin, which activates its phosphorylation and consequent polyubiquitination and degradation by the UPS. This inactivation of the Wnt/β-catenin pathway in periportal hepatocytes determines its different activity compared to PC hepatocytes. **B**. Deletion of β-catenin in mice determines a periportal-like liver while an APC deletion a perivenous like. (From Colnot, 2011) [4]

1.3 **Drug metabolism and hepatotoxicity**

Hepatocytes take up xenobiotics or drugs that reach the liver via the enterohepatic circulation, where they are metabolically processed into excretable products. These reactions can be divided into phase-I, which create highly reactive functional groups by oxidation or hydrolysis, and phase-II in which the reactive products of phase-I are conjugated into chemically inactive and highly polar (soluble) derivatives that are readily excreted (Fig 5).

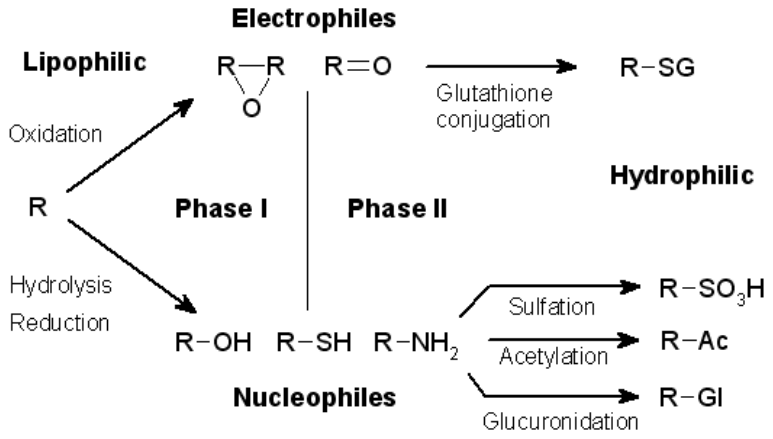

Figure 5: Biotransformation of xenobiotics in the liver. Xenobiotics are metabolized through Phase I and Phase II reactions. (Figure from http://en.wikipedia.org/wiki/Drug_metabolism)

Most phase-I reactions are mediated by enzymes called cytochrome P450 [5], a superfamily of hemoproteins of about 50 kDa that catalyze the introduction of a molecular oxygen into a substrate with simultaneous utilization of nicotinamide adenine dinucleotide phosphate (NADPH) [1]. There are 57 cytochrome P450 enzymes in the human genome, of which approximately 20 members in the CYP1, 2, 3 and 4 families are involved in drug metabolism [5].

Although xenobiotic biotransformation through the concerted action of phase-I and phase-II reactions should in principle eliminate all potential hepatotoxic compounds, hepatotoxicity is one of the most common adverse drug reactions and the most important

cause for drug withdrawal from the market [6]. Most drug-induced hepatic injuries in humans are unpredictable and poorly understood. However, decades of work in molecular toxicology have shed light into fundamental aspects of hepatotoxicity. Particularly, the role of bioactivation by phase-I enzymes has been well established as a crucial mechanism for hepatotoxicity [7].

1.4 Animal models of Hepatotoxicity and Regeneration: Acetaminophen and CCl_4 as model hepatotoxic compounds

The high expression of P450 enzymes and the direct exposure to drugs and xenobiotics via enterohepatic circulation, make the liver a highly susceptible organ for adverse drug reactions [7]. The role of bioactivation by P450 enzymes as a cause of hepatotoxicity is best understood by studies using the model compounds acetaminophen and CCl_4 [8].

1.4.1 Acetaminophen hepatotoxicity

Paracetamol, acetaminophen or APAP (n-acetyl-p-aminophen) is a worldwide used analgesic and antipyretic drug which is well tolerated by children, adults and even pregnant women when used at the recommended dosage. Nevertheless, acute liver intoxication by APAP overdose is one of the major causes of acute liver failure in the United States [9]. The toxicity of APAP depends on its metabolism by the P450 enzyme Cyp2E1. This has been demonstrated by the considerable resistance against APAP intoxication in mice with genetic deletion of Cyp2E1 [10, 11]. APAP is metabolized to the reactive metabolite NAPQI (n-acetyl-p-benzoquinoneimine) which is rapidly conjugated to glutathione (GSH) to be eliminated through the urine (Fig 6). When an overdose occurs, the cytoplasmic and mitochondrial levels of GSH are overwhelmed and the highly reactive NAPQI can bind to thiol groups of cellular proteins forming APAP-protein adducts [12, 13].

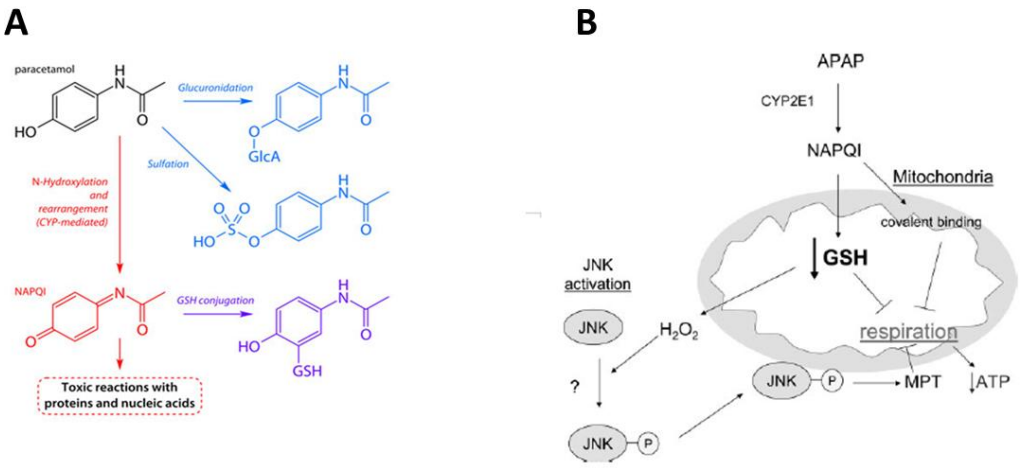

Figure 6: Paracetamol metabolism and mechanisms of toxicity. A) Summary of Paracetamol biotransformation includes direct conjugation reactions (glucoronidation, sulfation). However, bioactivation via Cyp2E1 generates the highly reactive intermediary NAPQI, which can be conjugated with GSH for elimination. When excessive NAPQI is formed, the GSH levels are overwhelmed and NAPQI can further react with proteins and nucleic acids (from http://drugdiscoveryopinion.com/tag/synthesis). **B)** NAPQI depletes mitochondrial GSH rendering the hepatocytes more sensitive to the highly oxidative environment generated by the respiratory chain. The accumulated H_2O_2 leaks to the cytoplasm which in turn activates JNK. Sustained JNK activation induces a translocation to the mitochondria. Furthermore, NAPQI binds covalently to mitochondrial proteins, thus altering the respiratory chain. These combined effects cause increased mitochondrial membrane permeability, which results in cytochrome-c release and depletion of ATP. All these effects promote cell killing [14, 15].

Over the last decades, critical events in APAP-induced hepatotoxicity have been revealed. These studies indicate that protein binding is just a primary event after intoxication which is further amplified through different pathways. A proposed model from Kaplowitz et al [14] suggests the following sequence of events: first, excessive NAPQI generates GSH depletion. Since mitochondrial GSH is needed for H_2O_2 detoxification, the former event causes H_2O_2 accumulation and leakage from the mitochondria to the cytosol, which activates the JNK pathway. The sustained activation of JNK in the cytoplasm induces its translocation to the mitochondria, where it can further promote mitochondrial permeability transition pore opening (MPT) and cytochrome c release. In addition, APAP binds to thiol groups of mitochondrial proteins which results in inactivating structural changes, disruption of the respiratory chain and finally ATP depletion. These combined events cause apoptosis and necrosis [14-16].

1.4.2 CCl_4 –induced hepatotoxicity

Many halogenated alkanes, including CCl_4, chloroform and iodoform are well known to cause severe liver damage [17]. Therefore, CCl_4 has been adopted as a model substance for studying mechanisms of hepatotoxic substances (reviewed in Weber, L.W.D 2003) [17]. Similar to APAP, CCl_4 is mainly metabolized through Cyp2E1, and to a minor extent by Cyp2B1and Cyp2B2 [18] to the highly reactive trichlormethyl radical (CCl_3^*). The CCl_3* be further oxidized, generating the even more reactive trichloromethylperoxy radical (CCl_3OO*) [17] (Fig 7).

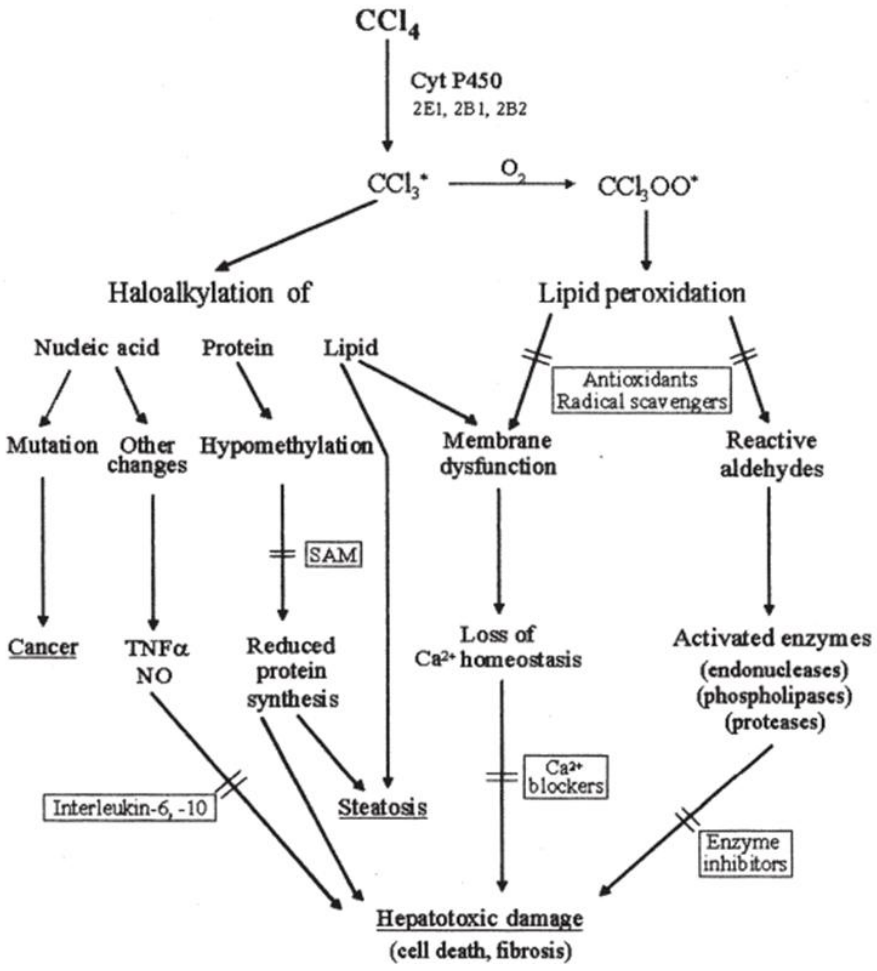

Figure 7: CCl_4 bioactivation and mechanisms of liver damage. After CCl_4 metabolism 2 sets of reactions are activated. First, CCl_3 can directly react with DNA causing mutations and hypomethylation. The last one can reduce protein synthesis levels and it can also directly cause membrane dysfunctions through binding to lipids. Second, CCl_3 can react with oxygen, forming the more reactive trichloromethylperoxy radical (CCl_3OO*). The last one causes also lipid peroxidation and membrane dysfunction. These reactive aldehydes as a byproduct of lipid peroxidation can further cause protein dysfunction. All this reactions together can induce a strong hepatotoxic damage [17, 18].

After conversion of CCl_4 to the reactive trichloromethyl radical and trichloromethylperoxy radical, two types of reactions set on [19]. First, CCl_3* can covalently bind to lipids, DNA and proteins. This causes cell damage primarily by inducing conformational changes on macromolecules. Second, the CCl_3OO* radicals can also cause damage as a result of a chain of lipid peroxidation reactions on cell membranes inducing mitochondrial and ER permeability, leading to a loss of calcium homeostasis and ATP depletion. Furthermore, the products of lipid peroxidation, including reactive aldehydes and 4-hydroxynonenal, can directly bind to proteins causing conformational changes. This leads to inhibition of enzyme activity, DNA and RNA hypomethylation, inhibition of protein synthesis and in the case of phospholipids inhibition of lipoprotein secretion [18]. These two types of damaging reactions set on changes in the cells which lead to hepatocyte damage and ultimately to cell death. Similar to APAP, the role of metabolic activation in CCl_4-induced hepatotoxicity is demonstrated by the protective phenotype in knockout mice for Cyp2E1 [17].

1.5 **Stress signaling pathways in hepatotoxicity**

The direct killing of hepatocytes by hepatotoxic compounds triggers the activation of signal transduction pathways in the liver [14, 20, 21]. These pathways have been associated to an intense inflammatory reaction and to a coordinated proliferation response that results in organ regeneration [22, 23]. The timing of expression, activation or recruitment of the most prominent cellular and molecular inflammatory mediators has been well documented. Among the best characterized cellular responses are the activation of non-parenchymal cells such as sinusoidal endothelial cells [23] and Kupffer cells [24] and recruitment of circulating monocytes and neutrophils [25]. Also, the induction of pro and anti-inflammatory cytokines such as TNFα, IFNγ, and interleukin-6 has been well characterized (reviewed in [22]). In this context, hepatocytes have been relegated as mere bystanders, whereby they only contribute cellular debris as a consequence of chemically-induced cell killing. The debris are recognized by sinusoidal endothelial cells or Kupffer cells via TLR9, which causes activation of signaling pathways such as NF-kB and STAT3, followed by expression of cytokines and chemokines including TNFα, IFNγ and IL-6 [26-29]. These studies have led to the view that signal

transduction pathways are only relevant on non-parenchymal cells, whereas hepatocytes are simply killed by the chemicals and the surviving population awaits the release of growth factors from non-parenchymal cells to engage tissue regeneration [23].

However, recent reports suggest that stress signal transduction pathways in hepatocytes are crucial to the progression of liver damage after exposure to hepatotoxic compounds. As described above, direct modifications of mitochondrial proteins by NAPQI can cause activation of JNK. Although these analyses were performed with whole liver extracts, it is fair to assume that the results are representative of alterations occurring in hepatocytes, where APAP is metabolized to NAPQI [14, 30]. In addition, cytokines such as TNFα released during the inflammatory response can also induce activation of JNK in hepatocytes [30]. Hence, it is not surprising that JNK is activated upon drug-induced hepatotoxicity. Several studies have demonstrated that JNK activation is fundamental for APAP-induced cell death. Several studies have demonstrated the role of JNK in APAP hepatotoxicity [15, 30, 31]. In a seminal paper, Kaplowitz et al [30]showed that the JNK inhibitor SP600125 strongly reduced APAP-induced liver injury, as demonstrated by reduced serum transaminases and smaller dead cell areas around central veins [30]. This effect was not observed for ERK1/2 (PD98059) or p38 (SB203589) inhibitors. Mice knockout for JNK 1 and JNK2 were also protected against APAP hepatotoxicity [30]. Importantly, neither the JNK inhibitor nor the JNK knockout influenced APAP biotransformation, indicating that JNK is one of the most important mediators of liver damage. The role of JNK in APAP hepatotoxicity was further demonstrated in mice with genetic deletion of ASK1, an activating kinase for JNK [32]. The model hepatotoxic compound CCl_4 also induces activation of JNK in mouse liver. However, JNK inhibition was not protective against CCl_4-induced liver injury [30]. These results suggest that either additional signaling pathways may be necessary to mediate cell killing by different hepatotoxic compounds, or that the role of JNK depends on a particular context of cellular stress.

1.6 **The Unfolded Protein Response (UPR)**

The molecular alterations induced by CCl_4, including macromolecule conformational changes and leakage of Ca^{2+} from the ER membranes, suggest that this compound may induce accumulation of misfolded proteins which in turn cause the activation of a set of sensors located in the endoplasmic reticulum (ER), initiating signaling events known as the unfolded protein response (UPR) [33] . In mammals, this response is initiated by three transmembrane proteins located in the ER: PERK (PKR-like ER-localized kinase), ATF6α (activating transcription factor 6α) and IRE1α (Inositol requiring 1 α). These proteins act as sensors for misfolded proteins, and are kept in an inactive state by the chaperone Bip (Binding Immunoglobulin protein). Upon accumulation of misfolded proteins in the ER lumen, Bip is released from the ER sensors and binds altered proteins, allowing the activation of the three ER stress sensors [33, 34] (Fig 8). The activation of the three ER-stress sensors results in a massive transcriptional response, driven by potent transcription factors such as Xbp1, ATF4, CHOP and ATF6, as discussed below.

PERK is a kinase which becomes activated by dimerization and trans-autophosphorylation. It phosphorylates the eukaryotic translation Initiation Factor 2-α (eIF-2α) which leads to global translation attenuation. The phosphorylation of eIF2α selectively enhances the translation of some mRNA species, including the potent transcription factor ATF4 (activating transcription factor 4), which in turn activates the transcription of genes related to increase the folding capacity of the ER like chaperones, proteins related to amino acid metabolism, antioxidant stress response and the transcription factor CHOP (C/EBP homologous protein) [35-37]. ATF4 and CHOP cooperate to induce the expression of GADD34 (growth arrest and DNA damage 34) which together with PP1 (protein phosphatase 1) dephosphorylate eIF2α providing a negative feedback mechanism that releases the break on mRNA translation [33, 35-37].

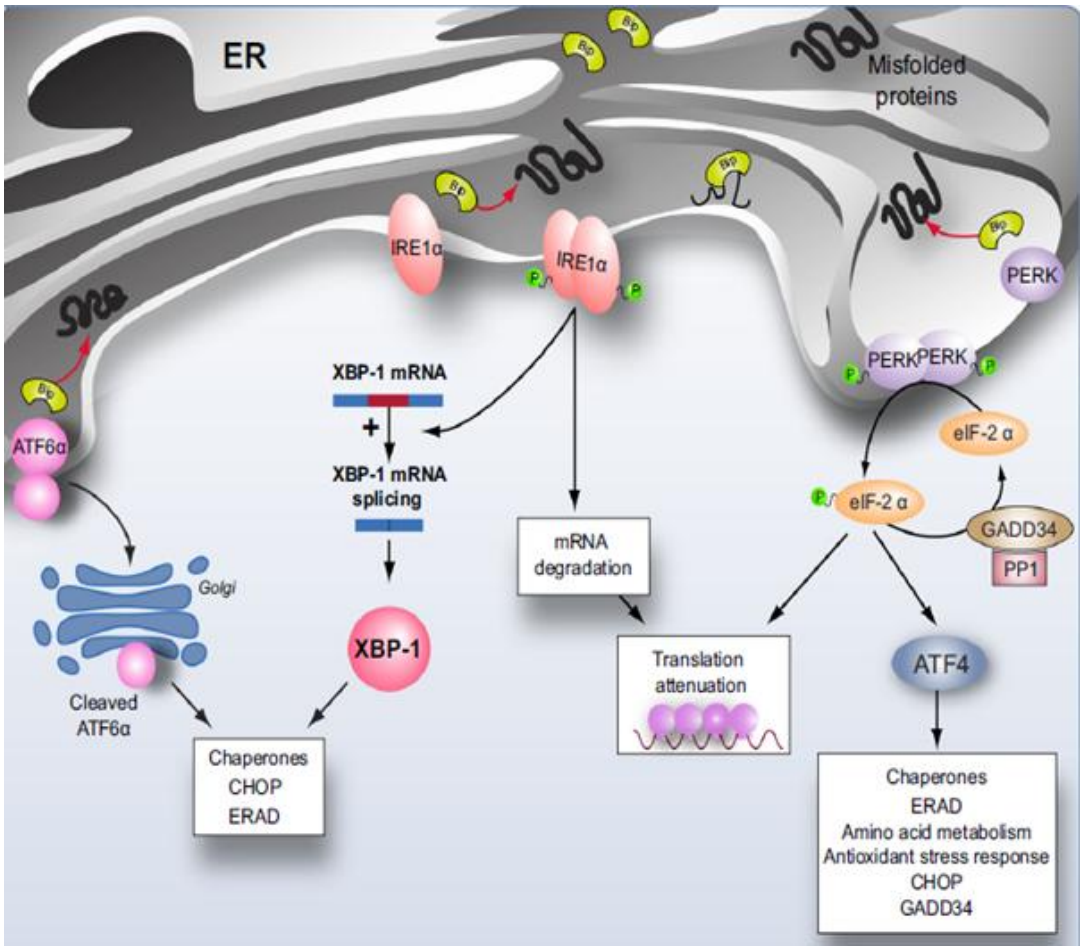

Figure 8: ER Stress Sensors. The ER-Stress response is mediated though the activation of three ER-transmembrane sensors: ATF6α, IRE1α and PERK. In an unactivated state the sensors bind to the chaperone protein Bip. Stimuli inducing the accumulation od missfolded proteins in the ER can bind to Bip. This causes its dissociation from the sensors leading to their activation. In general activation of the UPR induces the activation of pathways to restore homeostasis. It induces general translation attenuation to reduce the amount of client proteins entering the ER and specifically induces the transcription of proteins that increase its folding capacity such as chaperones like Bip [33].

IRE1α is a dual protein with a kinase and endoribonuclease domain. Upon Bip dissociation, IRE1α is activated by dimerization and transautophosphorylation which in turn activates its RNAse activity. This initiates the splicing of X-box-binding protein 1 mRNA (XBP1) generating a frame shift that results in enhanced translation of Xbp1 protein which acts as a potent transcription factor [35-37]. The spliced form sXBP1 binds to DNA response elements (ERSE, ERSE-II and UPRE) which in turn activate the transcription and translation of proteins which will increase the folding capacity of the ER such as chaperone proteins like Bip itself, ER-associated degradation (ERAD) components and CHOP [33].

ATF6α is also activated upon dissociation of Bip. However, this ER-stress sensor is not phosphorylated. Instead, it undergoes proteolytic cleavage in the Golgi apparatus, and the released cytosolic domain forms an active transcription factor that induces ER-chaperones like Bip, XBP1 and GRP94 (glucose related protein 94). It can also heterodimerize with sXBP1 activating the transcription of several sXBP1 target genes (Herp, EDEM, MDG1), Chop and ER-associated degradation (ERAD) components [35-37].

The activation of ER-stress pathways can have two different consequences. So far, the models indicate that short, mild ER-stress promotes reactions aimed to restore homeostasis at the ER, including the general attenuation of mRNA translation and induction of chaperones. Conversely, persistent or intense ER-stress can generate responses that cause cell death. The exact mechanisms leading to this outcome are not fully understood. So far, one of the best characterized ER-stress dependent apoptotic mechanisms is the transcription factor CHOP.

1.7 **CHOP-induced cell death**

A key mechanism of ER-stress induced cell killing is the transcription factor CHOP [36, 38]. This transcription factor can induce the expression of well- known pro-apoptotic genes such as Bim [39] and repress anti-apoptotic genes such as Bcl-2 [40]. In addition, CHOP has been reported to induce cell death via induction of Ero1l (endoplasmic oxidoreductin-1-like protein) [41]. Ero1l is an ER oxidase that which under physiological conditions promotes disulfide bond formation in newly synthesized proteins in the ER. However, overexpression of Ero1l promotes a hyperoxidizing environment that leads to cell death [41]. Ero1l can also activate the ER-calcium release channel IP3R1, thus promoting activation of the calcium-dependent kinase CaMKII which triggers several apoptotic pathways [41, 42] (Fig 9).

Another proposed mechanism for CHOP-dependent cell killing is the induction of GADD34, a phosphatase that dephosphorylates eIF2α [43], thus releasing the translation attenuation (Fig 9). A possible explanation for this is that under conditions of ER-stress, the already compromised ER becomes overloaded with newly synthetized proteins, which in turn may cause more ER-stress. In support of this, mice expressing an inactive form of GADD34 are resistant against ER-stress-induced renal cell apoptosis [44].

An intriguing mechanism for CHOP-dependent apoptosis is the induction of TRB3 (Tribbles-related protein 3) [45] (Fig 9). This protein was first described as an adaptor protein that inhibits Akt phosphorylation [46]. Expression of Trb3 upon tunicamycin induced ER-stress was strongly reduced in fibroblasts from CHOP knockout mice and by siRNA-mediated silencing of CHOP [45]. Furthermore, silencing Trb3 expression by siRNA protects fibroblasts against tunicamycin-induced apoptosis [45].

Altogether, these results suggest that ER-stress may be involved in CCl_4-induced hepatocyte killing.

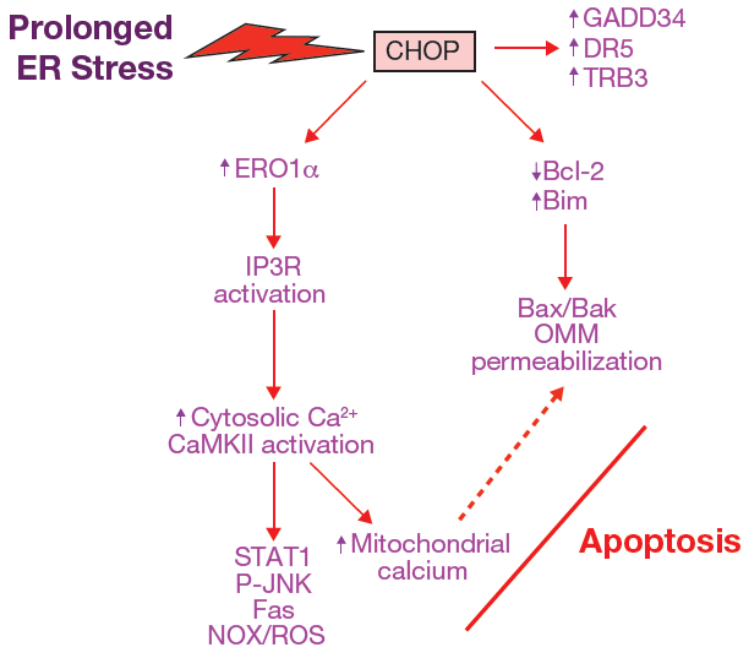

Figure 9: CHOP expression and apoptosis. Under prolonged ER-Stress conditions CHOP can induce the expression of proapoptotic genes such as Bim, DR5 and TRB3 while downregulating antipoptotic ones such as Bcl-2. The activation of CHOP can also induce GADD34 which dephosphorylates eIF2α and shuts the pathway down. Normally, p-Eif2α causes global translation attenuation.When this happens prematurely and the ER-Stress still remains unresolved, this will lead to an overload of the ER capacities generating more ROS and enhancing the stress. Induction of Ero1l by CHOP leads to activation of IP3R1 (inositol 1,4,5-trisphosphate receptor 1), a calcium-release in the ER. Cytoplasmic calcium release activates CaMKII which can induce further apoptosis mechanisms [36] .

2 Aims of this work

The aim of this study was to perform a genome wide unbiased analysis of the most important transcriptional regulatory networks in a model of carbon tetrachloride induced acute liver damage in mice. For this purpose, I used a combination of gene array analyses, bioinformatics and manual curation of the identified deregulated genes. Validation of the identified biological motifs associated to the transcriptional regulatory networks was performed by qRT-PCR, histological as well as molecular biology techniques such as western blot and PCR. These analyses identified a strong activation of ER-stress pathways during early stages of CCl_4-induced hepatotoxicity. Finally, I used CHOP knockout mice to determine the contribution of ER-stress to CCl_4 induced liver damage.

3 List of abbreviations

Akt	Ak (mouse bred) thymoma
ATF4	Activating transcription factor 4
ATF6α	Activating transcription factor 6α
APAP	n-acetyl-p-aminophen, Acetaminophen, Paracetamol
APC	Adenomatous polyposis coli
ASK1	Apoptosis signal-regulating kinase 1
BAD	BCL-2 antagonist of cell death
BAK	BCL-2-antagonist/killer
BAX	BCL-2-associated X protein
BC	Bile canaliculi
BCA	Bicinchonic acid assay
BCL-2	B-cell lymphoma-2
BH3	BCL-2 homology 3
BID	BH3-interacting domain death antagonist
BIM	BCL-2-like-11
BIK	BCL-2-interacting killer
BIP	Binding immunoglobulin protein
bp	Base pairs
BSA	Bovine serum albumin
CCl_4	Carbon tetrachloride

CCl_3	Trichloromethyl radical
°C	Grades Celsius
CEBPD	CCAAT-enhancer binding protein- delta
CHOP	C/EBP homologous protein
CV	Central vein
d	Density
DAB	3,3'-Diaminobenzidine
DAPI	4′,6-Diamidin-2-phenylindol
dH_2O	Distilled Water
DISC	Death induced signaling complex
DMEM	Dulbecco's Modified Eagle's Medium
DMSO	Dimethyl Sulfoxide
dNTPS	Deoxynucleoside triphosphates
ECL	Enhancer Chemiluminescence
EDTA	Ethylenediaminetetraacetic acid
EGTA	Ethylene Glycol Tetraacetic acid
eIF2α	Eukaryotic initiation factor 2 alpha
ER	Endoplasmic reticulum
ERAD	ER-assisted degradation
Ero1α	ER-oxidase 1 α
EtOH	Ethanol
FADD	Fas-Associated protein with Death Domain

FCS	Fetal calf serum
FDR	False discovery rate
FH	Fresh hepatocytes
Frz	Frizzled
GFP	Green fluorescent protein
GO	Gene Ontology
GOT	glutamate-oxaloacetate transaminase
GPT	glutamic pyruvic transaminase
GSH	Glutathione
h	Hour
H&E	Hematoxilin Eosin Staining
HEPES	4-(2-hydroxyethyl)-1-piperazineethanesulfonic acid
HKG	Housekeeping Gene
HNF4α	Hepatocyte nuclear factor 4 alpha
HRP	Horseradish peroxidase
IgG	Immunoglobulin
IHC	Immunohistochemistry
IF	Immunofluorescence
IL	Interleukin
i.p.	Intraperitoneal
IRE1α	Inositol requiring 1α
JNK	c-Jun N-terminale Kinase

KEGG	Kyoto encyclopedia from genes and genomes
KH- Buffer	Krebs-Henseleit buffer
KO	Knock out
L	Liter
LPS	Lipopolysaccharide
mA	Miliampere
MAPK	Mitogen-activated protein kinases
Mc	Collagen monolayer confluent
Mcl-1	Induced myeloid leukemia cell differentiation protein
mM	Milimolar
MPT	Mitochondrial permeability transition
mRNA	Messenger RNA
Ms	Collagen monolayer subconfluent
nM	Nanomolar
µM	Micromolar
NaCl	Sodium chloride
NaOH	Sodium hydroxide
NAPQI	N-acetyl-p-benzoquinone imine
NPC	Non parenchymal cells
PAGE	Polyacrylamide gel electrophoresis
PBS	Phosphate buffered saline solution
PC	Pericentral

PCA	Principal Component Analysis
PCR	Polymerase chain reaction
PCNA	Proliferating cell nuclear antigen
Pepck1	Phosphoenolpyruvate carboxykinase
PERK	PKR-like ER kinase
PHx	Partial hepatectomy
PFA	Paraformaldehyde
PRIMA	PRomoter Integration in Microarray Analysis
PV	Perivenous
PVDF	Polyvinylidene fluoride
RIDD	Related IRE1α dependent decay
ROS	Reactive oxygen species
RT	Room temperature
RT-PCR	Reverse transcriptase PCR
qRT-PCR	Quantitative real time PCR
S	Collagen sandwish
SDS	Sodium dodecyl sulfate
STAT3	Signal transducer and activator of transcription 3
sXBP1	Spliced XBP1
TBS-T	Tris Buffered Saline with Tween 20
TF	Transcription factor
TFBS	Transcription factor binding site

TNF-α	Tumor necrosis factor α
TRAF-2	TNF receptor-associated factor 2
TRB3	Tribbles 3
UPR	Unfolded protein response
UPS	Ubiquitin proteasome system
XBP1	X-box-binding protein 1

4 Materials

Table 1: Chemicals for liver perfusions

Chemical	**Company**
Albumine Fraction V	Sigma-Aldrich Corp., St. Louis, MO, USA
Amino acid solution	PAN Biotech GmbH. Aidenbach, Germany
Collagenase from Clostridium histolyticum	Sigma-Aldrich Corp., St. Louis, MO, USA
Calcium chloride	Sigma-Aldrich Corp., St. Louis, MO, USA
D-(+)- Glucose monohydrate	Sigma-Aldrich Corp., St. Louis, MO, USA
EGTA	Sigma-Aldrich Corp., St. Louis, MO, USA
Fetal calf serum	Biochrom AG, Berlin, Germany
HEPES	Carl Roth, Karlsruhe, Germany
Hydrochloric acid 4mol/L	Carl Roth, Karlsruhe, Germany
KH Buffer (Krebs-Henseleit buffer)	Sigma-Aldrich Corp., St. Louis, MO, USA
L- Glutamine	Sigma-Aldrich Corp., St. Louis, MO, USA
Magnesium sulfate	Sigma-Aldrich Corp., St. Louis, MO, USA
N-Acetyl-L-glutamic acid	Sigma-Aldrich Corp., St. Louis, MO, USA
Potassium chloride	Sigma-Aldrich Corp., St. Louis, MO, USA
Potassium dihydrogen phosphate	Sigma-Aldrich Corp., St. Louis, MO, USA
Sodium chloride	Sigma-Aldrich Corp., St. Louis, MO, USA

4.1 **Buffers for liver perfusions**

Collagenase Buffer	155 ml Glucose (9g/L)
	25 ml KH Buffer pH 7,4
	25 ml HEPES pH 8,5
	30 ml Amino acid solution (Costumer formulation, Cat.Nr.: SO-33100 PAN Biotech GmbH)
	10 ml $CaCl_2$ (19 gr/L)
	2,5 ml Glutamine (7g/L)
	Collagenase from Clostridium histolyticum (Sigma-Aldrich Corp., St. Louis, MO, USA, Cat.Nr.: C2674-16)150 mg
EGTA Buffer	248 ml Glucose (9g/L)
	40 ml KH Buffer pH 7,4
	40 ml HEPES pH 8,5
KH Buffer	Potassium chloride (KCl) 1.75 g/L
	Potasium hydrogen phosphate 1.6 g/L sodium chloride 60 g/L in dH_2O pH set with NaOH to 7.4

Suspension Buffer	400 mg Albumin Fraction V (BSA)
	30 ml Amino acid solution
	1.6 ml CaCl2 solution (19 g/l CaCl2* 2 H2O)
	124 ml Glucose solution (9 g/l)
	2 ml Glutamine (7 g/ml)
	20 ml HEPES pH 7.6
	20 ml KH buffer
	0.8 ml $MgSO_4$ solution
	(24,6 g/L $MgSO_4$ * $7H_2O$)

Table 2: Cell culture media and additives for primary mouse hepatocytes

Primary mouse hepatocytes were cultivated as previously described (Godoy et al 2013), using Williams Medium E, PAN Biotech GmbH; Cat.Nr.:P04-29510 supplemented with the following additives:

Additives	Final concentration	Company	Catalog number
Gentamycin	10 µg/ml	PAN Biotech GmbH. Aidenbach, Germany	P06-13001
Glutamine 200 mM	2 mM	PAN Biotech GmbH. Aidenbach, Germany	P04-82100
Penicillin-Streptomycin	100 U/ml Pen and 100 U/ml Strep	PAN Biotech GmbH. Aidenbach, Germany	P06-07100
Dexamethasone	100 nM	Sigma-Aldrich Corp., St. Louis, MO, USA	D4902
Insulin-transferrin-selenium 100X (ITS)	10 ng/ml	Sigma-Aldrich Corp., St. Louis, MO, USA	129K8402
Fetal calf serum (FCS) (added just for full media)	10%	PAN Biotech GmbH. Aidenbach, Germany	sample 149

Table 3: Reagents and media for collagen preparation

Reagents and Media	Company	Catalog number
DMEM low glucose media 1,0 g/L 10x	Amimed, Allschwil, Switzerland	1-25K03-I
Rat tail Collagen	Roche, Mannheim, Germany	11 171 179 001
NaOH	Merk, Darmstadt, Germany	1.06462
Acetic acid 0,09%	Carl Roth, Karlsruhe, Germany	3738.5

Table 4: Reagents for hepatocytes in vitro culture and in vivo injections

Reagents	Company	Catalog number
DMSO	Sigma-Aldrich Corp., St. Louis, MO, USA	472301
CCl_4	Carl Roth, Karlsruhe, Germany	7345.1
LPS	Sigma-Aldrich Corp., St. Louis, MO, USA	L3012-5MG
Paracetamol (4-Acetamidophenol 98 %)	Sigma-Aldrich Corp., St. Louis, MO, USA	A 7302
Olive oil	Sigma-Aldrich Corp., St. Louis, MO, USA	75343-1L
Tunicamycin	Sigma-Aldrich Corp., St. Louis, MO, USA	T7765

Table 5: Reagents for BCA protein quantification, RNA isolation and cell counting

Reagents	Company	Catalog number
EDTA	Carl Roth, Karlsruhe, Germany	8040.3
Trypan Blue	Sigma-Aldrich Corp., St. Louis, MO, USA	T6146
BCA Protein Assay	Thermoscientific, Wilmington, USA	23225
QIAzol Lysis Reagent	Qiagen, Hilden, Germany	79306
Methanol	J.T. Baker Griesheim, Germany	8045
Isopropanol	Carl Roth, Karlsruhe, Germany	6752.2

Table 6: Reagents for SDS PAGE and western blot

Reagents	Company	Catalog number
Acrylamide 30%, Rotiphorese	Carl Roth, Karlsruhe, Germany	3029.1
APS (Ammonium persulphate solution)	Sigma-Aldrich Corp., St. Louis, MO, USA	3678-25g
Roti-Blot A	Carl Roth, Karlsruhe, Germany	L510.1
Roti-Blot K	Carl Roth, Karlsruhe, Germany	L511.1
Bromphenolblue	Merk, Darmstadt, Germany	211705
DTT (Dithiothreitol)	Sigma-Aldrich Corp., St. Louis, MO, USA	D9779
Glycine	Carl Roth, Karlsruhe, Germany	HN07.3
Nonidet P40	Roche, Mannheim, Germany	11754599001
Ponseau S	Carl Roth, Karlsruhe, Germany	5938.1
Magic Mark XP western protein standard	Invitrogen GmbH, Darmstadt, Germany,	LC5602
Precision Plus Protein standards	Bio-Rad Laboratories, Munich, Germany	161-0374
SDS pellets	Carl Roth, Karlsruhe, Germany	.LN 30.1
TEMED	Carl Roth, Karlsruhe, Germany	2367.1
Western Lightning® Plus-ECL. Enhanced Chemiluminescence Substrate	Perkin-Elmer, Massachusetts, USA	NEL105001.EA

4.2 Prepared buffers and solutions for SDS PAGE and western blot

RIPA Buffer	50 mM Tris-Cl (pH 7.5)
	150 mM NaCl
	1% Nonidet P-40 (NP-40)
	0,5% Sodium deoxycholate
	0,1% SDS
	Protease Inhibitor Cocktail (Sigma München, Germany, Cat.Nr. P8340) 1:100
	Phosphatase Inhibitor Cocktail II (Sigma München, Germany, Cat.Nr.P5726) 1 :100
	Phosphatase Inhibitor Cocktail III (Sigma München, Germany, Cat.Nr.P0044) 1 :100
Anode Buffer	Roti-Blot A 80 ml
	Methanol 160 ml
	dH_2O 560 ml
10% APS	10 gr APS in 100 ml dH_2O
10% SDS	10 gr SDS pellets in 100 ml dH_2O
Cathode Buffer	Roti-Blot K (Roth) 80 ml

	Methanol 160 ml
	dH_2O 560 ml
Laemmli Buffer (5x)	2.25 mL 1M Tris-HCl, pH 6.8
	5 mL Glycerol
	0.5 g 10% SDS
	5 mg Bromphenol blue
	2.5 mL 1M DTT
Running buffer (10x)	30.3 g Tris Base
	144.0 g Glycine
	10.0 g SDS
	Add 1 L dH_2O
Separation buffer	36.34 g Tris in 100 mL dH_2O (pH 8.8)
Stacking buffer	5.69 g Tris in 100 mL dH_2O (pH 6.7)
TBS (10x)	265 g NaCl
	60 g Tris

	Add 5 L of dH_2O (pH 7.4)
TBS-T	250 mL dH_2O
	250 mL TBS
	2.5 mL Tween-20
	Add 2.5 L of dH_2O
Ponseau S solution	1g Ponseau S
	500 mL 3% Triclorite acetic acid
Mild Stripping Buffer, Abcam	15 g Glycine
	1 g SDS
	10 ml Tween 20.Adjust pH to 2.2.
	Add 1 L of dH_2O
PBS 10x	10g KCl
	10g KH2PO4
	400g NaCl
	46g Na2HPO4
	Add 5 L of dH_2O (pH 7.4)

Table 7: List of primary antibodies

Antigen	Origin	Catalog number	Company
β-Actin	Mouse	A2228	Sigma-Aldrich Corp., St. Louis, MO, USA
CEBPD M17	Rabbit	sc-3636	Santa Cruz Biotechnology, Inc., California, USA
CHOP	Mouse	2895	Cell Signaling New England Biolabs GmbH, Frankfurt am Main, Germany
CHOP (GADD153)	Rabbit	sc-575	Santa Cruz Biotechnology, Inc., California, USA
eIF2α	Rabbit	9722	Cell Signaling New England Biolabs GmbH, Frankfurt am Main, Germany
GAPDH	Rabbit	2118	Cell Signaling New England Biolabs GmbH, Frankfurt am Main, Germany
HNF1	Rabbit	sc-8968	Santa Cruz Biotechnology, Inc., California, USA
HNF4α	Goat	sc-6556	Santa Cruz Biotechnology, Inc., California, USA
Ly-6G/-6C (neutrophil marker)	Rat	ab2557	Abcam, Cambridge, UK
PCNA	Mouse	2586	Cell Signaling New England Biolabs GmbH, Frankfurt am Main, Germany
p-Akt	Rabbit	9271	Cell Signaling New England Biolabs GmbH, Frankfurt am Main, Germany
p-eIF2α	Rabbit	3398	Cell Signaling New England Biolabs GmbH, Frankfurt am Main, Germany
p-p44/42 MAPK (Erk1/2)	Rabbit	9101	Cell Signaling New England Biolabs GmbH, Frankfurt am Main, Germany
p-SAPK/JNK (T183/Y185)	Rabbit	4668	Cell Signaling New England Biolabs GmbH, Frankfurt am Main, Germany
p-STAT3 (Tyr705)	Rabbit	9145	Cell Signaling New England Biolabs GmbH, Frankfurt am Main, Germany
Trb3	Rabbit	1032	Merck Millipore, Berlin, Germany

Table 8: List of secondary antibodies for western blot

Antigen	Origin	Catalog number	Company
Rabbit IgG	Goat	7074	Cell Signaling New England Biolabs GmbH, Frankfurt am Main, Germany
Mouse IgG	Horse	7076	Cell Signaling New England Biolabs GmbH, Frankfurt am Main, Germany

Table 9: Reagents for histology

Reagents	Company	Catalog number
Citric acid monohydrate	Carl Roth, Karlsruhe, Germany	3958.2
4% PFA (Rotihistofix)	Carl Roth, Karlsruhe, Germany	P087.5
Avidin/Biotin Blocking Kit	Vector Laboratories, Lörrach, Germany	SP-2001
VECTASTAIN Elite ABC Kit (Rabbit IgG)	Vector Laboratories, Lörrach, Germany	PK-6101
VECTASTAIN Elite ABC Kit (Goat IgG)	Vector Laboratories, Lörrach, Germany	PK-6105
Alexa555-labeled donkey anti Rabbit	Life technologies	A-31572
DAB Peroxidase substrate kit	Vector Laboratories, Lörrach, Germany	SK 4100
Dako Pen	Dako, Hamburg, Germany	REF S2002
Acetic acid	Carl Roth, Karlsruhe, Germany	3738.5
Eosin Y disodium salt	Sigma-Aldrich Corp., St. Louis, MO, USA	E4382
Tris	Carl Roth, Karlsruhe, Germany	4855.2
Tween 20	Sigma-Aldrich Corp., St. Louis, MO, USA	P7949
Microscopy Entellan	Merk, Darmstadt, Germany	1.07960.0500
Hydrochloric Acid 4 N	Carl Roth, Karlsruhe, Germany	N676.1
Mayer´s Hemalum solution	Merk, Darmstadt, Germany	1.09249.0500
Hydrogen peroxide 30%	Carl Roth, Karlsruhe, Germany	9681.1
Albumin bovine Fraction V	Serva Electophoresis, Heidelberg, Germany	11926
Ethanol 99%	Merk, Darmstadt, Germany	100983
Xylol AnalaR Norampur	VWR, Langenfeld, Germany	UN1307
Roti Histol	Carl Roth, Karlsruhe, Germany	6640.1
Paraffin Histowax Surgipath paraplast	Leica Microsystems, Wetzlar, Germany	3901006
Fluorescence preservation reagent	Calbiochem, Darmstadt, Germany.	345787

4.3 **Buffers for PCR**

TBE buffer (10x)	Boric acid 55 g
	Tris 108 g
	40 ml 0.5 M Na_2EDTA pH 8
	Add 1 L dH_2O
Ficoll loading buffer	Bromphenol blue 125 mg
	Ficoll 7.5 g
	Add 50 ml dH_2O

Table 10: Chemicals for PCR

Reagents	Company	Catalog number
Agarose	Biozym Scientific GmbH, Hessisch Oldendorf, Germany	840004
Boric acid	Carl Roth, Karlsruhe, Germany,	5935.1
DEPC treated Water	Invitrogen GmbH, Darmstadt, Germany	46-2224
DNA ladder, 100 bp	Invitrogen GmbH, Darmstadt, Germany	15628-050
Ethidium Bromide	Invitrogen GmbH, Darmstadt, Germany	15585-011
Ficoll	Sigma-Aldrich Corp., St. Louis, MO, USA	F4375
Taq DNA Polymerase kit	5-Prime, Hamburg, Germany	2900169

Table 11: PCR primers

Primers were purchased from Eurofins, Ebersberg, Germany

Primers	Sequence 5´→3´
XBP1 Forward	GAACCAGGAGTTAAGAACACG
XBP1 Reverse	AGGCAACAGTGTCAGAGTCC

Table 12: Reagents for qRT-PCR

Reagents	Company	Catalog number
High capacity cDNA Reverse Transcription Kit (include: RT-Random primer, dNTPS, Reverse transcriptase, RT-Buffer)	Applied Biosystems, Karlsruhe, Germany	4368813

Table 13: Reagents for qRT-PCR

Reagents	Company	Catalog number
TaqMan Universal Master Mix II	Applied Biosystems, Karlsruhe, Germany	4440038

Table 14: TaqMan probes

All TaqMan probes were purchased from Applied Biosystems, Karlsruhe, Germany

Target gene	Catalog number
Bcl2	Mm00477631_m1
Bcl2l11 – Bim	Mm00437796_m1
Bcl2l1 – Bcl-xl (mouse)	Mm00437783_m1
Ccl2	Mm00441242_m1
CHOP (Ddit3)	Mm01135937
Cflar (mouse)	Mm01255576_m1
PERK (Eif2ak3)	Mm00438700
GAPD	Mm4352932E
GADD34-Ppp1r15a	Mm01205601
Ero1l	Mm00469296_m1
IRE1α (Ern1)	Mm00470233
Lcn2	Mm01324470_m1
Mcl1 (mouse)	Mm00725832_s1
Mt2	Mm00809556_s1
TNFR12	Mm00489103_m1
Trib3	Mm00454879

5 Methods

5.1 In vivo models of liver damage, inflammation and regeneration

A set of fundamentally different models of liver stress was applied to obtain a comprehensive overview of transcriptional regulatory networks in liver tissue. This included mouse models of acute liver damage by the hepatotoxins CCl_4 and paracetamol, endotoxin (lipopolysaccharide)-induced inflammation and surgically-induced stress (partial hepatectomy). In addition, a model of drug-induced ER-stress with tunicamycin was included. All experiments were performed in male C57Black6/N or C57B6/J mice (8-12 weeks old, Charles Rivers, Sulzfeld, Germany). CHOP knockout mice (on a C57BL/6J background) (Ref paper CHOP KO Zinzsner DevCell 98) were purchased from Jackson laboratories (Stock number 005530). Mice were fed ad libitum with Ssniff R/M-H, 10 mm standard diet (Ssniff, Soest, Germany). All experiments were approved by the local Ethic committees. 4-5 mice were used for each time point in each model. At the indicated time points, mice were anesthetized with an intraperitoneal injection of Rompun® 2% (20 mg/kg) and ketamine (120 mg/kg) for collection of blood and liver tissue. The liver was resected, washed in PBS and sectioned for further analysis. Sections of about 0.5 cm^2 were snap frozen in liquid nitrogen and stored at -80°C for subsequent isolation of proteins or RNA. Details for sample preparation are described below.

5.1.1 CCl_4-induced acute liver damage

To obtain information about the transcriptional regulatory networks induced in early and late stages after acute liver damage, the model compound CCl_4 was selected. For maximal liver damage, C57B6/N mice received a single intraperitoneal injection of 1.6 g/kg CCl_4 dissolved in olive oil as previously described [47]. As controls, mice received a single injection of olive oil. The solutions were freshly prepared before the injection and mixed by vortexing. Blood and tissue samples were collected after 2h, 8h, and days 1, 2, 4, 6, 8, and 16 of CCl_4 injection. Control (i.e. olive oil) samples were collected at day 1 and day 8 after olive oil injection. The

volume injected was 4 ml/kg per mice. Healthy liver tissue was collected from untreated mice.

In a separate set of experiments, C57B6/J and CHOP knockout mice received CCl_4 in two different doses. A high dose of 1.6 g/kg was used to induce maximal liver damage as described for C57B6/N mice. For a minimal liver injury, mice received a single injection of 0.132 g/kg CCl_4 in olive oil. In both experiments, liver and blood were collected after 2h, 8h, 24h and 72h. Four to five mice were used for each condition and time point, from wild type and CHOP knockout mice respectively. As control, mice received a single injection of olive oil for 24h.

5.1.2 **Paracetamol model of acute liver damage**

To compare with a different model of drug-induced acute liver damage, the hepatotoxic compound paracetamol was chosen. For this, C57B6/N received a single dose of 500 mg/kg paracetamol dissolved in sterile PBS, at a concentration of 14.9 g/l. The final volume injected was 33.5 µl per gram of body weight. To ensure proper paracetamol solubilization, the solutions were freshly prepared and heated at in a water bath a 55 °C [15, 48]. Before injection, the solutions were cooled down and sterile filtered. As a control, mice received a single injection of PBS for 24h.

5.1.3 **Tunicamycin-induced ER-stress in vivo**

Tunicamycin was used to generate a model of ER-stress in vivo. For this, C57B6/J mice received a single intraperitoneal injection of tunicamycin (5 mg/kg), dissolved in 150 mM glucose / 5% DMSO to a concentration of 0.5 mg/ml. The final volume injected was 20 µl per gram body weight. Liver samples were collected after 8h.

5.1.4 **Model of inflammation: LPS injection**

For lipopolysaccharide (LPS) model, mice received a single intraperitoneal injection of LPS (750 ng/kg) dissolved in sterile PBS for 24h.

5.1.5 **Partial hepatectomy (PHx)**

The model of 70% partial hepatectomy was performed by our cooperation partners at the Department of General, Visceral and Vascular Surgery, University Hospital Jena. All surgical interventions were performed under inhalation of 2% isoflurane mixed with an oxygen flow of 0.3 L/min (isoflurane vaporizer, Sigma Delta, UK) in S1 operation room. A precise vessel-oriented, parenchyma-preserving surgical technique was used for 70% partial hepatectomy using a modification of the technique described by Madrahimov [50] for rats. a 10x magnification. A ligature (6-0 silk) was applied loosely to the pedicle of LLL. The The procedure started with a laparotomy via a transverse abdominal incision. The whole liver was well exposed by elevating the xiphoid process. Skin and muscle were fixed by retractors, and the small bowel was moved out to the left side of the abdomen and covered with saline soaked gauze. The liver was freed from the falciform ligament and triangular ligamentum. The liver lobes were positioned so that hilum of left lateral lobe (LLL) and median lobe (ML) were clearly visible. All subsequent steps were performed using a stereo microscope with ligature was tightened keeping a distance of about 3 mm from the cava while the LLL remained in its anatomical position and the lobe resected. Next, cholecystectomy was performed after double ligating the cystic duct and cystic artery using a 7-0 prolene suture. For resection of the median lobe, a virtual line was drawn between the left side of the cava and the gallbladder. The clamp was placed, roughly perpendicular to the surface of the left median lobe (LML), about 3mm lateral to this line and the left median lobe removed. Proximal to the clamp, a piercing suture was positioned according to vascular anatomy to ligate the left median hepatic vein and the clamp removed. Then, the right median lobe (RML) was clamped in similar way. After resection, two piercing sutures were placed to ligate the right and median hepatic vein as well as the arterial and portal supply. Finally, the abdomen was irrigated with warm saline solution and closed with a 2 layer running suture (6-0 prolene). At the end of anaesthesia, animals were allowed to recover on a heating pad. Temgesic (0.05 mg/kg) was applied subcutaneously after operation and at an interval of 12 hours in next 3 days. Animals were monitored daily for body weight development and activity using a scoring system [51]. Briefly, mice with normal activity, physiological position, no jaundice, and no signs of bleeding were regarded as healthy (+++); animals showing a weaker activity, hunched back position and/or signs of jaundice or bleeding were regarded as weak (++); and animals with no spontaneous activity and lying position and signs of jaundice or bleeding were regarded as

severely ill (+). At the indicated time points, mice were anesthetized and the liver was resected, washed in ice cold PBS and sectioned for further analysis. Sections of about 0.5 cm^2 were snap frozen in liquid nitrogen and stored at -80°C for subsequent isolation of proteins or RNA.

5.2 Collection and analysis of blood samples

5.2.1 Blood sample collection and plasma separation

To determine the severity of liver damage, the activity of liver transaminases GOT and GPT were analyzed in the plasma of mice treated with CCl_4 or paracetamol at each time point and condition, and compared to the levels of control and healthy mice. Blood collections proceeded as follows. Mice were anesthetized by intraperitoneal injection of Rompun® 2% (20 mg/kg) and ketamine (120 mg/kg), fixed on a grid and opened through the abdominal cavity. About 400 µl of blood were collected from the heart using a 26G cannula in a 1ml syringe containing 25 µl EGTA (32 mg/ml). The blood was carefully mixed by up and down movements in the syringe with the EDTA solution and transferred into a pre-chilled, sterile 1.5 ml tube. The sample was immediately centrifuged at 13,000 rpm, 10 min at 4°C. The supernatant, corresponding to 200 µl of plasma was collected in pre-chilled 1.5 ml tubes and stored at -80°C for further quantification of transaminases.

5.2.2 Determination of GOT and GPT activity in plasma

The activity of liver transaminases GOT (glutamate-oxaloacetate transaminase) and GPT (glutamic pyruvic transaminase) in plasma of control and treated mice was determined at the LADR laboratory in Recklinghausen (LADR, medizinisches Versorgungszentrum, Recklinghausen, Germany).

5.3 **Primary hepatocytes isolation and culture**

Primary mouse hepatocytes were obtained by a two-step perfusion technique from male Black6N mice (8-12 week old) as previously described [52, 53]. Briefly, mice received an intraperitoneal injection of a mixture of anesthesia (Ketamin 120 mg/kg) and a sedative (Rompun® 2% 20 mg/kg). The complete sedative effect and the inhibition of pain in the mouse was determined 5-7 min after the injection by observing suppression of reflexes (ataxia, no reaction to pain by pressing of the paws). Afterwards, the mouse was placed on a flat grid and fixed with adhesive tape, and the abdominal cavity was opened to proceed for liver perfusion. First, a 24G cannula was inserted into the inferior vena cava, connected to a peristaltic pump with a rate flow of 15 ml/min. The liver perfusion started with EGTA buffer at 37 °C. When the cannulation was successful the liver color turned pale immediately, then the vena cava was incised to assure a proper outflow of the buffers. After 5 min of EGTA buffer, the perfusion continued with a collagenase buffer at 37 °C until cell detachment from the liver matrix was observed by slightly pressing the liver with a forceps, which occured after 15-20 min of collagenase buffer perfusion. The liver was then completely excised from the mouse and transferred to a sterile hood. Afterwards, the liver capsule was disrupted using forceps to release the liver cells in a suspension buffer. The liver cell suspension was then filtered through a 100 µm cell strainer and centrifuged at 50g for 5 min at 4°C. After centrifugation the supernatant was discarded. The pellet, corresponding to the hepatocyte fraction, was resuspended in 10 ml suspension buffer. A portion of the cell suspension is mixed1:5 with trypan blue for cell counting in a Neubauer cell chamber. The percentage of viable cells was determined by trypan blue exclusion; the minimal viability was 97%. Hepatocytes were then cultivated in either collagen-I coated dishes (i.e. monolayer) or between two layers of collagen-I gel (collagen sandwich). The monolayer cultures were performed either in confluent (MC) or subconfluent (MS) conditions, using 104,166 cells/cm^2 or 13,000 cells/cm^2, respectively. For collagen sandwich cultures (S), hepatocytes were plated at 88,542 cells/cm^2. Detailed protocols for the cultivation of hepatocytes are described in Godoy et al 2013 [23].

5.4 RNA isolation from primary mouse hepatocytes and liver tissue

RNA was isolated from cultured hepatocytes and from mouse liver tissue using the phenol/chloroform method (Trizol®, Qiagen, Hilden, Germany) according to the manufacturer's description. For freshly isolated hepatocytes, 1 million cells in suspension medium were allowed to decant in a 1.5 ml conical tube placed on ice for 10 minutes. The medium was quickly removed and the cells homogenized in 1 ml of Trizol® (Qiagen, Hilden, Germany) by 10 repetitive aspirations in a micropipette. For hepatocytes in culture, the medium was removed and the cells were homogenized in 1 ml Trizol® (Qiagen, Hilden, Germany) with a micropipette. For liver tissue, snap frozen sections were homogenized in a 1.5 ml tube with 1 ml Trizol® (Qiagen, Hilden, Germany) using a plastic pestle and subsequent sonication on ice. RNA concentration and integrity and were determined spectrophotometrically in a Nanodrop®2000 (ThermoScientific, Waltham MA, USA) and in a Bioanalyzer® (Agilent, Waldbronn, Germany) respectively.

5.5 cDNA synthesis and Polymerase Chain Reaction

5.5.1 cDNA synthesis

For complementary DNA synthesis, 2 µg of RNA were transcribed using the High Capacity cDNA reverse transcription kit (Applied Biosystems, Darmstadt, Germany) as previously described (Godoy et al 2013). The resulting cDNA was diluted 10 fold and used as template for real-time PCR. The temperatures and cycles for the qRT-PCR reaction are indicated on table 15. After cDNA synthesis the samples were either stored at -20°C.

Table 15: Thermocycler Program for Reverse –Transcriptase PCR

Step	Temperature	Time
1	25	10 min
2	37	2h
3	85	5 min
4	4	---

5.5.2 **Real Time qPCR**

Quantitative, real time PCR reactions were performed using 2.5 µl of cDNA, TaqMan Universal Master Mix II and TaqMan primer probes (from Applied Bio systems, Karlsruhe, Germany) in an ABI Prism 7300 Sequence detection system (Applied Biosystems, Karlsruhe, Germany). The reagents were mixed as indicated in Table 15. A list of TaqMan probes is provided in (section 4, Table 13). The reaction steps are described below (table 16). The relative mRNA content was normalized to the GAPDH mRNA expression in each sample. For calculations of relative gene expression the $2^{-\Delta\Delta Ct}$ method was used [54]. All qPCR reactions performed and analyzed using technical duplicates.

Table 16: Master mix conditions for qPCR reactions

Reagent	Volume per reaction (µl)
TaqMan Universal Master Mix	10
TaqMan probe	1
DEPC-Water	6.5
cDNA	2.5

Table 17: ABI Prism 7300 conditions for qPCR

Stage	Temperature	Time	Repetitions
1	50	2 min	1
2	95	15 min	1
3	94 55 72	15s 30s 35s	40
4	95 60 95 60	15 20 15 15	1

5.5.3 **Analysis of Xbp1 splicing by PCR**

The PCR reaction for XBP1 was performed using the Taq DNA Polymerase kit of 5-Prime (Hamburg, Germany) with primers from Eurofins (Ebersberg, Germany) in the T-Gradient Thermocycler from Biometra at the temperatures and cycles indicated below (the sequence used primers are indicated table 11). The whole PCR products were further mixed with 5 µl Ficoll (see section 4.4) and shortly spin down for further loading into 1.5% Agarose gels. The samples ran in 1x TBE Buffer at 150 V for ~2 h. The electrophoresis results were detected using UV light and the Fusion FX7 image acquisition system from Vilber Lourmat (Eberhardzell, Germany).

Table 18: Thermocycler Program for XBP1 PCR reaction

Step	Temperature°C	Time	Go back to step	Number of cycle repetitions
1	94	2m		
2	94	30s		
3	58	1m		
4	72	1m		
5	72	10m	2	39
6	4		---	

5.6 Affymetrix gene array analysis

Whole genome gene array analysis from liver tissue and from cultivated primary hepatocytes was performed using Affymetrix GenChip® Mouse Genome 430 2.0 arrays (Santa Clara, CA, USA). In case of liver tissue, the analysis was conducted using RNA from C57B6/N mouse liver after CCl_4 administration (1.6 g/kg), LPS intraperitoneal injection or partial hepatectomy as described above. For the CCl_4 model, the following time points were analyzed: 2h, 8h, and days 1, 2, 4, 6, 8 and 16 after CCl_4 injection. For LPS, a single time point of 24h was performed. For partial hepatectomy, the following time points were analyzed: 1h, 6h, 12h, and days 1, 2, 3, 4 and 7. For the CCl_4 model, control (olive oil) and healthy (untreated) liver were also collected and analyzed. For LPS, control (PBS treated) livers were used. For partial hepatectomy, liver tissues from 5 independent control mice were used. For cultivated hepatocytes, samples were collected from cells in monolayer confluent, monolayer subconfluent or sandwich cultures at days 1, 2, 3, 5, and 7. Three independent hepatocyte preparations were used.

The analysis of RNA expression by gene array was conducted as follows. Briefly, five µg RNA were transcribed into cDNA by oligo dT primers, and reverse transcribed to biotinylated cRNA with the Gene Chip IVT® Labeling kit (Affymetrix, High Wycombe, UK). Cleanup of the IVT product was done using CHROMA SPIN-100 columns (Clontech,

USA). Spectrophotometric analysis was used for quantification of cRNA with acceptable A260/A280 ratio of 1.9 to 2.1. After that the cRNA was fragmented using Affymetrix's protocol. Labeled and fragmented cRNA was hybridized to Mouse Genome 430 2.0 Affymetrix GeneChips for 16h at 45° C according to the manufacturer's instructions. Microarrays were washed using an Affymetrix fluidics station 450 and stained initially with streptavidin-phycoerytherin. For each sample the signal was further enhanced by incubation with biotinylated goat anti-streptavidin followed by a second incubation with streptavidin-phycoerytherin and a second round of intensities were measured. Microarrays were scanned with an Affymetrix scanner controlled by Affymetrix Microarray Suite software.[55]

5.7 Microarray processing and statistical analysis

Affymetrix gene expression data were pre-processed using 'affyPLM' packages [56] of the Bioconductor Software [57].To obtain the genes with the most evidence of differential expression, a linear model fit was applied for each gene using 'limma' (Linear Models for Microarray Data) packages [58] of [57]. Data obtained from fresh hepatocytes were used as reference. The custom chip definition file from Brainarray [59] based on Unigene ID's was used to annotate the microarrays. A false positive rate of a=0.05 with FDR correction and a fold change greater 2 was taken as the level of significance. Processing and visualization (Principal Component Analysis) of data were performed using MATLAB tools (The MathWorks Inc., Natick, MA).

5.8 Fuzzy clustering of gene expression profiles

The time-profiles of the differentially expressed genes in cultivated mouse hepatocytes were scaled between their respective absolute temporal extreme values to focus subsequent cluster analysis on the qualitative behavior of the expression profiles. The time series were clustered using fuzzy c-means [60] (fuzzy exponent = 1.5; maximum number of iteration = 200; minimum cost function improvement = 10-10). The optimum number N of cluster was

estimated by repeated calculation (number of iterations = 100) of the fuzzy cluster index 'Separation Index'.

5.9 Gene Ontology (GO) and KEGG Pathway analyses

Genes which show change ratios greater (or less) than 2-fold in the triplicate arrays at any one of the time points have been considered as up or downregulated and subjected for gene ontology (GO) and pathway analyses. Differentially regulated genes were categorized using the manually curated Gene Ontology of the Biobase Knowledge Library (BKL) of the ExPlain™ webservice (BioBase GmbH, Wolfenbüttel, Germany).

5.10 Promotor analysis

To identify transcription factors (TFs) whose binding sites are enriched in a given set of promoters, the algorithm PRIMA (PRomoter Integration in Microarray Analysis; Elkon et al., 2003) of the Expander Software 6.1 (EXPression ANalyzer and DisplayER [61] was used. Genes that are significantly (p-value cut off is 0.05) changed greater than 2-fold were used for analysis. All genes from mouse (Ensembl release 42) were used as background set, the threshold of the p-value was set to 0.01 and the region was scanned from -3000 to +200.

5.11 Spearman rank correlation analysis

To calculate the strength of the relationship between cultivation (MC, MS, S) and the in vivo models CCl_4, PHx and LPS, we used spearman rank correlation. The changes in gene expression at different time points in cultivation (MC, MS, S) versus changes in CCl_4, PHx and LPS were used for the calculation of the correlation coefficients. Affimetrix Gene Array analysis of CCl_4 induced liver damage

Whole genome gene array analysis with Affymetrix chip was performed from CCl_4 1.6 g/kg treated Bl6N mice at different time points using the Affymetrix GenChip® Mouse Genome 430 2.0 arrays (Santa Clara, CA, USA). Briefly, five µg RNA were transcribed into cDNA by oligo dT primers, and reverse transcribed to biotinylated cRNA with the Gene Chip IVT® Labeling kit (Affymetrix, High Wycombe, UK). Cleanup of the IVT product was done using CHROMA SPIN-100 columns (Clontech, USA). Spectrophotometric analysis was used for quantification of cRNA with acceptable A260/A280 ratio of 1.9 to 2.1. After that the cRNA was fragmented using Affymetrix's protocol. Labeled and fragmented cRNA was hybridized to Mouse Genome 430 2.0 Affymetrix GeneChips for 16h at 45° C according to the manufacturer's instructions. Microarrays were washed using an Affymetrix fluidics station 450 and stained initially with streptavidin-phycoerytherin. For each sample the signal was further enhanced by incubation with biotinylated goat anti-streptavidin followed by a second incubation with streptavidin-phycoerytherin and a second round of intensities were measured. Microarrays were scanned with an Affymetrix scanner controlled by Affymetrix Microarray

5.12 Protein extraction and western blot analyses

5.12.1 Protein isolation from liver tissue

Protein extracts and immunoblots were performed as previously described (Godoy et al 2009, Godoy et al 2013). Briefly, hepatocytes or snap frozen liver tissue were homogenized by sonication in ice cold radioimmunoprecipitation (RIPA) buffer (2% NP40, 0.5% DOC, 0.1% SDS, 250 mM NaCl, 2.5 mM EDTA, 50 mM Tris pH 7.2) supplemented with protease inhibitors (Protease inhibitor cocktail) and phosphatase inhibitors (Phosphatase inhibitor cocktail-I and phosphatase inhibitor cocktail-II), all from Sigma (München, Germany). The homogenates were incubated on ice for 30 min, and centrifuged for 10 min at 13.000 rpm, 4°C. The clear supernatant containing solubilized proteins was collected in a pre-chilled 1.5 ml tube.

5.12.2 **Protein quantification (BCA Assay)**

Proteins were quantified according to the bicinchoninic acid (BCA) assay using a kit from Thermo scientific (see under materials table 5). All reagents were mixed according to the manufacturer specifications together with an aliquot of each protein lysate sample (2, 5 µl to 10 µl depending on the estimated protein concentration). The samples were incubated at 60°C for 30 minutes. An aliquot of RIPA buffer was also included as a blank. Each sample was measured at 540 nm using a spectrophotometer (V-530, Jasco). The protein concentration was determined by the absorbance given by the mean value of 3 independent measurements relative to a standard curve and the used protein lysate dilution.

5.13 **SDS page and Western blot**

5.13.1 **Protein lysate preparation for electrophoresis**

For analysis of signal transduction (i.e phosphorylations) and expression of the cell cycle marker PCNA, 50 µg of liver protein extracts were mixed with Laemmli Buffer (see under materials 4.2) and denaturized by heating for 5 min at 95°C in a thermo block. Afterwards, the samples were centrifuged for 1 min at 12,000 rpm, placed on ice for 5 min then and loaded into 10% SDS gels (using gels prepared with 1.5 mm combs). The preparation of SDS/PAGE gels is described below.

5.13.2 **SDS-Acrylamide gel casting**

SDS/PAGE gels were casted under a fume hood using the Bio-Rad Mini-PROTEAN hand cast system. 10% SDS-Agarose gels 1.5 mm with10 wells were made using the mixtures indicated below (Table 20) and stored in a humid bag at 4-8 °C for a maximum of 1 week.

Table 19: Separation and Stacking gel composition

Separation gel compounds	Volume for 2 gels 10% SDS	Stacking gel compounds	Volume for 2 gels
H_2O	6.4 ml	H_2O	4.8 ml
Acrylamide	5.28 ml	Acrylamide	1.0 ml
Separation buffer	4.0 ml	Separation buffer	0.8 ml
10% SDS	160 µl	10% SDS	65 µl
TEMED	6.4 µl	TEMED	5.0 µl
10% APS	160 µl	10% APS	100 µl

5.13.3 **SDS-Acrylamide gel electrophoresis**

SDS/PAGE gel electrophoresis was performed using the Mini-PROTEAN®Tetra Cell system for gel electrophoresis (Bio-Rad, Hercules, California, USA). The electrophoresis ran at a constant current of 25 mA per gel (Power Pack 300 from Bio-Rad, Hercules, California, USA) for ~3h in a 1x running buffer (see under materials 4.2.).

5.13.4 **Semi dry Blotting**

Once proteins were separated by electrophoresis, they were blotted into a PVDF membrane (Polyscreen transfer membrane, Perkin Elmer, Cat Nr.: NEF 1002001PK) using the Trans-Blot® SD Semi-Dry Transfer Cell system from Bio-Rad (Hercules, California, USA). To do this, the gel was placed between a sandwich of 12 blotting papers (Blotting paper 703, VWR, Cat Nr.:732-0591) previously saturated in anode buffer, the PVDF membrane and 4 blotting papers previously saturated in cathode buffer. To ensure that no bubbles were present between the layers, the blot-paper-gel pile was slightly pressed out by rolling a pipette. After this procedure the blotting chamber was closed and the proteins were blotted at a constant current of 250 mA per gel for 40 min.

5.13.5 **Proteins immunodetection by chemiluminiscense**

5.13.5.1 **Membrane blocking:**

After blotting proteins, the membranes were incubated in a blocking solution of either 5% BSA or 5% milk in TBS-T, depending on the antibodies used, for 1h in a shaker at room temperature.

5.13.5.2 **Incubation with the first antibody:**

After blocking the membranes, they were incubated with a solution of antibodies against the desired protein, in either 5% BSA or 5% milk in TBS-T, overnight at 4°C on a shaker. Afterwards, the membranes were washed three times in TBS-T for 10 min. A detailed list with all used antibody conditions is provided under 5.19.5.3

5.13.5.3 **Incubation with secondary antibody.**

After washing, the membranes were incubated with horse radish peroxidase-labeled secondary antibodies diluted in 5% BSA or 5% milk in TBS-T. The incubation was performed for a minimum of 1h on a shaker at room temperature. After this time, the membranes were washed 3 times for 10 min with TBS-T.

Table 20: Antibody conditions used for western blot

First Antibody	Dilution	Incubation time	Second antibody	Dilution	Incubation time
β-Actin	1:500 in 5% BSA	30 min at RT	Mouse	1:5000 in 5% BSA	30 min
CHOP	1:1000 in 5% BSA	Overnight at 4-8 °C	Mouse	1:1000 in 5% BSA	1h at RT
eIF2α	1:1000 in 5% BSA	Overnight at 4-8 °C	Rabbit	1:1000 in 5% BSA	1h at RT
GAPDH	1:1000 in 5% BSA	Overnight at 4-8 °C	Rabbit	1:1000 in 5% BSA	1h at RT
PCNA	1:2000 in 5% Milk	Overnight at 4-8 °C	Mouse	1:1000 in 5% Milk	1h at RT
p-Akt	1:1000 in 5% BSA	Overnight at 4-8 °C	Rabbit	1:1000 in 5% BSA	1h at RT
p-eIF2α	1:1000 in 5% BSA	Overnight at 4-8 °C	Rabbit	1:1000 in 5% BSA	1h at RT
p-p44/42 MAPK (Erk1/2)	1:1000 in 5% BSA	Overnight at 4-8 °C	Rabbit	1:1000 in 5% BSA	1h at RT
p-SAPK/JNK (T183/Y185)	1:1000 in 5% BSA	Overnight at 4-8 °C	Rabbit	1:1000 in 5% BSA	1h at RT
p-STAT3 (Tyr705)	1:1000 in 5% BSA	Overnight at 4-8 °C	Rabbit	1:1000 in 5% BSA	1h at RT

5.13.6 **Chemiluminescence reaction:**

To detect the protein of interest, the membranes were incubated in 5 ml of ECL solution (Perkin Elmer, Waltham MA, USA) and placed in Fusion FX7 image acquisition system (Vilber Lourmat, Eberhardzell, Germany) for detection of chemiluminiscense.

5.14 **Liver Tissue fixation**

After blood collection (see 5.2) the liver of the mouse was completely excised. Two liver lobes were collected in plastic cassettes and fixed for 2 days in 4% PFA solution at 4-8°C, followed by washed for 2 days in sterile PBS at 4-8°C. After this time the liver lobes were embedded in paraffin (see 5.15)

5.15 **Paraffin embedding of liver tissue**

After proper fixation, the liver lobes were embedded in paraffin using the Microm STP 120 Spin Tissue Processor from Thermo Scientific, according to the program specified below. After this process, the liver lobes were submerged in paraffin with the Microm HM450 automated embedding device.

Table 21: Paraffin Embedding Program for liver lobes

Step	Treatment	Time in minutes
1	70% ethanol	30
2	70% ethanol	60
3	90% ethanol	30
4	90% ethanol	30
5	99% ethanol	30
6	99% ethanol	35
7	99% ethanol	60
8	Xylol	30
9	Xylol	35
10	Xylol	60
11	Paraffin Histowax	80
12	Paraffin Histowax	105

5.16 **Liver slices for histological analyses**

Paraffin liver sections of 5 µm obtained with a Microm HM450 microtome and mounted on glass microcopy slides by incubation for 20 min at 60°C.

5.16.1 **Tissue deparaffinization**

For tissue deparaffinization, the liver slices were incubated three times for 10 min in xylene.

5.16.2 **Tissue rehydration**

Deparaffinized liver sections were rehydrated by tandem incubations in decreasing concentrations of isopropanol (98%, 96%, 90%, 80%, and 70%, respectively) for 5min each, and a final incubation in distilled water for 10 seconds.

5.17 **Hematoxilin and eosin staining of paraffin liver sections**

To determine the extent of liver injury, liver sections were stained with hematoxilin and eosin, and examined under bright field microscopy. This staining allows the identification of dead cell areas. The staining procedure was performed as follows. After rehydration, the samples were incubated for 5 min. in Mayers Hematoxylin solution (1:5 solution, filtered before use), followed by washing in running tub water for 15 min. Afterwards, the tissue sections were incubated for 3 min in 1% Eosin solution (Eosin Y 1% with 1 drop of acetic acid) and further washed for 10 seconds in distilled water. Finally, the samples were dehydrated gradually in organic solvent starting from 5 seconds incubation in 70%, 80%, 90% isopropanol and finishing with an incubation of 3 min in Roti-Histol. After this procedure, the samples were covered with a cover slide glass with Entellan, allowed to air dry overnight, and examined under bright light microscopy for quantification of dead cell areas.

5.18 **Quantification of dead cell areas**

Digital images of the H&E stained liver sections were acquired on an Olympus BX41 microscope (Olympus, Hamburg, Germany) and analyzed with the Cell^M software

(Olympus, Hamburg, Germany). In order to precisely quantify the dead cell area, first a measurement of the whole image area was taken. Later, the dead cell areas were localized as the areas showing no hepatocytes nuclei. Five pictures from 3 mice were quantified to calculate the % dead cell area, according to the formula shown below.

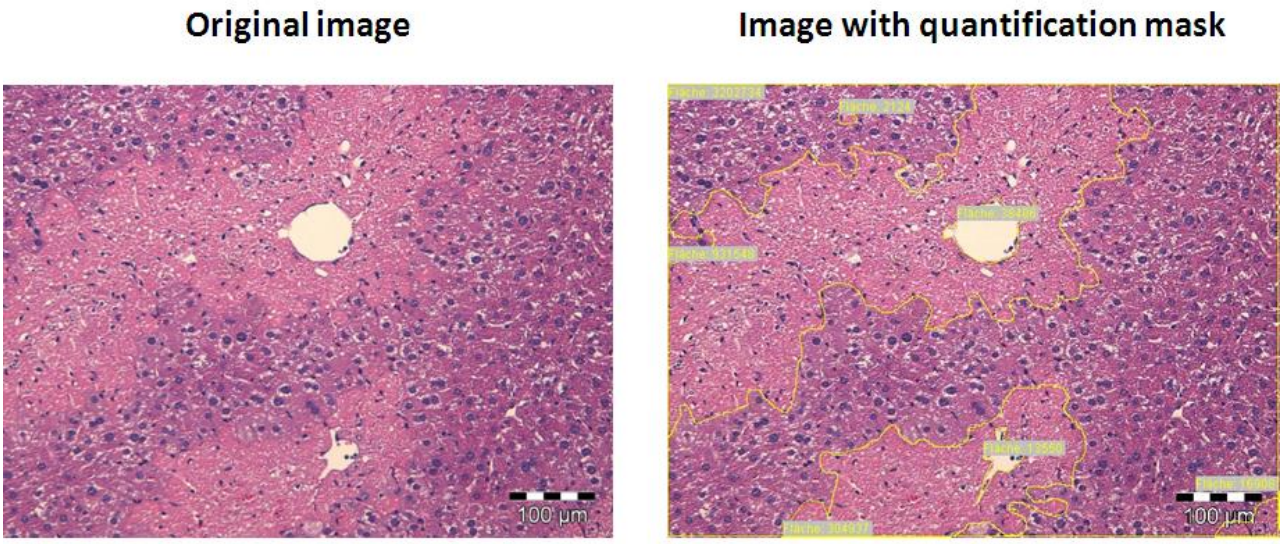

$$\%\ \textbf{Dead Cell Area} = \frac{\text{Area of lesion - Central Vein}}{\text{Total Image area} - \text{Veins}} \times 100$$

Figure 10: H&E Staining quantification. Pictures from H&E stainings were taken and quantified measuring the areas were hepytocyte nuclei were loss. For a more accurate determination of the necrotic areas, the empty areas corresponding to veins were substracted from the total area according formula shown above. 5 pictures from 3 mice were quantified to calculate the % dead cell area.

5.19 **Immunohistochemistry:**

The expression of CHOP, CEBP/δ, HNF4α, HNF1 and neutrophils in mouse liver sections was performed by immunohistochemistry. For every staining, a histological control (staining without first antibody) was included. The procedure for immunohistochemistry was as

follows. Paraffin tissue sections were deparaffinized according to 5.16.1. After dewaxing, the samples were rehydrated with increasing concentrations of ethanol: 100%, 95%, 90%, 70%, 50%, and 30%, respectively, for 5min each, and a final incubation in distilled water for 10 seconds. To unmask the antigens, a microwave citrate antigen retrieval procedure was used. The tissue samples were submerged in freshly prepared citrate buffer (10 mM, pH 6.0) and heated in a microwave oven 2 times for 7 minutes each. Afterwards the samples were cold down at room temperature for 30 min and washed with PBS, 2 times for 5 min. To block endogenous peroxidase activity, the samples were further incubated in 15% H_2O_2 in the dark for 15 min and washed 3 times for 5 min each in PBS. To block unspecific binding sites, the samples were incubated for 30 min in 3% BSA in 0.1%Tween in a dark humid chamber. To ensure the solution stays on the tissue, the samples were surrounded by a circle with a hydrophobic barrier pen (Dako Pen REF S2002). A further blocking step was performed by incubation with the Avidin /Biotin blocking Kit.2 for 15min. Afterwards, the avidin solution was discarded and the samples incubated for additional 15 minutes with a biotin solution.

The first antibody solutions were prepared in 0.3% BSA / 0.1%Tween. The antibody concentrations used are summarized in Table 22. All incubations were performed overnight at 4°C in a humidified chamber. The next day, the samples were washed 3 times for 5 minutes each with 1x PBS buffer, and incubated for 30 minutes in a dark humid chamber with secondary antibodies, diluted to 1:500 in 2 ml PBS with 30 µl blocking serum. After this procedure the samples were washed 3 times for 5 minutes each with PBS buffer. For Signal amplification the VECTASTAIN Elite ABC Kit (Vector Laboratories, Burlingame, USA) was used following the manufacturer's instructions. To detect the bound antibodies, the samples were incubated in a dark humid chamber for 10min. with DAB (3, 3'-diaminobenzidine) Peroxidase substrate kit, later on the samples were washed for 10 min. with tap running water. The positive signals were identified by a brown color. The tissue sections were counterstained with 5% Mayer solution in water for 90 seconds, and washed for 10 minutes with running tap water. After the staining treatment, the samples were rehydrated gradually in organic solvent starting from 5 seconds incubation in 70%, 80%, 90% ethanol and finishing with an incubation of 3 min in Roti-Histol. After this procedure, the samples were covered with a cover glass slide and fixed with Entellan.

Table 22: Antibodies for immunohistochemistry

Antigen	Used dilution
CHOP	1:250
CEBP/δ	1:100
HNF1	1:100
HNF4α	1:500
Ly-6G/6C	1:100

5.20 **Immunofluorescence analysis of Trb3 expression**

For detection of Trb3 by immunofluorescence 5 µm liver sections were deparaffinized and rehydrated as described above. Afterwards, unspecific binding sites were blocked by incubation with 3% BSA / 0.1% Tween®20 in PBS for 30 min at room temperature. After removing the blocking solution, the sections were incubated overnight at 4°C with anti Trb3 polyclonal antibodies (ST1032, Merck-Millipore, Darmstadt, Germany) at a 1:100 dilution in BSA 0.3% / 0.1% Tween®20 in PBS. Subsequently, the antibody solution was removed and samples were washed three times for 10 min with PBS at room temperature. Afterwards, the samples were incubated for 1h at room temperature with secondary antibodies labeled with Alexa 555 (Life Technologies, Karlsruhe, Germany) at 1:100 dilution in BSA 0.3% / 0.1% Tween®20 in PBS. After removing the secondary antibody solutions, the samples were washed three times for 10 min with PBS, and incubated with 4`,6-diamidino-2-phenylindole (DAPI, Life Technologies, Karlsruhe, Germany) at 0.5 ng/ml for 30 min at room temperature, covered with a glass slide using FluoReserve reagent (Calbiochem-Merck, Darmstadt, Germany) and allowed to air dry for 30 min. The tissues were examined on an Olympus FV-1000 confocal microscope (Olympus, Hamburg, Germany). The excitation and emission wavelengths were used as specified by the manufacturer. The colors assigned to Trb3 and DAPI were red and blue respectively.

6 Results

6.1 Induction of acute liver damage by CCl_4

To identify the transcriptional regulatory networks at early and late time points during acute liver damage and regeneration, a mouse model of CCl_4-induced damage was chosen. For this purpose, male C57B6N mice received a single dose of 1.6 g/kg CCl_4 or control vehicle (olive oil). Blood and liver tissue samples were collected at early (2h and 8h) and late time points (day 1, 2, 4, 6, 8 and 16). For each time point five mice were used. Control and vehicle treated livers were of smooth appearance and with intense red color due to the high vascularization of this organ. In CCl_4 treaded livers, white puncta appeared between day 1 and day 2 after CCl_4 administration which reflects macroscopic features of tissue damage. A representative picture of the macroscopic morphology of control and CCl_4 treated liver (day 1) is shown in Fig. 11.

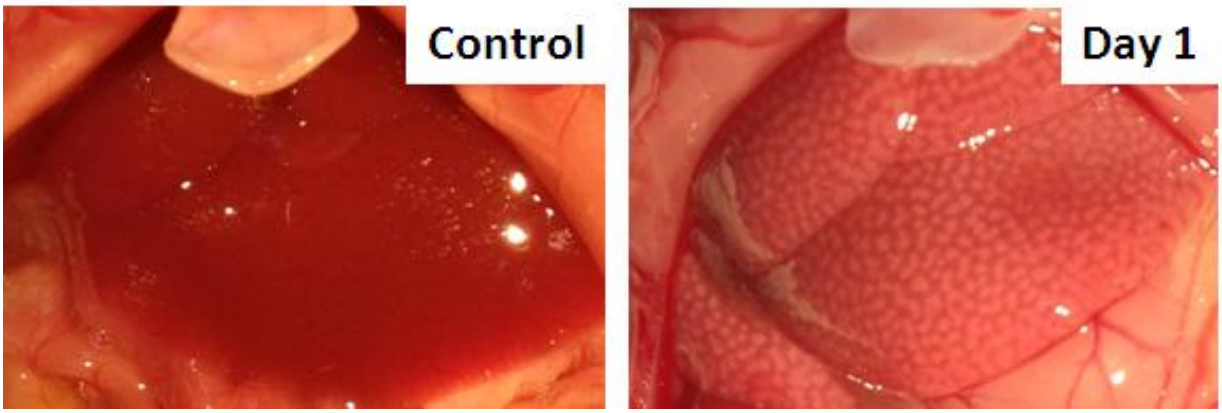

Figure 11: Macroscopical changes induced by an acute injection of CCl_4 (1.6 g/kg). Control mouse liver has a smooth appearance and intense red coloration. At day 1 after CCl_4 1.6 g/kg treatment extensive white puncta were observed throughout the entire organ, indicating extensive tissue injury. These puncta were still visible by day 2 and were almost completely absent by day 4 (not shown). Representative pictures of 5 mice per condition.

Microscopic assessment of liver damage was assessed by H&E stainings of paraffin embedded liver sections. Already 8h after CCl_4 injection, a differential staining pattern was observed around central veins (Fig 12), while clear tissue injury was observed at days 1 and 2 after CCl_4 administration, which was not only reflected by a weaker coloring of eosin in the

cytoplasm, but also by a clear disappearance of hepatocyte nuclei (Fig 12). The location of the injury is well documented to coincide with the zonal expression of Cyp2E1, which is expressed in pericentral hepatocytes [62] and metabolizes CCl_4 to its highly reactive intermediaries that cause hepatotoxicity [17]. At day 4, these dead cell areas were almost completely absent. However a clear cellular infiltration was observed around central veins, which reflects the regeneration process due to hepatocyte proliferation and the well-documented inflammatory reaction which is needed for this response [47, 63].

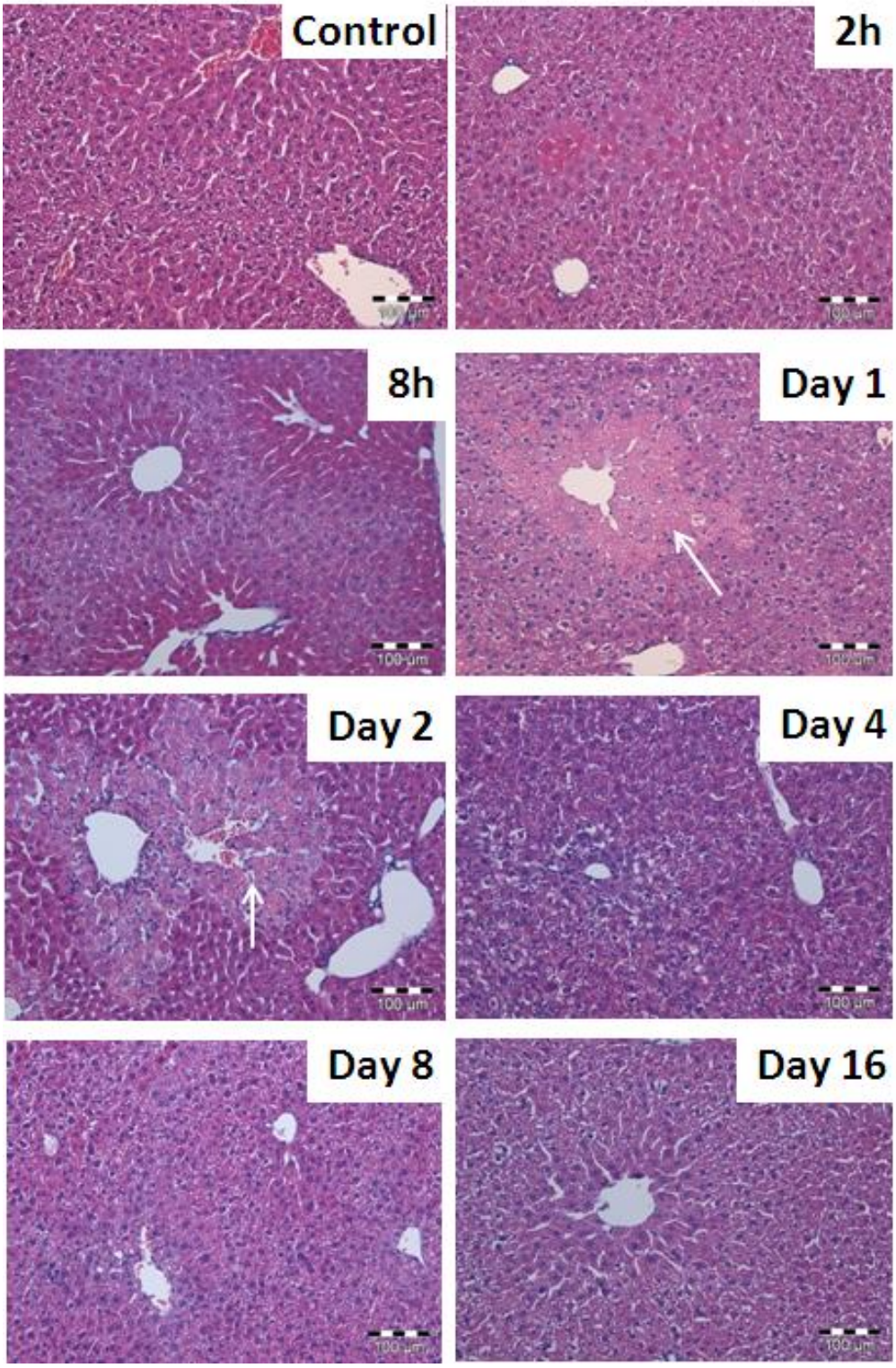

Figure 12: Histological examination of liver damage by H&E staining. Paraffin embedded liver sections stained with H&E were examined under bright light microscopy (100X magnification). The well-documented centrilobular dead cell areas were clearly identified at day 1 and day 2 after CCl_4 administration (with arrows). At day 4, these injuries were completely closed, and intense infiltration could be observed near central veins. By day 8 a full recovery was observed. Scale bars represent 100 µm.

To accurately determine the extent of liver damage at the histological level, the dead cell areas were quantified as described in the methods section 5.18. This quantification indicated a transient tissue damage at days 1and 2 with about 25% of liver lobule injury (Fig 13). At later time points, these dead cell areas were completely removed, and the lobules reached a normal histological pattern by day 8, consistent with previous reports [47].

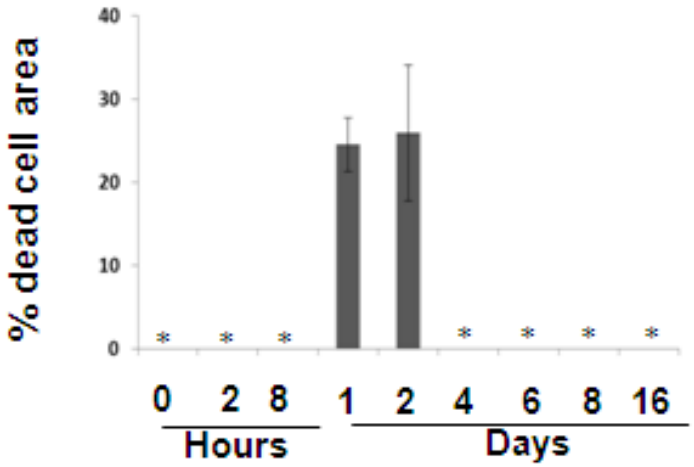

Figure 13: Quantification of dead cell areas in mouse liver after CCl_4 administration. The extent of tissue damage was assessed by quantification of the dead cell areas as described in methods. The quantification revealed a tissue injury of about 25% at days 1 and 2. At all other time points, no dead cell areas were observed. The bars are the mean values of three mice per time point. Error bars indicate standard error. * no detectable dead cell area.

A further measurement of liver damage was performed by quantification of the release of liver transaminases GOT and GPT into the bloodstream. Consistent with the dead cell area quantification, the maximum activity of both GOT and GPT was observed at days 1 and 2 after CCl_4 administration (Fig 14). However, this analysis was more sensitive than quantification of dead cell areas, because a significant increase of both GOT and GPT was detected already 2h after CCl_4 administration (Fig 14). Consistent with previous reports [47] the levels of transaminase activity in plasma returned to normal at day 4, which correlates with the regeneration observed by histological examination (Fig 14). Control (vehicle) did not result in detectable GOT or GPT release.

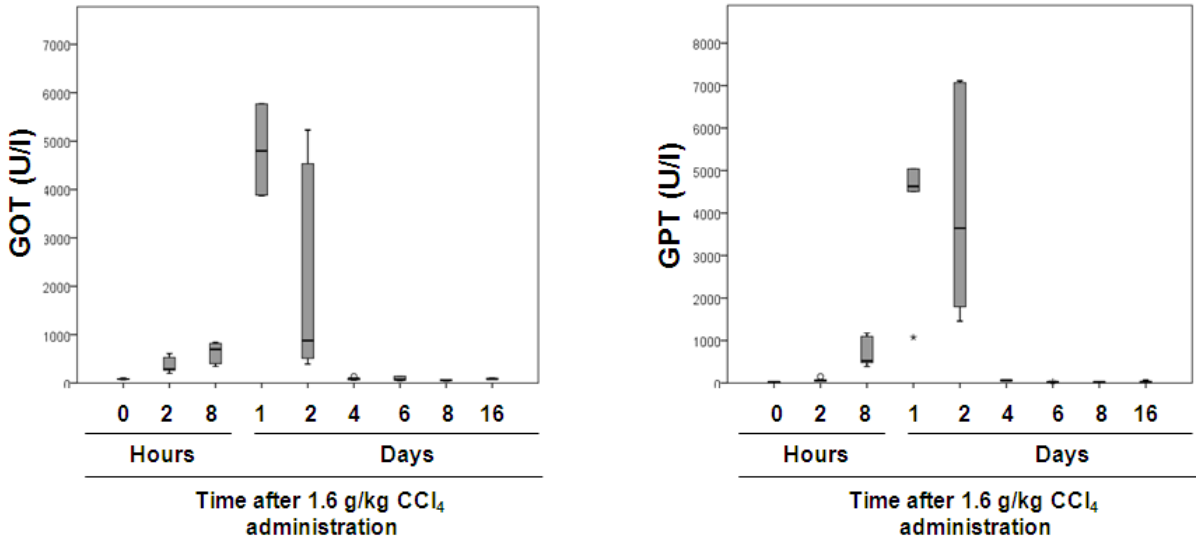

Figure 14: Plasma transaminase activity after CCl_4 administration. At the indicated time points, blood was collected from the heart and the activity of the liver transaminases GOT and GPT in plasma were analyzed as described in methods. Increased GOT and GPT activities were observed as early as 2h after CCl_4 administration. Consistent with the histological analyses, a peak in GOT and GPT was observed at days 1 and 2 after CCl_4 injection. The horizontal line in the middle of a box shows the median of the sample. The edges of a box mark the 25th and 75th percentiles. The whiskers show the range of values that fall within 1.5 box-lengths. Values >1.5 box-lengths from the 25th or 75th percentiles are marked by a dot. Data was generated using 5 mice per time point.

These results indicate that a robust and reproducible experimental setup of acute liver damage and regeneration was achieved, which was well suited for further transcriptomics analyses.

6.2 Affymetrix gene array analysis of CCl_4-induced liver damage

To obtain an unbiased overview of CCl_4-induced gene expression alterations, RNA was isolated from the livers of 5 independent mice at each time point (2h to 16 days) and analysed with whole-genome Affymetrix 430 2.0 gene arrays. The expression levels at each time after CCl_4 or vehicle (olive oil) treatment were compared to those of normal, healthy liver. The analysis detected 1, 469 genes at least 2-fold deregulated ($p<0.05$; FDR adjusted) (Godoy et al 2013, in revision; Campos et al 2013, in revision). Principal component analysis indicated that a good clustering of gene expression was obtained for each time point after CCl_4 administration (Fig 15). This analysis also revealed a quick transcriptional response whereby samples at 2h clearly deviated from control liver in the principal component space (Fig 15).

This time-resolved transcriptional response continued deviating from healthy liver until day 1 (Fig 15). The samples from day 2 onwards progressively moved towards the reference state, and largely overlapped with control liver at the latest time points (days 6 to 16) (Fig 15). This time-dependent motion in the principal component space seems to reflect a quick response upon CCl_4 exposure and infliction of liver damage between 2h and day 1, followed by a regeneration process from day 2 on. Importantly, the deregulated genes observed in liver tissue after CCl_4 administration are expressed almost exclusively in hepatocytes, as demonstrated by the analysis of freshly isolated hepatocytes from mouse livers at days 1 and 3 after CCl_4 injection (Fig 15). Therefore, further bioinformatics analyses would allow a direct assessment of transcriptional responses mostly in hepatocytes.

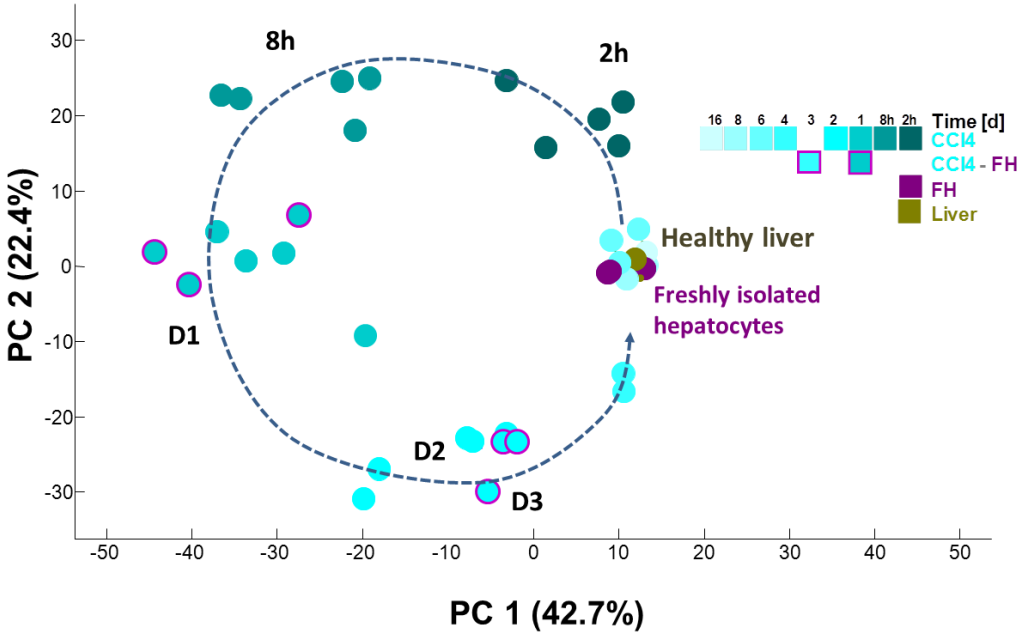

Figure 15: Principal Component Analysis of gene expression in mouse liver and in hepatocytes after CCl_4 administration. The graph represents the coordinates of the principal component 1 (PC1) and principal component 2 (PC2), which account for 42.7% and 22.4% of the deregulated genes in the transcriptional response after CCl_4, respectively. The position of the samples of 2h, 8h, day 1 and day 2 after CCl_4 injection indicated that a robust time-dependent clustering was obtained with 5 independent samples per time point. In addition, transcriptional patterns of freshly isolated hepatocytes from livers treated with CCl_4 for 1 or 3 days (circles with purple borders) clustered closely with those of whole liver tissue at the corresponding time points, indicating that the transcriptional response observed in liver homogenates largely reflects expression in hepatocytes and not in non-parenchymal cells.

A heatmap analysis of all 1,469 differentially expressed genes revealed a complex pattern of up and downregulated genes (Fig 16), with a large number of genes deregulated over 5-fold (Fig 16). The heatmap also indicated that the strongest gene deregulation occurs between 2h and day 2 after CCl_4 administration, in line with the pattern in the principal component space of Figure 15.

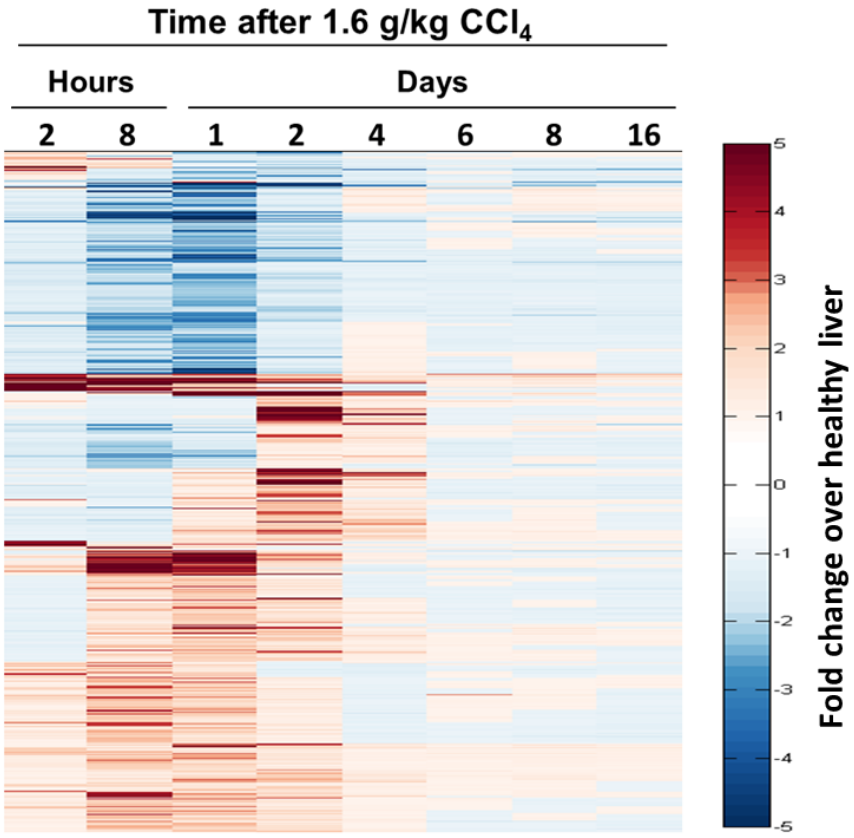

Figure 16: Heat map representation of deregulated genes in mouse liver after CCl_4 administration. The color code indicates fold of change over healthy liver. The strongest transcriptional alterations are observed between 2h and 4 days after CCl_4 injection.

6.3 MAPK and inflammation-associated signaling pathways are induced early upon CCl_4 administration, followed by a cell-cycle response

The strong induction of gene expression observed between 2h and day 4 after CCl_4 administration suggested that signal transduction pathways were activated during the early phase of tissue injury. To obtain a more precise assessment of the pathways activated, protein extracts from healthy and CCl_4-treated mouse liver at 2h, 8h and days 1, 2 and 4 were analyzed by western blot. Phosphorylation of STAT3, JNK and ERK were strongly induced at 2h after CCl_4 administration (Fig 17). While JNK phosphorylation returned to basal levels after 8h, STAT3 remained phosphorylated above control levels up to 2 days after CCl_4 administration (Fig 17). ERK phosphorylation showed a biphasic behavior, with peaks at 2h and at day 2 after CCl_4 injection (Fig 17). A similar biphasic pattern was observed for Akt phosphorylation, although its maximal activation was observed at day 1 (Fig 17). These signaling patterns are consistent with previous reports [63-65] and indicate that the liver quickly starts processing information in the form of signal transduction and gene expression regulation upon exposure to the hepatotoxicant CCl_4.

A well-documented event in this model of acute liver damage is the induction of hepatocyte proliferation which is needed to restore the loss of parenchyma observed in Fig. 12 [47]. Analysis of PCNA (proliferating cell nuclear antigen) revealed a strong proliferation response between day 2 and day 4 after CCl_4 administration (Fig 17). This result is also consistent with previous reports, which indicate that the hepatocyte proliferation response occurs between 1 and 3 days after CCl_4-induced liver damage [47].

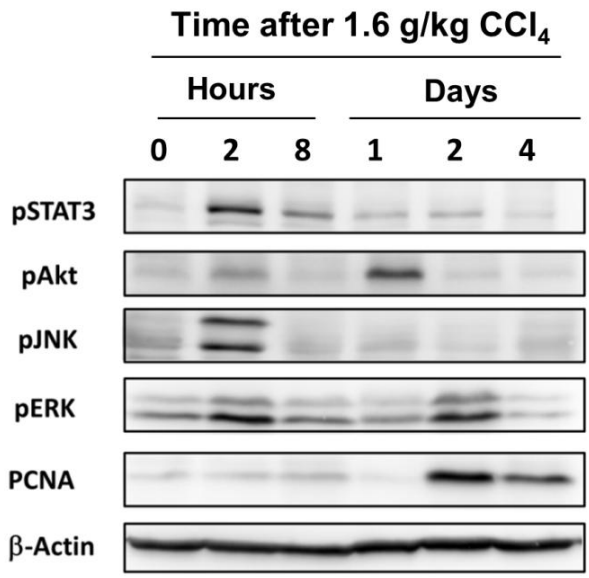

Figure 17: Western blot analysis of signal transduction pathways at early and late points after CCl_4 induced liver damage. Protein extracts from mouse liver tissue after CCl_4 injection were used for analysis of phosphorylation of signal transduction proteins. The phosphorylation of MAPK proteins JNK and Erk1/2, and also the inflammation-associated STAT3 protein were observed at 2h after CCl_4 injection, indicating that several signaling pathways were activated early after CCl_4 injection. This early signaling activity was consistent with the strong gene expression alterations observed at 2h after CCl_4 administration (Fig 16). The phosphorylation of Akt also occurred at 2h however a second peak with a stronger signal was observed at day 1. The proliferation marker PCNA was observed upregulated at days 2 and 4. β-actin was used as loading control. The results are representative of 5 independent mice per time point and condition.

These results indicated that most signal transduction events are probably taking place very early upon CCl_4 administration. Thus, they may be responsible for the strong initial wave of gene expression observed by gene array. However, it is not possible to accurately link the observed signaling pathways to the complex transcriptional response identified by gene array. Such causal associations require a more refined analysis of time-resolved gene expression patterns. Therefore, a time-resolved gene clustering approach was undertaken.

6.4 Time-dependent fuzzy clustering of gene expression in liver upon CCl_4-induced hepatotoxicity

The clear clustering between each biological replica (i.e. mouse liver) offers good conditions to study time-dependent gene clusters. For this purpose, the gene expression values were scaled between their respective absolute temporal extreme values (i.e. maximal or minimal)

and subsequently clustered using the fuzzy-c-means algorithm [66]. This analysis revealed seven distinct time-dependent gene clusters (Fig. 18), of which 1, 2, 3, 5 and 6 included upregulated genes, whereas clusters 4 and 7 contained downregulated genes (Fig 18). Only eight out of the 1,469 genes could not be fitted into any of the identified clusters, indicating that the clusters contained the vast majority of deregulated genes.

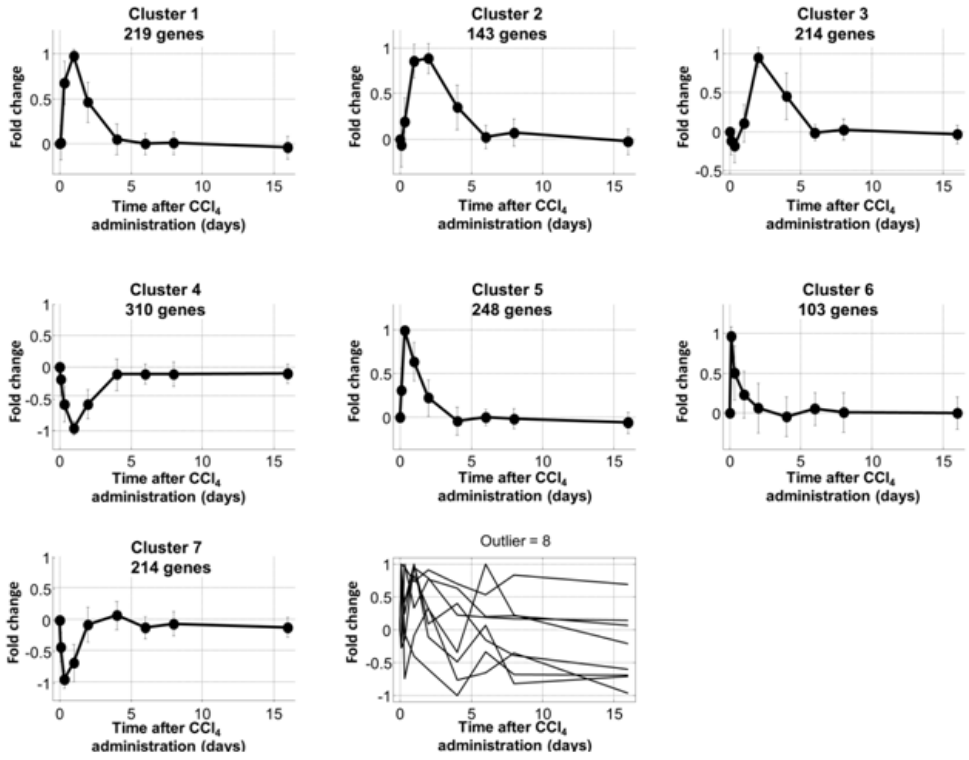

Figure 18: Time resolved clustering of deregulated genes in mouse liver upon CCl_4 administration. Seven time-dependent gene clusters were generated by the fuzzy-c-means algorithm. Graphs indicate the average expression of the mean-scaled expression value for all genes in each cluster.

A heatmap representation of the time-dependent gene clusters showed that the strongest upregulation occurred in clusters 3 and 6, which peaked at day 2 and 2h respectively, whereas the strongest downregulations were observed on cluster 4, which peaked at day 1 (Fig 19). This analysis suggested that the early transcriptional response observed at 2h involves mostly upregulated genes, which includes some of the strongest induced genes in this model.

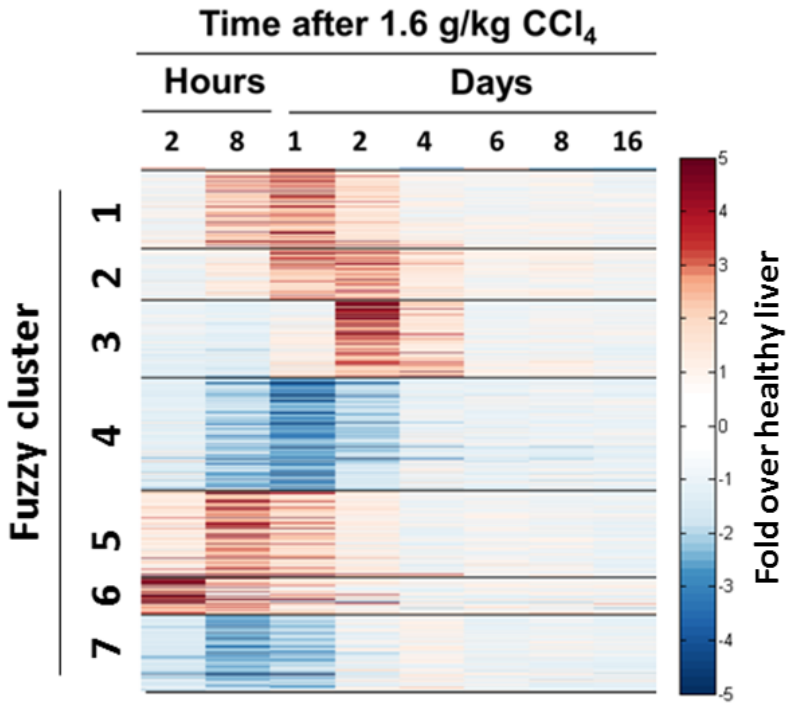

Figure 19: Heat map representation of the time-dependent fuzzy gene clusters of deregulated genes in mouse liver upon CCl_4 administration. The color code indicates fold of change over healthy liver. The strongest upregulations were observed on clusters 3 and 6, which peak at day 2 and 2h respectively.

Although the mere number of deregulated genes, clustering and the intensities of gene deregulation did not indicate per se any biological meaning, the well-established time-dependent gene clusters provided the basis for a more precise dissection of further bioinformatics analyses, to extract biological motifs overrepresented at different time points.

6.5 Gene ontology and KEGG analyses identify biological motifs of proliferation and metabolism

One of the most robust methods for extracting biologically meaningful context from a gene list is gene ontology (GO, http://www.geneontology.org/), an expert curated database assigning genes to various functional categories [67]. The GO database consists of three main categories: biological process (BP), molecular function (MF) and cellular component (CC).

Each main category contains multiple subcategories with a subset of genes associated to more specific terms or functions. For example, within “biological process” (GO:0008150), the main category “single-organism cellular process” (GO:004763) contains the subcategory “cell cycle” (GO:0007049), which contains several sub-terms such as M-phase, nuclear division, etc. (http://www.geneontology.org/). Statistical tests such as Fisher’s exact test can be used to assess the overrepresentation or enrichment of deregulated genes within GO subsets. This procedure was used to identify biological motifs enriched within the time-dependent gene clusters described in figure 20.

Analysis of GO “biological process” revealed a high enrichment of cell cycle-associated terms in cluster 3 (Fig 20), such as “cell cycle” (p=5.66E-43), “mitosis” (1.45E-41) and “M-phase” (p=5.91E-43) (Fig 20). Cluster 3 contains upregulated genes which are induced within day 1 and day 4, and reach their maximum at day 2 (Figs 19 and 20). The overrepresentation of cell cycle-associated terms within cluster 3 is consistent with the fact that a strong hepatocyte proliferation response is induced as a consequence of the initial injury caused by CCl_4 [47], and also with the proliferative markers observed in Fig 17 (PCNA western blot).

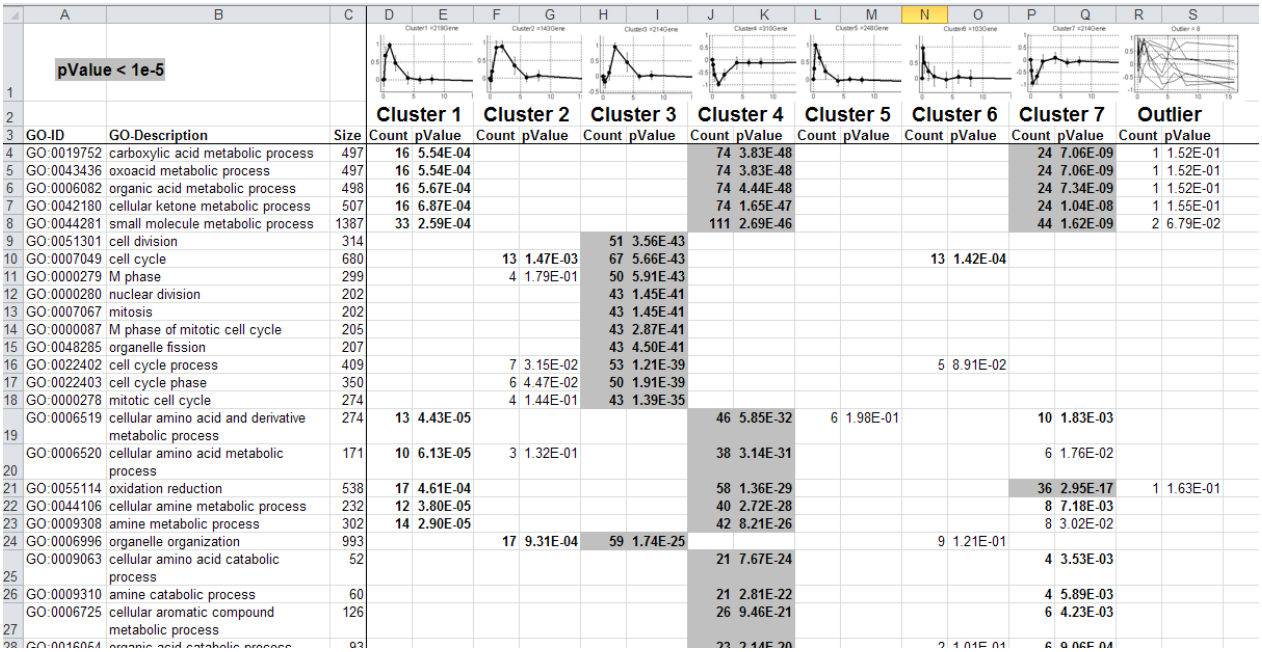

	A	B	C	D	E	F	G	H	I	J	K	L	M	N	O	P	Q	R	S
1	pValue < 1e-5																		
2				Cluster 1		Cluster 2		Cluster 3		Cluster 4		Cluster 5		Cluster 6		Cluster 7		Outlier	
3	GO-ID	GO-Description	Size	Count	pValue	Count	pValue	Count	pValue	Count	pValue	Count	pValue	Count	pValue	Count	pValue	Count	pValue
4	GO:0019752	carboxylic acid metabolic process	497	16	5.54E-04					74	3.83E-48					24	7.06E-09	1	1.52E-01
5	GO:0043436	oxoacid metabolic process	497	16	5.54E-04					74	3.83E-48					24	7.06E-09	1	1.52E-01
6	GO:0006082	organic acid metabolic process	498	16	5.67E-04					74	4.44E-48					24	7.34E-09	1	1.52E-01
7	GO:0042180	cellular ketone metabolic process	507	16	6.87E-04					74	1.65E-47					24	1.04E-08	1	1.55E-01
8	GO:0044281	small molecule metabolic process	1387	33	2.59E-04					111	2.69E-46					44	1.62E-09	2	6.79E-02
9	GO:0051301	cell division	314					51	3.56E-43										
10	GO:0007049	cell cycle	680			13	1.47E-03	67	5.66E-43					13	1.42E-04				
11	GO:0000279	M phase	299			4	1.79E-01	50	5.91E-43										
12	GO:0000280	nuclear division	202					43	1.45E-41										
13	GO:0007067	mitosis	202					43	1.45E-41										
14	GO:0000087	M phase of mitotic cell cycle	205					43	2.87E-41										
15	GO:0048285	organelle fission	207					43	4.50E-41										
16	GO:0022402	cell cycle process	409			7	3.15E-02	53	1.21E-39					5	8.91E-02				
17	GO:0022403	cell cycle phase	350			6	4.47E-02	50	1.91E-39										
18	GO:0000278	mitotic cell cycle	274			4	1.44E-01	43	1.39E-35										
19	GO:0006519	cellular amino acid and derivative metabolic process	274	13	4.43E-05					46	5.85E-32	6	1.98E-01			10	1.83E-03		
20	GO:0006520	cellular amino acid metabolic process	171	10	6.13E-05	3	1.32E-01			38	3.14E-31					6	1.76E-02		
21	GO:0055114	oxidation reduction	538	17	4.61E-04					58	1.36E-29					36	2.95E-17	1	1.63E-01
22	GO:0044106	cellular amine metabolic process	232	12	3.80E-05					40	2.72E-28					8	7.18E-03		
23	GO:0009308	amine metabolic process	302	14	2.90E-05					42	8.21E-26					8	3.02E-02		
24	GO:0006996	organelle organization	993			17	9.31E-04	59	1.74E-25					9	1.21E-01				
25	GO:0009063	cellular amino acid catabolic process	52							21	7.67E-24					4	3.53E-03		
26	GO:0009310	amine catabolic process	60							21	2.81E-22					4	5.89E-03		
27	GO:0006725	cellular aromatic compound metabolic process	126							26	9.46E-21					6	4.23E-03		
28	GO:0016054	organic acid catabolic process	93							23	2.14E-20			2	1.01E-01	6	9.06E-04		

Figure 20: Analysis of GO "biological process" overrepresentation in time-dependent gene clusters. The figure shows a snapshot of the results obtained for overrepresentation of GO "biological processes". The strongest overrepresentation of GO motifs were observed in clusters containing down regulated genes (cluster 4 and 7), which showed a high enrichment of GO terms associated with metabolism, and in cluster 3 which contained a strong overrepresentation of cell cycle-associated GO terms. Gray colored boxes indicate p-value<10^{-5}.

Another interesting observation from the GO analysis was that both clusters of downregulated genes (clusters 4 and 7) were highly enriched in metabolism associated GO terms, including "small molecule metabolic process" (p=2.69E-46), "carboxylic acid metabolic process" (p=3.83E-48) and "oxoacid metabolic process" (3.83E-48) (Fig 20). These results indicated that a dramatic loss of metabolic functions takes place during the process of liver damage and regeneration. However, the metabolism-associated GO terms in this analysis were too general for a precise characterization of the metabolic pathways repressed or lost after CCl_4 administration. Therefore, further GO enrichment analyses were performed.

Similar to the previous results, analysis of GO "molecular function" showed a high enrichment of metabolism terms in downregulated gene clusters (cluster 4 and 7) (Fig 21). However, the function-associated GO terms were more indicative of specific metabolic functions. For example, the GO terms "oxidoreductase activity" (p=9.27E-32), "heme binding" (p=1.96E-12) and "iron ion binding" (p=1.61E-14) suggested that enzymes which contain heme groups are among the most prominent group of downregualted genes. In the

liver, such heme-containing proteins include the cytochrome P450 enzymes [5], which would indicate that this metabolic component of liver function is one of the most severely affected by the process of damage and regeneration.

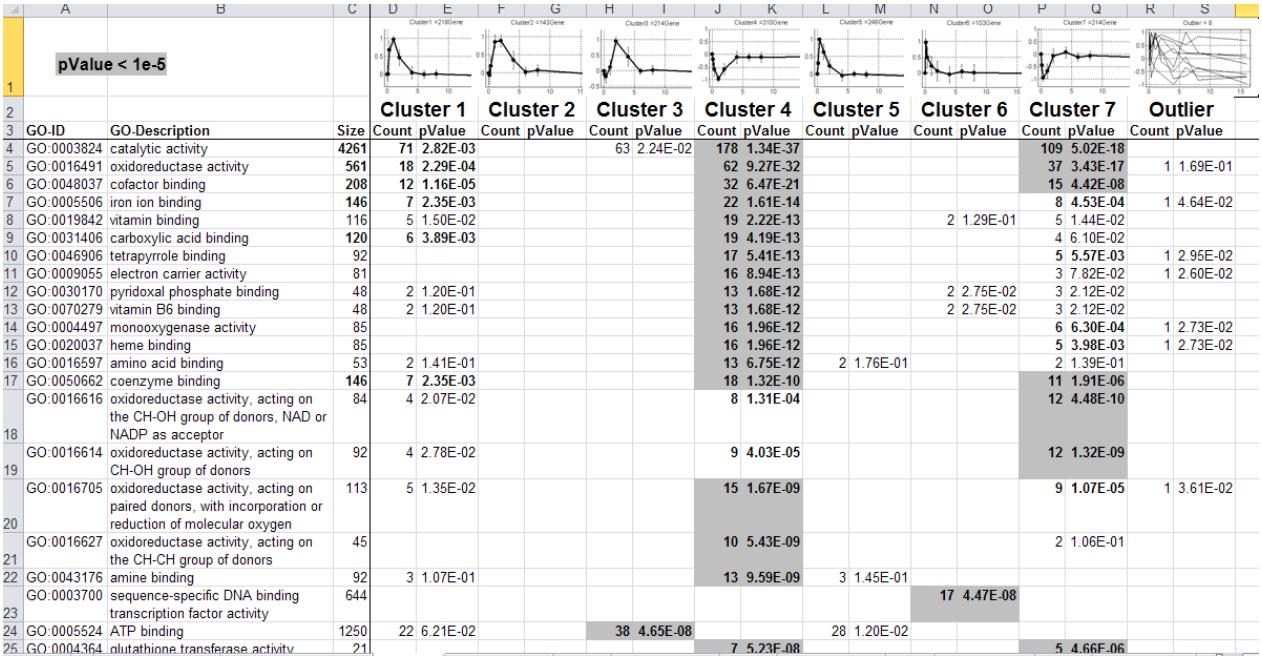

	A	B	C	D	E	F	G	H	I	J	K	L	M	N	O	P	Q	R	S
1	pValue < 1e-5																		
2				Cluster 1		Cluster 2		Cluster 3		Cluster 4		Cluster 5		Cluster 6		Cluster 7		Outlier	
3	GO-ID	GO-Description	Size	Count	pValue	Count	pValue	Count	pValue	Count	pValue	Count	pValue	Count	pValue	Count	pValue	Count	pValue
4	GO:0003824	catalytic activity	4261	71	2.82E-03			63	2.24E-02	178	1.34E-37					109	5.02E-18		
5	GO:0016491	oxidoreductase activity	561	18	2.29E-04					62	9.27E-32					37	3.43E-17	1	1.69E-01
6	GO:0048037	cofactor binding	208	12	1.16E-05					32	6.47E-21					15	4.42E-08		
7	GO:0005506	iron ion binding	146	7	2.35E-03					22	1.61E-14					8	4.53E-04	1	4.64E-02
8	GO:0019842	vitamin binding	116	5	1.50E-02					19	2.22E-13			2	1.29E-01	5	1.44E-02		
9	GO:0031406	carboxylic acid binding	120	6	3.89E-03					19	4.19E-13					4	6.10E-02		
10	GO:0046906	tetrapyrrole binding	92							17	5.41E-13					5	5.57E-03	1	2.95E-02
11	GO:0009055	electron carrier activity	81							16	8.94E-13					3	7.82E-02	1	2.60E-02
12	GO:0030170	pyridoxal phosphate binding	48	2	1.20E-01					13	1.68E-12			2	2.75E-02	3	2.12E-02		
13	GO:0070279	vitamin B6 binding	48	2	1.20E-01					13	1.68E-12			2	2.75E-02	3	2.12E-02		
14	GO:0004497	monooxygenase activity	85							16	1.96E-12					6	6.30E-04	1	2.73E-02
15	GO:0020037	heme binding	85							16	1.96E-12					5	3.98E-03	1	2.73E-02
16	GO:0016597	amino acid binding	53	2	1.41E-01					13	6.75E-12	2	1.76E-01			2	1.39E-01		
17	GO:0050662	coenzyme binding	146	7	2.35E-03					18	1.32E-10					11	1.91E-06		
18	GO:0016616	oxidoreductase activity, acting on the CH-OH group of donors, NAD or NADP as acceptor	84	4	2.07E-02					8	1.31E-04					12	4.48E-10		
19	GO:0016614	oxidoreductase activity, acting on CH-OH group of donors	92	4	2.78E-02					9	4.03E-05					12	1.32E-09		
20	GO:0016705	oxidoreductase activity, acting on paired donors, with incorporation or reduction of molecular oxygen	113	5	1.35E-02					15	1.67E-09					9	1.07E-05	1	3.61E-02
21	GO:0016627	oxidoreductase activity, acting on the CH-CH group of donors	45							10	5.43E-09					2	1.06E-01		
22	GO:0043176	amine binding	92	3	1.07E-01					13	9.59E-09	3	1.45E-01						
23	GO:0003700	sequence-specific DNA binding transcription factor activity	644											17	4.47E-08				
24	GO:0005524	ATP binding	1250	22	6.21E-02			38	4.65E-08			28	1.20E-02						
25	GO:0004364	glutathione transferase activity	21							7	5.23E-08					5	4.66E-06		

Figure 21: Analysis of GO "molecular function" overrepresentation in time-dependent gene clusters. The figure shows a snapshot of the results obtained for overrepresentation of GO "molecular function". Similar as in "biological process", the strongest overrepresentation of GO motifs were observed in clusters containing down regulated genes (cluster 4 and 7), which showed a high enrichment of GO terms associated with enzyme activity. Cluster 6 contained a strong overrepresentation of sequence-specific-associated GO terms. Gray colored boxes indicated p-value<10^{-5}.

Analysis of the GO "cell component" terms supported the previously generated hypothesis of cell proliferation and loss of metabolic functions (Fig 22). In this case, proliferation-associated terms such as "chromosome" (p=2.14E-36), "kinetochore" (p=4.01E-15) and "condensed chromosome" (p=1.15E-13) were strongly enriched in cluster 3, whereas metabolism-associated terms such as "mitochondrion" (p=4.22E-18) and "microsome" (p=1.88E-15) were highly overrepresented in downregulated genes (cluster 4 and 7).

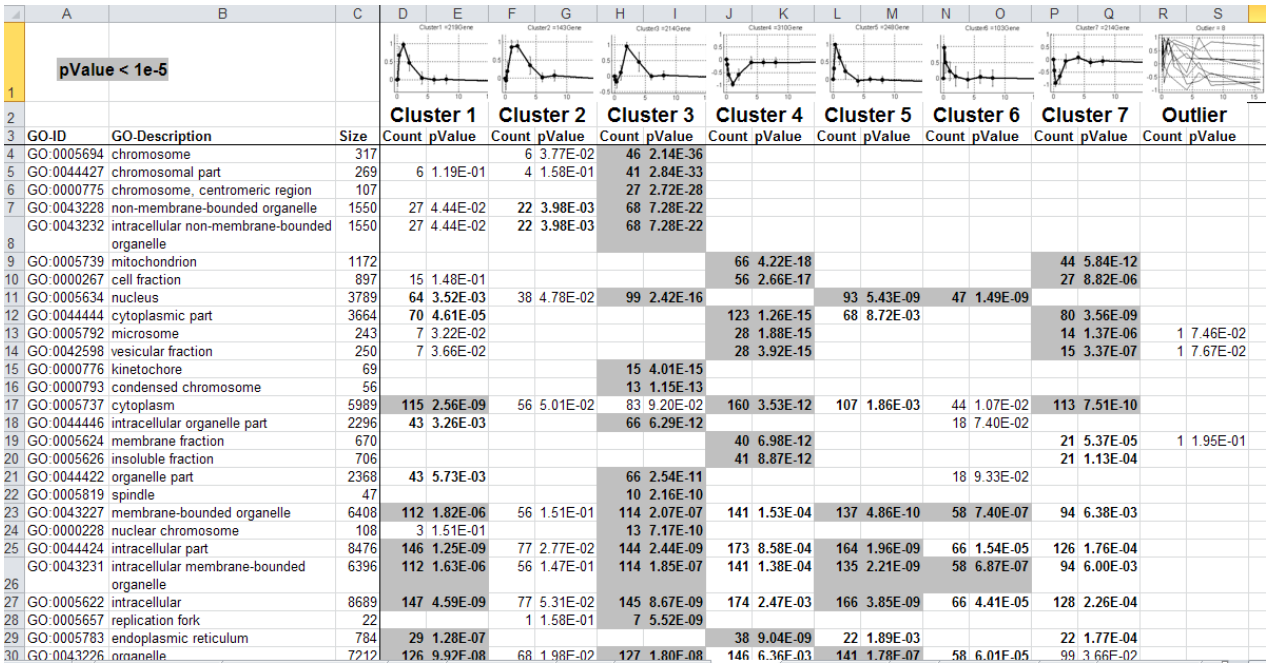

	A	B	C	D	E	F	G	H	I	J	K	L	M	N	O	P	Q	R	S
1	pValue < 1e-5																		
2				Cluster 1		Cluster 2		Cluster 3		Cluster 4		Cluster 5		Cluster 6		Cluster 7		Outlier	
3	GO-ID	GO-Description	Size	Count	pValue	Count	pValue	Count	pValue	Count	pValue	Count	pValue	Count	pValue	Count	pValue	Count	pValue
4	GO:0005694	chromosome	317			6	3.77E-02	46	2.14E-36										
5	GO:0044427	chromosomal part	269	6	1.19E-01	4	1.58E-01	41	2.84E-33										
6	GO:0000775	chromosome, centromeric region	107					27	2.72E-28										
7	GO:0043228	non-membrane-bounded organelle	1550	27	4.44E-02	22	3.98E-03	68	7.28E-22										
8	GO:0043232	intracellular non-membrane-bounded organelle	1550	27	4.44E-02	22	3.98E-03	68	7.28E-22										
9	GO:0005739	mitochondrion	1172							66	4.22E-18					44	5.84E-12		
10	GO:0000267	cell fraction	897	15	1.48E-01					56	2.66E-17					27	8.82E-06		
11	GO:0005634	nucleus	3789	64	3.52E-03	38	4.78E-02	99	2.42E-16			93	5.43E-09	47	1.49E-09				
12	GO:0044444	cytoplasmic part	3664	70	4.61E-05					123	1.26E-15	68	8.72E-03			80	3.56E-09		
13	GO:0005792	microsome	243	7	3.22E-02					28	1.88E-15					14	1.37E-06	1	7.46E-02
14	GO:0042598	vesicular fraction	250	7	3.66E-02					28	3.92E-15					15	3.37E-07	1	7.67E-02
15	GO:0000776	kinetochore	69					15	4.01E-15										
16	GO:0000793	condensed chromosome	56					13	1.15E-13										
17	GO:0005737	cytoplasm	5989	115	2.56E-09	56	5.01E-02	83	9.20E-02	160	3.53E-12	107	1.86E-03	44	1.07E-02	113	7.51E-10		
18	GO:0044446	intracellular organelle part	2296	43	3.26E-03			66	6.29E-12					18	7.40E-02				
19	GO:0005624	membrane fraction	670							40	6.98E-12					21	5.37E-05	1	1.95E-01
20	GO:0005626	insoluble fraction	706							41	8.87E-12					21	1.13E-04		
21	GO:0044422	organelle part	2368	43	5.73E-03			66	2.54E-11					18	9.33E-02				
22	GO:0005819	spindle	47					10	2.16E-10										
23	GO:0043227	membrane-bounded organelle	6408	112	1.82E-06	56	1.51E-01	114	2.07E-07	141	1.53E-04	137	4.86E-10	58	7.40E-07	94	6.38E-03		
24	GO:0000228	nuclear chromosome	108	3	1.51E-01			13	7.17E-10										
25	GO:0044424	intracellular part	8476	146	1.25E-09	77	2.77E-02	144	2.44E-09	173	8.58E-04	164	1.96E-09	66	1.54E-05	126	1.76E-04		
26	GO:0043231	intracellular membrane-bounded organelle	6396	112	1.63E-06	56	1.47E-01	114	1.85E-07	141	1.38E-04	135	2.21E-09	58	6.87E-07	94	6.00E-03		
27	GO:0005622	intracellular	8689	147	4.59E-09	77	5.31E-02	145	8.67E-09	174	2.47E-03	166	3.85E-09	66	4.41E-05	128	2.26E-04		
28	GO:0005657	replication fork	22			1	1.58E-01	7	5.52E-09										
29	GO:0005783	endoplasmic reticulum	784	29	1.28E-07					38	9.04E-09	22	1.89E-03			22	1.77E-04		
30	GO:0043226	organelle	7212	126	9.92E-08	68	1.98E-02	127	1.80E-08	146	6.36E-03	141	1.78E-07	58	6.01E-05	99	3.66E-02		

Figure 22: Analysis of GO "cell component" overrepresentation in time-dependent gene clusters. The figure shows a snapshot of the results obtained for overrepresentation of GO "cell component". The strongest overrepresentation of GO motifs were observed in cluster 3, which showed a high enrichment of GO terms associated with nucleus, chromosomes and DNA, consistent with the strong proliferation response observed between days 2 and 4 (Fig 17, PCNA analysis). Clusters 4 and 7 were enriched in GO terms associated with mitochondria, consistent with the previously observed enrichment in metabolism on those clusters. Gray colored boxes indicated p-value<10^{-5}.

Another well-established approach for identification of biological motifs in gene array data is the Kyoto Encyclopedia of Genes and Genomes (KEGG http://www.genome.jp/kegg/) [68]. KEGG is a manually curated database which connects known information on molecular interactions networks, such as pathways and complexes, with databases such as GO [68]. Consistent with the previous results, analysis of KEGG pathway enrichment in the time-dependent gene clusters identified a regeneration (i.e. cell cycle) motif in cluster 3, including terms such as "DNA replication" (p=1.52E-15) and "cell cycle" (p=1.23E-13) (Fig 23). Also, metabolism-associated terms were found highly represented in downregulated gene clusters (cluster 4 and 7), including "metabolic pathways" (p=6.74E-7), but also more specific liver-metabolism associated terms, such as "metabolism of xenobiotics by cytochrome P450" (p=8.42E-11) and "drug metabolism-cytochrome P450" (p=5.08E-8) (Fig 23).

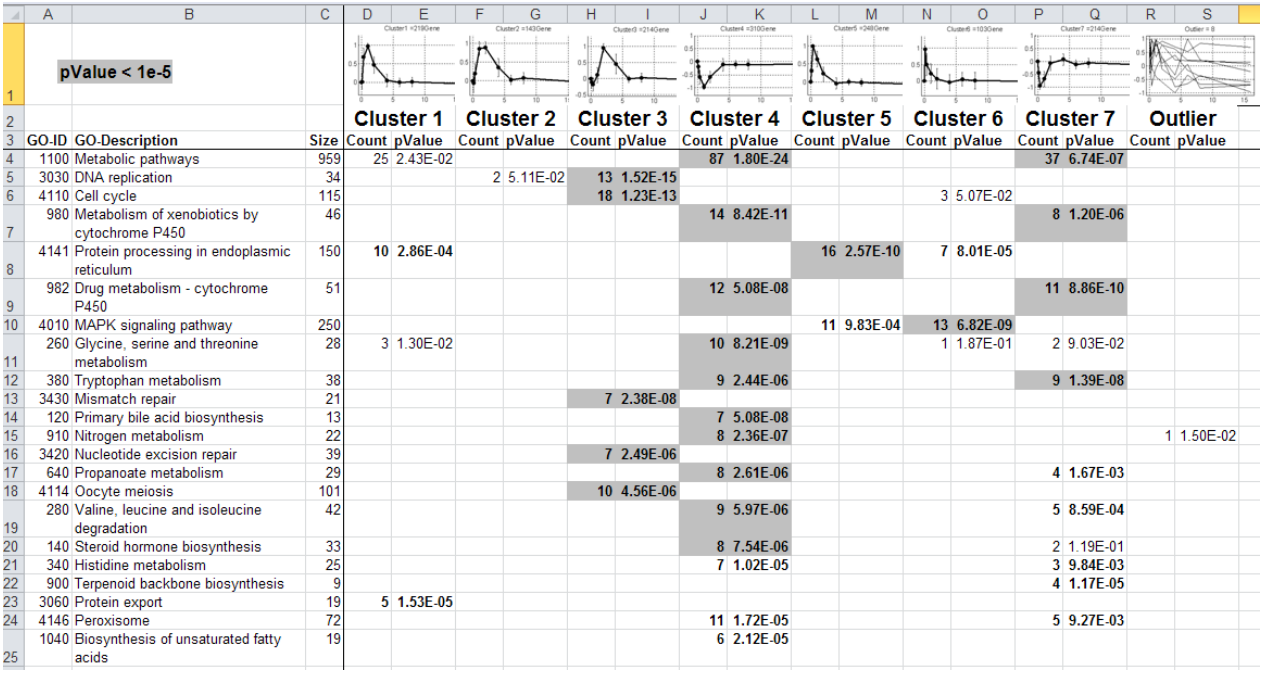

	A	B	C	D	E	F	G	H	I	J	K	L	M	N	O	P	Q	R	S
1	pValue < 1e-5																		
2				Cluster 1		Cluster 2		Cluster 3		Cluster 4		Cluster 5		Cluster 6		Cluster 7		Outlier	
3	GO-ID	GO-Description	Size	Count	pValue	Count	pValue	Count	pValue	Count	pValue	Count	pValue	Count	pValue	Count	pValue	Count	pValue
4	1100	Metabolic pathways	959	25	2.43E-02					87	1.80E-24					37	6.74E-07		
5	3030	DNA replication	34			2	5.11E-02	13	1.52E-15										
6	4110	Cell cycle	115					18	1.23E-13					3	5.07E-02				
7	980	Metabolism of xenobiotics by cytochrome P450	46							14	8.42E-11					8	1.20E-06		
8	4141	Protein processing in endoplasmic reticulum	150	10	2.86E-04							16	2.57E-10	7	8.01E-05				
9	982	Drug metabolism - cytochrome P450	51							12	5.08E-08					11	8.86E-10		
10	4010	MAPK signaling pathway	250									11	9.83E-04	13	6.82E-09				
11	260	Glycine, serine and threonine metabolism	28	3	1.30E-02					10	8.21E-09			1	1.87E-01	2	9.03E-02		
12	380	Tryptophan metabolism	38							9	2.44E-06					9	1.39E-08		
13	3430	Mismatch repair	21					7	2.38E-08										
14	120	Primary bile acid biosynthesis	13							7	5.08E-08								
15	910	Nitrogen metabolism	22							8	2.36E-07							1	1.50E-02
16	3420	Nucleotide excision repair	39					7	2.49E-06										
17	640	Propanoate metabolism	29							8	2.61E-06					4	1.67E-03		
18	4114	Oocyte meiosis	101					10	4.56E-06										
19	280	Valine, leucine and isoleucine degradation	42							9	5.97E-06					5	8.59E-04		
20	140	Steroid hormone biosynthesis	33							8	7.54E-06					2	1.19E-01		
21	340	Histidine metabolism	25							7	1.02E-05					3	9.84E-03		
22	900	Terpenoid backbone biosynthesis	9													4	1.17E-05		
23	3060	Protein export	19	5	1.53E-05														
24	4146	Peroxisome	72							11	1.72E-05					5	9.27E-03		
25	1040	Biosynthesis of unsaturated fatty acids	19							6	2.12E-05								

Figure 23: Analysis of KEGG pathways overrepresentation in time-dependent gene clusters. The figure shows a snapshot of the results obtained for overrepresentation of KEGG pathways. Similar as in "biological process", the strongest overrepresentations of KEGG pathways were observed in clusters containing down regulated genes (cluster 4 and 7), which showed a high enrichment of metabolic pathways. In cluster 3, a high enrichment of KEGG pathways associated with proliferation were observed, consistent with the strong proliferation response observed between days 2 and 4 (Fig 17, PCNA analysis). Cluster 6 contained a strong overrepresentation of the MAPK signaling pathway, consistent with the strong activation of MAPK signaling 2h after CCl_4 administration (Fig 17). Gray colored boxes indicated p-value<10^{-5}.

In conclusion, the timing of the overrepresented GO and KEGG terms cell-cycle (i.e. regeneration) were consistent with the analysis of proliferation markers (Fig 17, PCNA western blot) and with previous reports [47], indicating that the clustering approach selected accurately segregated biologically meaningful gene clusters. Furthermore, the GO and KEGG enrichment analysis on gene clusters identified a massive repression of metabolism associated genes.

6.6 Transcription factor binding site enrichment analysis identifies basic principles of transcriptional regulation after CCl_4 intoxication

With the advent of whole-genome sequencing and the cumulative knowledge on DNA sequences (or motifs) recognized by transcription factors [69, 70] it is nowadays possible to estimate the contribution of specific transcription factors to the regulation of gene clusters. Similar to the GO-term overrepresentation analysis, algorithms have been designed to search for overrepresented transcription factor binding sites (TFBS) within predefined sequences in gene promoters [67] . Using the PRIMA algorithm [71], an overrepresentation of TFBS in each time-dependent gene cluster was undertaken. The first remarkable feature of this analysis was that upregulated gene clusters seemed to contain a large number of overrepresented TFBS (Fig 24), whereas downregulated gene clusters seemed to be controlled by a more restricted number of transcription factors (Fig 24). Among the highest overrepresented TFBS in the upregulated gene clusters was E2F, which is consistent with the fact that upregulated genes were associated to cell cycle, and that E2F proteins play fundamental roles in cell cycle progression [72, 73].

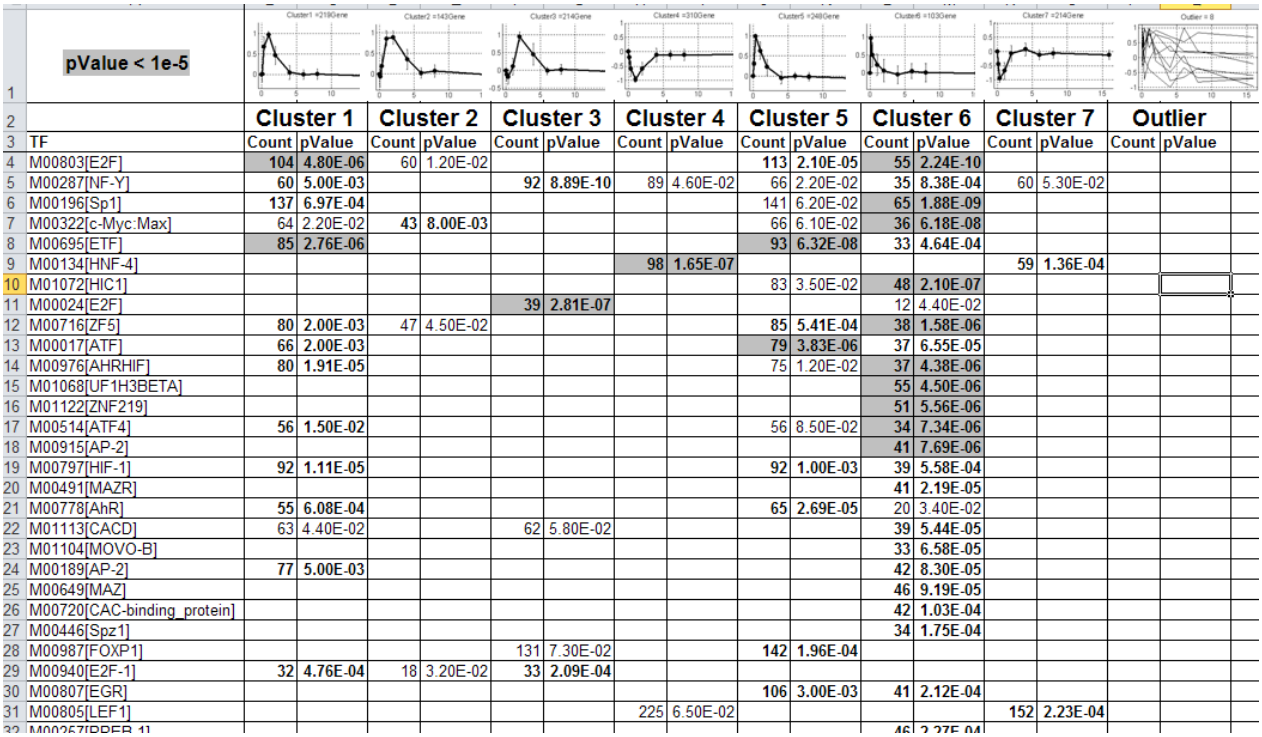

pValue < 1e-5	Cluster 1		Cluster 2		Cluster 3		Cluster 4		Cluster 5		Cluster 6		Cluster 7		Outlier	
TF	Count	pValue	Count	pValue	Count	pValue	Count	pValue	Count	pValue	Count	pValue	Count	pValue	Count	pValue
M00803[E2F]	104	4.80E-06	60	1.20E-02					113	2.10E-05	55	2.24E-10				
M00287[NF-Y]	60	5.00E-03			92	8.89E-10	89	4.60E-02	66	2.20E-02	35	8.38E-04	60	5.30E-02		
M00196[Sp1]	137	6.97E-04							141	6.20E-02	65	1.88E-09				
M00322[c-Myc:Max]	64	2.20E-02	43	8.00E-03					66	6.10E-02	36	6.18E-08				
M00695[ETF]	85	2.76E-06							93	6.32E-08	33	4.64E-04				
M00134[HNF-4]							98	1.65E-07					59	1.36E-04		
M01072[HIC1]									83	3.50E-02	48	2.10E-07				
M00024[E2F]					39	2.81E-07					12	4.40E-02				
M00716[ZF5]	80	2.00E-03	47	4.50E-02					85	5.41E-04	38	1.58E-06				
M00017[ATF]	66	2.00E-03							79	3.83E-06	37	6.55E-05				
M00976[AHRHIF]	80	1.91E-05							75	1.20E-02	37	4.38E-06				
M01068[UF1H3BETA]											55	4.50E-06				
M01122[ZNF219]											51	5.56E-06				
M00514[ATF4]	56	1.50E-02							56	8.50E-02	34	7.34E-06				
M00915[AP-2]											41	7.69E-06				
M00797[HIF-1]	92	1.11E-05							92	1.00E-03	39	5.58E-04				
M00491[MAZR]											41	2.19E-05				
M00778[AhR]	55	6.08E-04							65	2.69E-05	20	3.40E-02				
M01113[CACD]	63	4.40E-02			62	5.80E-02					39	5.44E-05				
M01104[MOVO-B]											33	6.58E-05				
M00189[AP-2]	77	5.00E-03									42	8.30E-05				
M00649[MAZ]											46	9.19E-05				
M00720[CAC-binding_protein]											42	1.03E-04				
M00446[Spz1]											34	1.75E-04				
M00987[FOXP1]					131	7.30E-02			142	1.96E-04						
M00940[E2F-1]	32	4.76E-04	18	3.20E-02	33	2.09E-04										
M00807[EGR]									106	3.00E-03	41	2.12E-04				
M00805[LEF1]							225	6.50E-02					152	2.23E-04		
M00267[PPER-1]											46	2.27E-04				

Figure 24: Analysis of transcription factor binding site (TFBS) enrichment in time-dependent gene clusters. The figure shows a snapshot of the results obtained for overrepresentation of TFBS. The TFBS with the strongest overrepresentation were ETF, Sp1, c-Myc and ETF, all of which were highly enriched in upregulated gene clusters. Conversely, HNF4α was the most overrepresented TFBS in downregulated gene clusters. Gray colored boxes indicated p-value<10^{-5}.

Conversely, HNF4α was the most enriched TFBS among downregulated genes (p=1.65E-7) (Fig 24). Considering the well-reported role of HNF4α in the expression of hepatocyte-specific genes, and particularly for metabolism-associated genes [74], an enrichment of HNF4α binding sites in these downregulated genes suggested that HNF4α may be affected during the phase of damage and regeneration. Analysis of HNF4α expression in liver tissue of control mice revealed the expected strong nuclear signal in hepatocytes, which was observed over the whole liver parenchyma (Fig 25). However, the signal for HNF4α progressively disappeared from the nuclei of hepatocytes during the early phase of liver damage, starting at 8h and almost completely disappeared at day 1 (Fig 25). This effect was not due to loss of hepatocytes, since also periportal hepatocytes, which under normal conditions also express HNF4α, did not show HNF4α expression on day 1 after CCl_4 (Fig 25). This rapid downregulation of nuclear HNF4α was almost completely recovered between days

2 and 4 (Fig 25), consistent with the progressive recovery in the expression of metabolism-associated genes in clusters 4 and 7 (Fig 20-23).

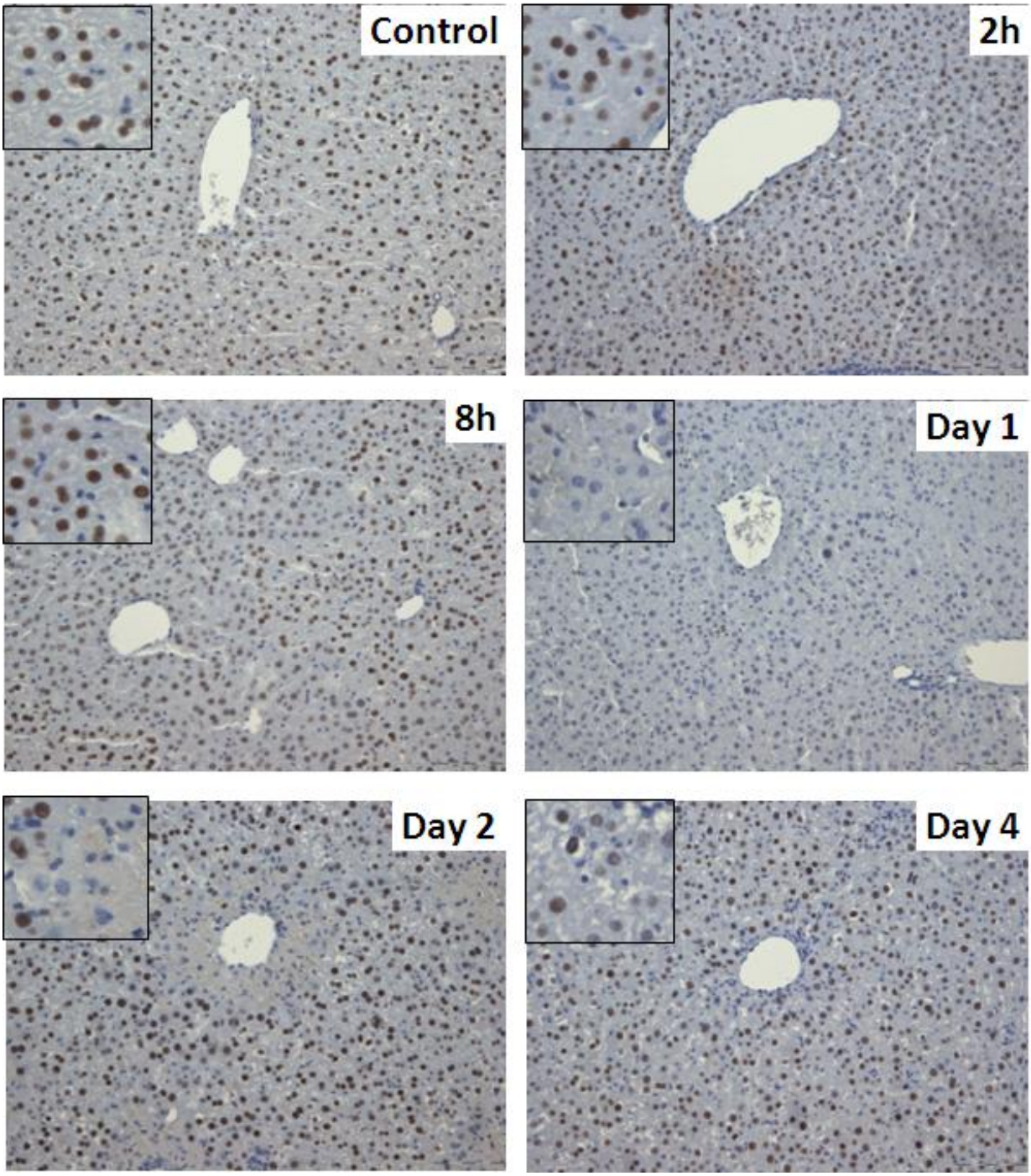

Figure 25: Immunohistochemical analysis of HNF4α in mouse liver reveals a transient downregulation during early time points after induction of damage by CCl_4. The expression and localization of the transcription factor HNF4α was assessed in paraffin embedded liver sections. In healthy (control) livers, HNF4α was found expressed throughout the liver parenchyma, and exclusively in hepatocyte nuclei. Upon CCl_4 injection, the staining intensity of HNF4α progressively decreased, and disappeared almost completely on day 1. The expression of HNF4α was recovered in livers 2 days after CCl_4 administration. Scale bars represent 100 µm.

Gene array analysis did not detect a downregulation of HNF4α mRNA. Consistent with this, qRT-PCR analysis detected only a slight decrease in HNF4α expression between days 1 and 4 (Fig 26). However the magnitude of this downregulation did not correlate with the profound reduction in HNF4α staining, suggesting that the loss of HNF4α was due to posttranscriptional events.

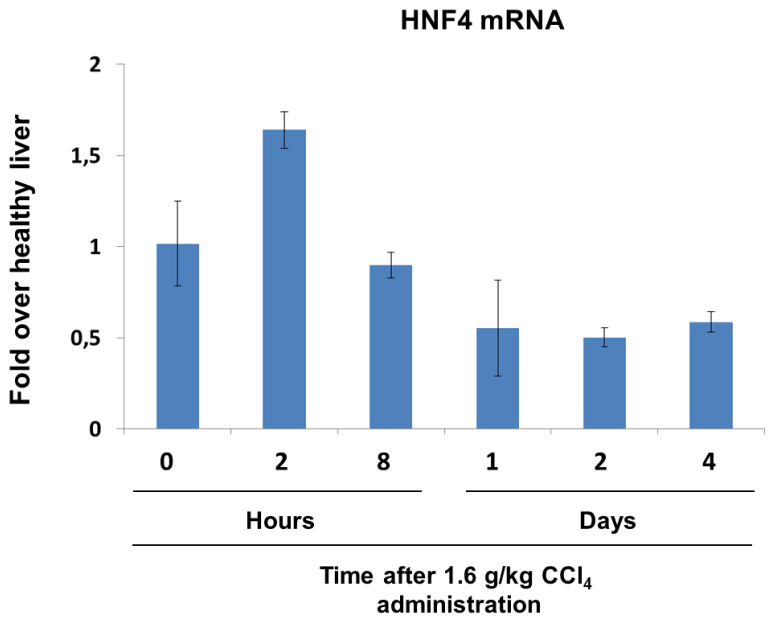

Figure 26: The expression of HNF4α mRNA is slightly decreased in livers upon CCl_4 intoxication. Expression of HNF4α mRNA was quantified in mouse liver tissue by qRT-PCR and normalized to the expression of GAPDH. The fold change was determined using healthy liver tissue as control (0 hours of CCl_4). Bars correspond to the average of 5 independent biological replicas. Error bars indicate standard error.

This led to the hypothesis that perhaps other TFs involved in control of metabolic functions in hepatocytes could also be affected in a similar fashion as HNF4α. Consistent with this, histological analysis of HNF1 also revealed a transient disappearance from hepatocyte nuclei during the early phase of liver damage, which was evident at 8h after CCl_4 administration, and progressively returned to normal levels on day 2 (Fig 27).

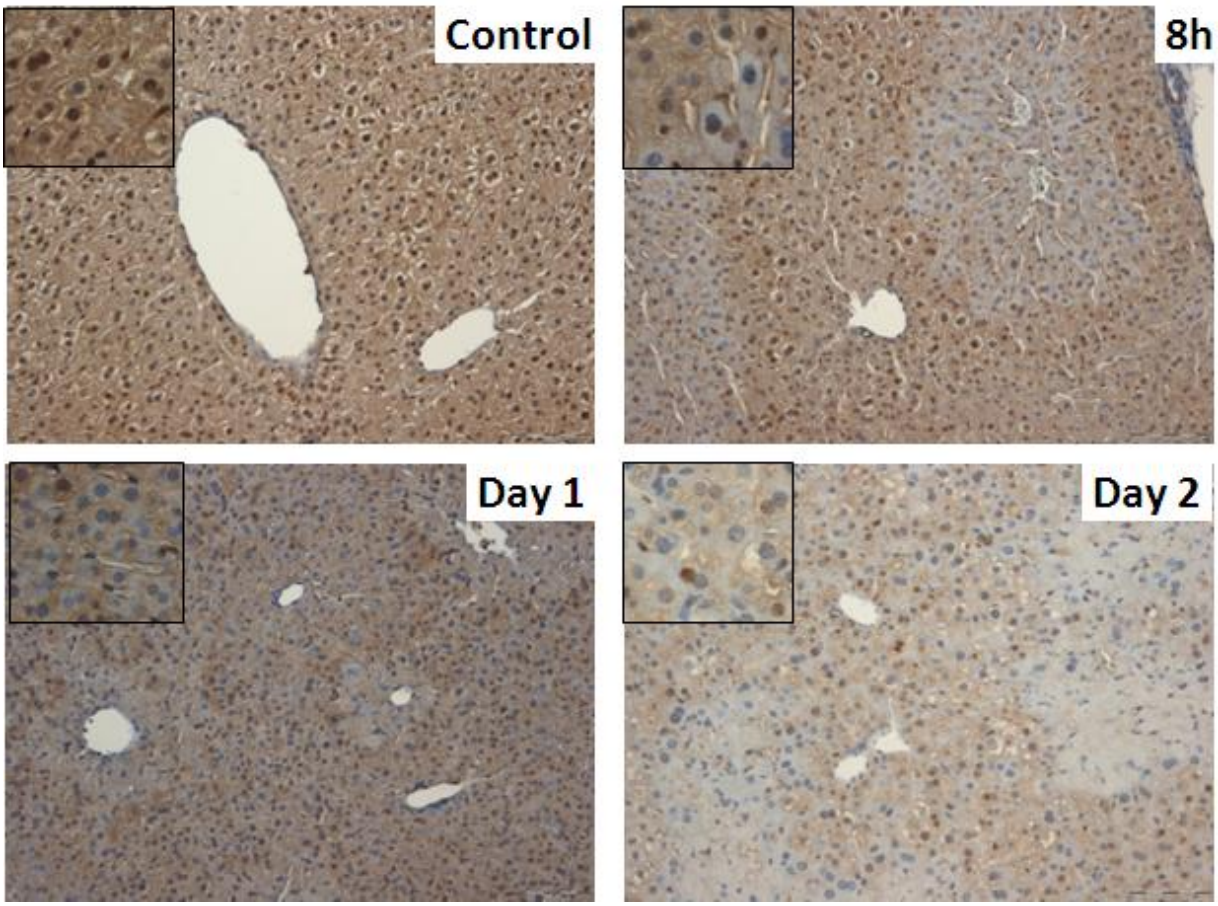

Figure 27: Immunohistochemical analysis of HNF1 in mouse liver reveals a transient downregulation during early time points after induction of damage by CCl_4. Similar to HNF4α, the expression and localization of the transcription factor HNF1 in healthy (control) livers was found throughout the liver parenchyma and exclusively in hepatocyte nuclei. Upon CCl_4 injection, the staining intensity of HNF1 progressively decreased, becoming weaker around central veins at 8h after CCl_4 injection, and disappeared from hepatocyte nuclei on day 1. Similarly as observed with HNF4α, the expression of HNF1 in hepatocytes started to recover by day 2. Scale bars represent 100 µm.

These results indicated that gene clustering allowed a more precise characterization of biological motifs and transcriptional regulatory networks. First, a well-orchestrated regeneration response was clearly detected in cluster 3, which was validated by immunoblotting of the cell cycle marker PCNA and is consistent with previous reports [47]. Second, a novel feature was discovered which involved a massive repression of metabolism-associated genes, which starts as early as 8h (cluster 7) and recovers on day 4 (cluster 4). Analysis of TFBS enrichment in these gene clusters supported a role of well-known proliferation-associated TFs such as E2F, whereas it unraveled a potential role for the

downregulation of HNF4α and HNF1 (and potentially other metabolism-associated TFs) during liver damage and regeneration.

In conclusion, a combination of time-resolved gene clustering and bioinformatics analyses (GO and KEGG motifs) and TFBS enrichment analysis provided important insights into the biological processes occurring in the liver during early and late phases of damage and regeneration. However, these analyses did not identify the precise mechanistic processes (i.e. signal transduction) that cause the strong transcriptional responses in the aforementioned gene clusters. This required a knowledge-based, manual curation of the data, starting with a closer examination of the individual deregulated genes.

6.7 CCl_4 induces a strong inflammatory response

Among the early-induced genes in cluster 6 was the acute phase response-associated transcription factor CEBP/δ [75] (Fig 28). Histological analysis demonstrated that CEBP/δ was expressed in hepatocyte nuclei, with a maximal signal at 8h after CCl_4 administration (Fig 29). This early induction of CEBP/δ is consistent with the early activation of STAT3 (Fig 17) which is known to drive the expression of this transcription factor upon inflammatory stimuli [75, 76]. At later time points, the acute phase response gene SAA3 and the macrophage marker genes CD68 and CD14 were also upregulated (Fig 28). These results suggested that an inflammatory response was activated early upon CCl_4 administration, and prompted for a further examination of inflammation-associated genes.

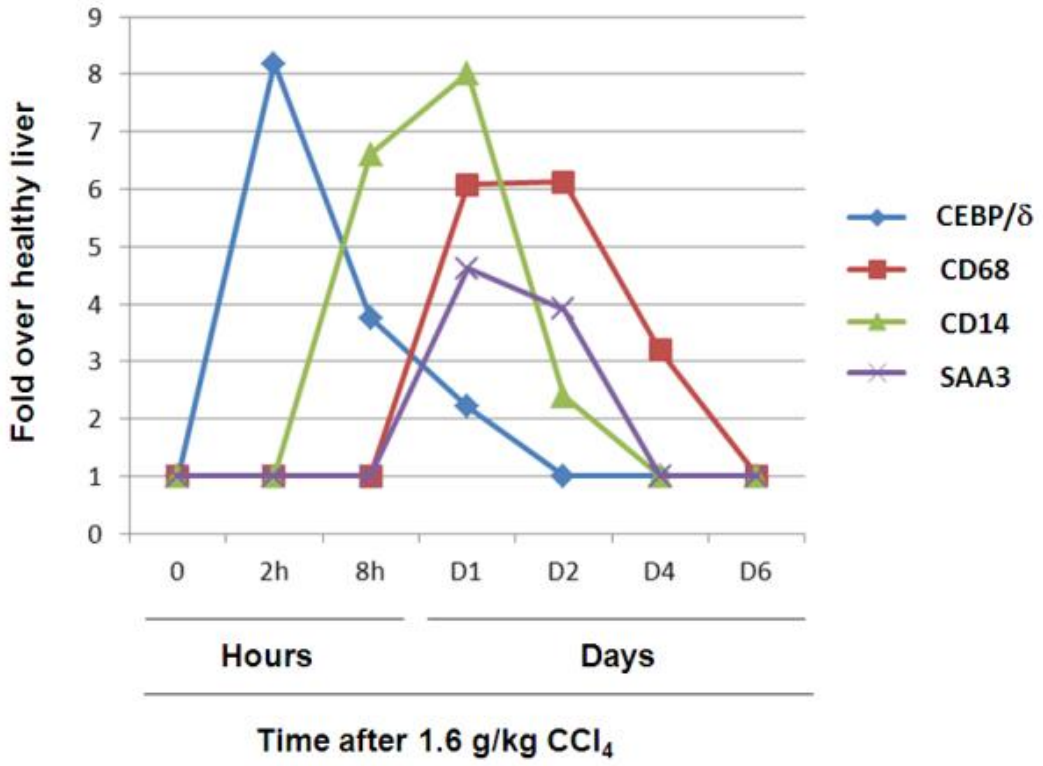

Figure 28: Expression of inflammation markers in liver tissue after CCl_4 intoxication. Upon CCl_4 injection, the inflammation-associated markers CEBP/δ, CD68 CD14 and SAA3 were strongly induced. The curves indicate mRNA expression intensity compared to healthy (0 hours) liver tissue. Values correspond to the average of 5 independent biological replicas per time point and condition ($p<0.05$, FDR adjusted).

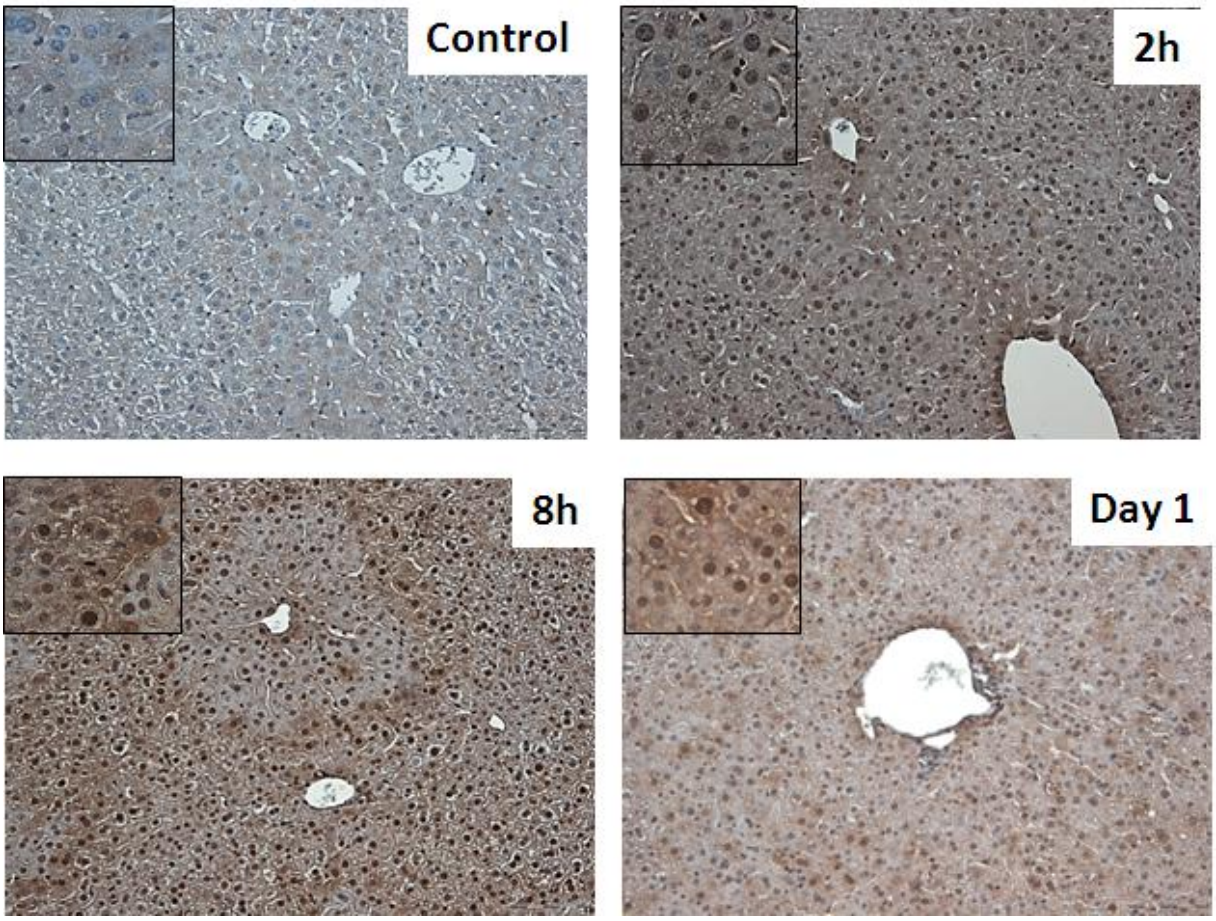

Figure 29: The inflammation-associated transcription factor CEBP/δ is induced in hepatocytes upon CCl_4 intoxication. The expression and localization of the transcription factor CEBP/δ was assessed in paraffin embedded liver sections. In healthy (control) livers, no expression of CEBP/δ was observed, whereas at 2h and 8h a strong nuclear expression of CEBP/δ was detected in hepatocyte nuclei. The expression of CEBP/δ started to decrease on day 1 after CCl_4 administration. The pictures are representative of 5 mice per time point and condition. Scale bars represent 100 µm.

Also during early time points after CCl_4 injection, the two potent chemokines Cxcl1 (also known as Gro1) and Cxcl2 (also known as Gro2 or MIP-2) were strongly induced (Fig 30). Furthermore, the chemokines Ccl2 (also known as monocyte chemoattractant protein-1) and Ccl6 were also induced (Fig 30).

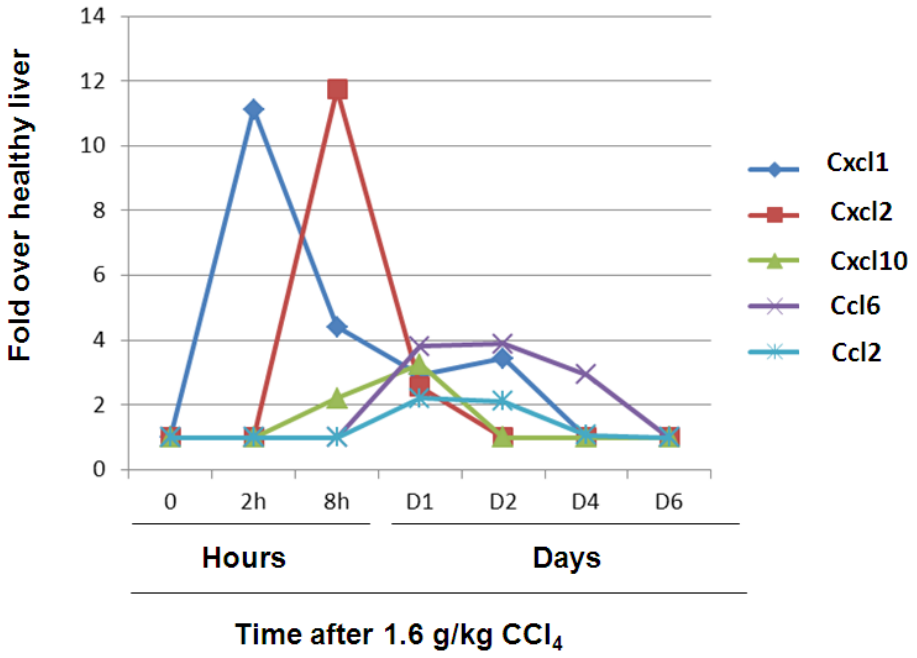

Figure 30: Expression of chemokines in liver tissue after CCl_4 intoxication. Upon CCl_4 injection, the chemokines Cxcl1, Cxcl2, Cxcl3, Ccl6 and Ccl2 were strongly induced. The curves indicate mRNA expression intensity compared to healthy (0 hours) liver tissue. Values correspond to average of 5 independent biological replicas per time point and condition ($p<0.05$, FDR adjusted).

The induction of Ccl2 was also confirmed by qRT-PCR (Fig 31). This analysis indicated that the time points when this induction occurred correspond to the gene array results. However, the actual mRNA induction was much stronger as indicated by the gene array, reaching expression over 40-fold above healthy liver (Fig 31). These results suggest that the gene array analysis may underestimate the contribution of cytokine expression during CCl_4-induced liver damage and regeneration. This may explain why bioinformatics analyses did not identify an overrepresentation of inflammation, and supports the fact that a manual curation of gene array data strengths the identification of biological processes revealed by bioinformatics.

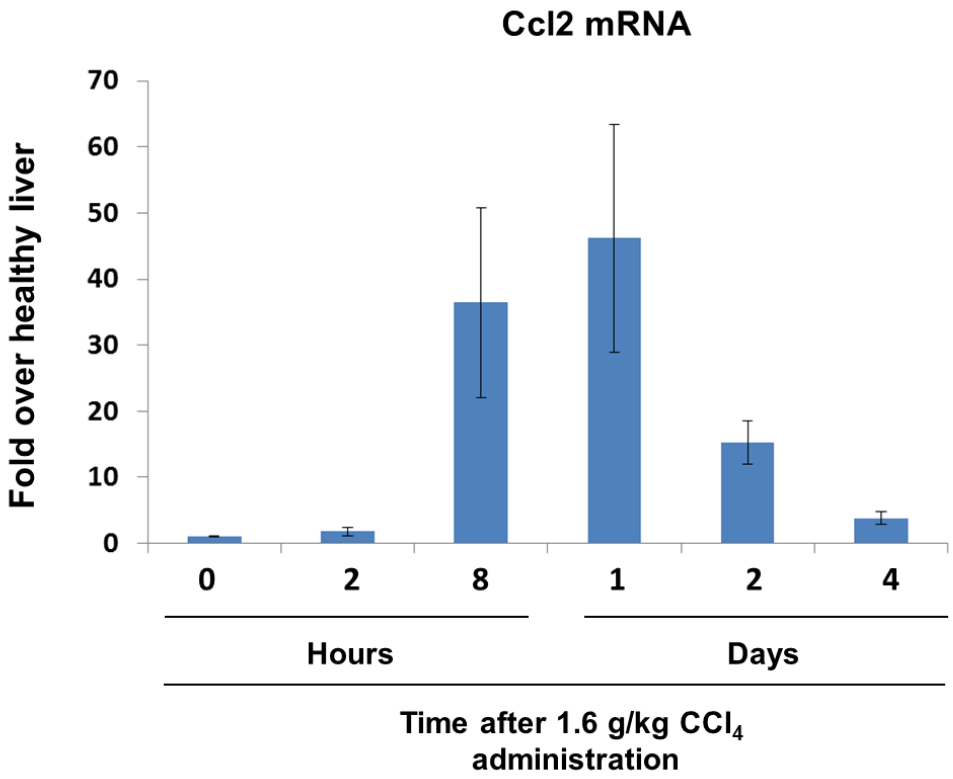

Figure 31: Expression of the chemokine Ccl2 was strongly induced in livers upon CCl_4 intoxication. Expression of Ccl2 mRNA was quantified in mouse liver tissue by qRT-PCR, and normalized to the expression of GAPDH. The fold change was determined using healthy liver tissue as control (0 hours of CCl_4). Bars correspond to the average of 5 independent biological replicas. Error bars indicate standard errors.

The chemokines identified by gene array act as potent mediators for leukocyte recruitment [77]. Consistent with this, immunostaining for Ly-6G/C, a marker of neutrophils, revealed a strong neutrophil infiltration on day 1, particularly around the dead cell areas (Fig 32).

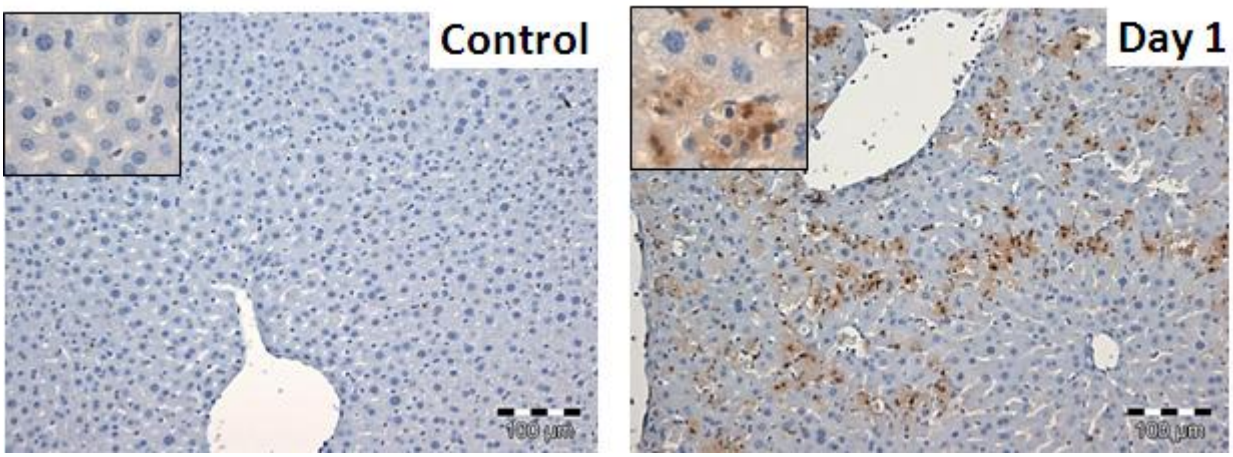

Figure 32: A strong infiltration of neutrophils occurs in livers upon CCl_4 intoxication. The expression and localization of neutrophils in liver tissue was determined by immunostaining with the antibody against the epitope Ly-6G/C, which is expressed in neutrophils. On healthy (control) livers, very few neutrophils were observed. However, on day 1 after CCl4 administration, a strong infiltration of neutrophils was observed around pericentral hepatocytes. The pictures are representative of 5 mice per time point and condition. Scale bars represent 100 µm.

The strongest upregulated gene in liver after CCl_4 administration was lipocalin-2 (Lcn2), which is a well-known acute phase response gene [78] (Fig 33A). Induction of Lcn2 mRNA was confirmed by qRT-PCR (Fig 33B). These results suggested that a large part of the transcriptional response induced during liver damage and regeneration occur concomitant with an inflammatory process.

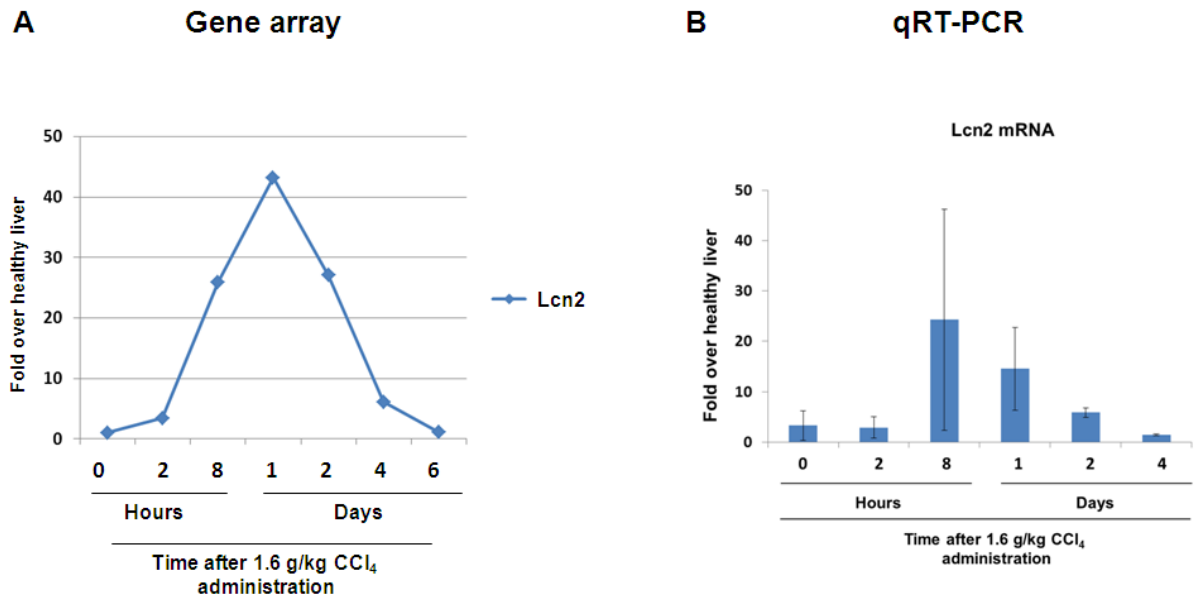

Figure 33: Expression of the acute phase response lipocalin-2 (Lcn2) in liver tissue after CCl_4 intoxication. **A)** Upon CCl_4 injection, the acute phase response gene Lcn2 was strongly induced. The curve indicates mRNA expression intensity compared to healthy (0 hours) liver tissue. Values correspond to the average of 5 independent biological replicas per time point and condition ($p<0.05$, FRD adjusted). **B)** Expression of Lcn2 mRNA was quantified in mouse liver tissue by qRT-PCR, and normalized to the expression of GAPDH. The fold change was determined using healthy liver tissue as control (0 hours of CCl_4). Bars correspond to average of 5 independent biological replicas. Error bars indicate standard error.

6.8 Inflammation and repression of metabolic functions are stereotypical responses in stressed hepatocytes

The observation that a strong inflammation response occurs in parallel to a massive repression of metabolic functions in hepatocytes, led to the question whether these responses would also occur in other models of hepatocyte stress. To obtain a thorough assessment of transcriptional responses in different stress conditions, gene array analyses were performed on three additional models of hepatocyte stress: two in vivo models, namely partial hepatectomy and lipopolysaccharide exposure, and the in vitro model of isolation and cultivation of hepatocytes.

A correlation analysis (spearman rank) revealed strong correlation of gene expression response between liver tissue after partial hepatectomy and liver after CCl_4 administration, particularly between days 1 and 2 in both models (Fig 34A). Similarly, a high correlation was

observed between days 1 and 3 after CCl_4 intoxication and liver tissue 24h after LPS administration (Fig 34B). Surprisingly, the highest correlations were observed between liver after CCl_4 administration and cultivated hepatocytes (Fig 34C). The observation that the maximal correlations between all in vivo models were observed at day 1, and also that this time point was the strongest correlated with cultivation-induced transcriptional alterations, led to the hypothesis that similar biological events may occur in all these profoundly different models of hepatocyte stress. To assess whether the biological motifs of inflammation and repression of metabolic functions were occurring in all models investigated, qRT-PCR analysis of selected genes representative of inflammation or metabolism were analysed. Remarkably, all inflammation-associated genes were strongly induced in all models (Fig 35). Furthermore, Lcn2 was the strongest upregulated gene in all models, indicating that this gene is a robust and sensitive indicator of stress-induced inflammation in hepatocytes. A repression of metabolism-associated genes was also observed in all tested models. However not all genes responded equally. While expression of the bile salt pump Bsep was strongly repressed in cultivation and in liver after CCl_4, this repression was less intense in livers after LPS or after partial hepatectomy (Fig 35). A similar response was observed for the bile salt synthesis enzyme Cyp7a1 (Fig 35). Nevertheless, these results strongly suggested that inflammation and repression of metabolic functions constitute a stereotypic response in stressed hepatocytes.

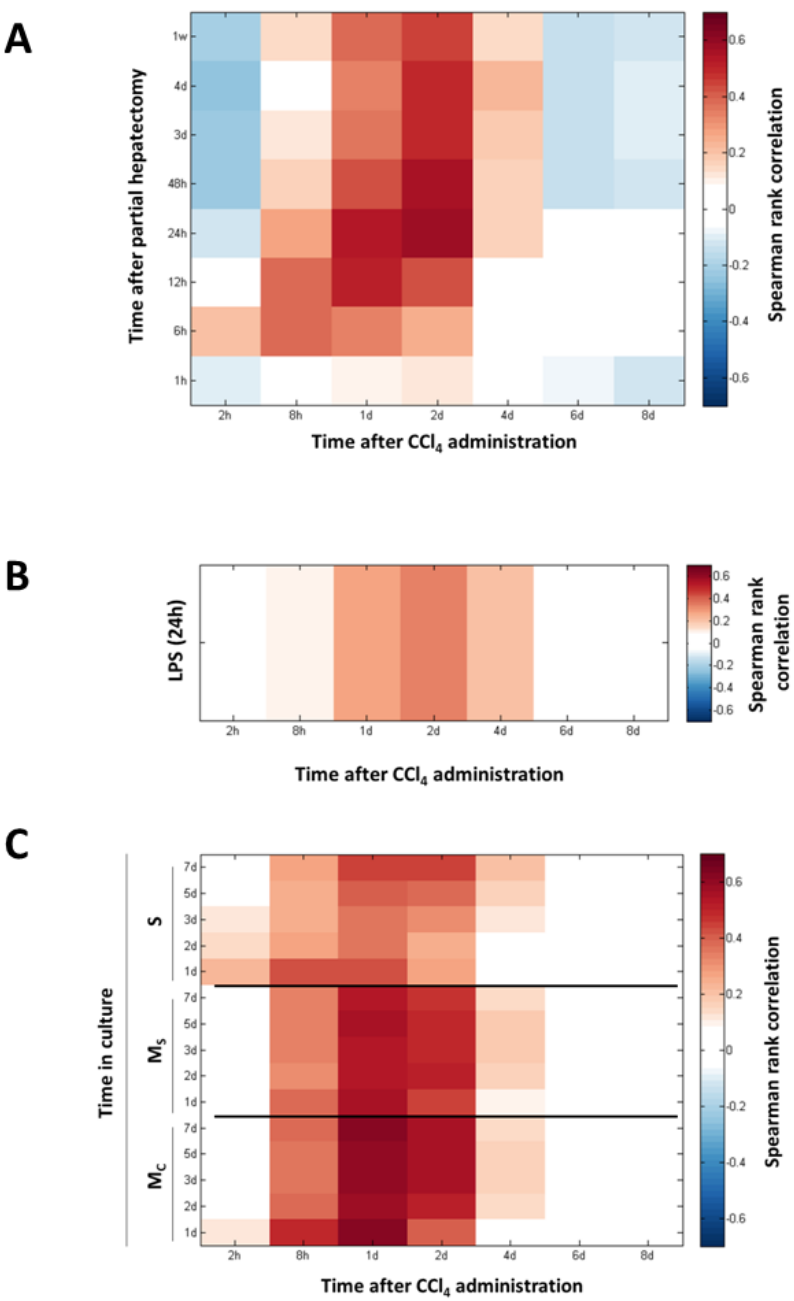

Figure 34: High correlation of global gene expression between different models of hepatocyte stress. Spearman rank correlation analysis revealed a high correlation of differentially expressed genes between CCl_4 intoxication and partial hepatectomy (**A**), CCl_4 intoxication and LPS exposure (**B**), and between CCl_4 intoxication and hepatocyte cultivation (**C**). The highest correlations were observed between 24 to 48 hours after CCl_4 intoxication and partial hepatectomy, and between 24h after CCl_4 intoxication and hepatocyte cultivation on monolayer confluent (M_C) conditions for 1 till 7 days. Lower correlations were observed between CCl_4 intoxication and sandwich (S) cultured hepatocytes, indicating that this culture system may repress some of the stress responses induced by isolation and cultivation.

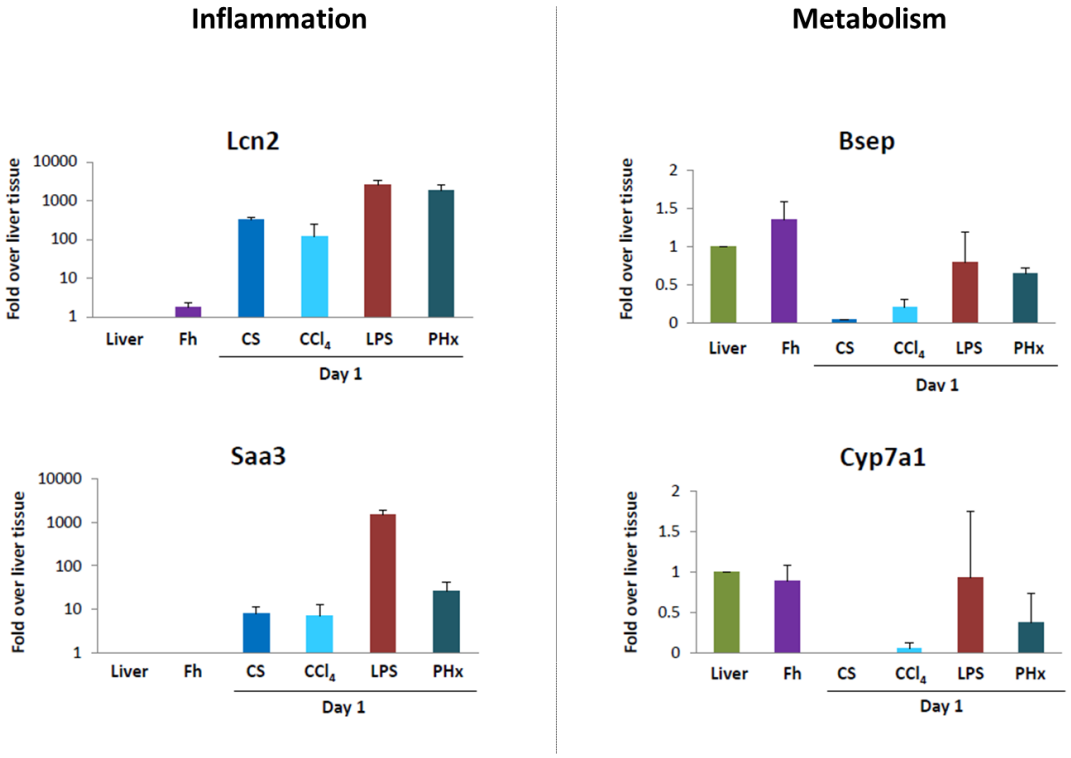

Figure 35: A stereotypic stress response in different models of hepatocyte stress consists of induction of inflammation and repression of metabolism-associated genes. Expression of the inflammation associated genes Lcn2 and SAA3 was detected in all models of liver stress analyzed in this study, namely hepatocyte isolation and cultivation in sandwich (S), CCl_4-induced liver damage (CCl_4), LPS exposure in vivo (LPS) and partial hepatectomy (PHx). Also, a repression of the metabolism-associated genes Bsep and Cyp7a1 was detected in all models used in this study. However, the intensity of downregulation varied between the models, whereby the strongest gene repressions were observed in cultivation and CCl_4-intoxication, while less intense gene downregulations occurred in PHx and LPS exposed livers. The fold change was determined using healthy liver tissue as control (0 hours of CCl_4) and normalized to the levels of GAPDH. Bars correspond to the average of 5 independent biological replicas. Error bars indicate standard error.

6.9 Gene cluster analysis shows the induction of ER-Stress related pathways

The time-resolved cluster analysis described above indicated that a massive transcriptional response was induced in hepatocytes within 2h after CCl_4 administration, before extensive liver damage occurs. During this time frame, CCl_4 is metabolized and the highly reactive metabolites, including CCl_3* and other oxidative radicals [17] induce intracellular alterations in hepatocytes, including modifications on macromolecules and Ca^{+2} leakage from the ER

[17]. These observations suggested that intracellular events in hepatocytes may cause the initial mechanisms leading to the transcriptional responses observed by gene array.

The oxidative radicals generated in hepatocytes and the macromolecule alterations may result in altered protein folding in the ER [17], and cause the activation of ER-stress responses [36, 37]. These responses include various potent transcription factors such as Xbp1, CHOP and ATF6 [36, 37] and can mediate the expression of hundreds of genes [37]. A closer examination on the gene array provided evidence supporting a role of ER-stress in the transcriptional response to CCl_4 in hepatocytes. First, KEGG pathway enrichment analysis identified the term "Protein processing in the endoplasmic reticulum" highly overrepresented on upregulated gene clusters 5, 6 and 1 (p=2.57E-10, p=8.01E-5 and p=2.86E-4, respectively) (Campos et al, 2013, in revision) (Fig 23). Second, binding sites for ER-stress dependent transcription factors were enriched in gene clusters 1, 4 5 and 6, including binding sites for ATF4, Xbp1 and CHOP (Campos et al, 2013, in revision).

Further analysis of ER-stress dependent biomarkers confirmed the early activation of these pathways upon CCl_4 adminstration (Fig 36). First, splicing of Xbp1 mRNA was clearly detected between 2h and 8h after CCl_4 injection (Fig 36A), indicating that the ER-stress sensor IRE1α was activated during these time frame. Second, phosphorylation of eIF2α, which depends on the ER-stress sensor PERK, was induced between 2h and 2 days after CCl_4 administration (Fig 36A). Third, induction of the transcription factor CHOP was strongly detected at the protein level 8h after CCl_4 injection (Fig 36A), while its transcript was induced between 8h and day 1 (Fig 36B). These results clearly demonstrated that ER-stress induced signaling was strongly induced very early upon CCl_4 intoxication in mouse liver.

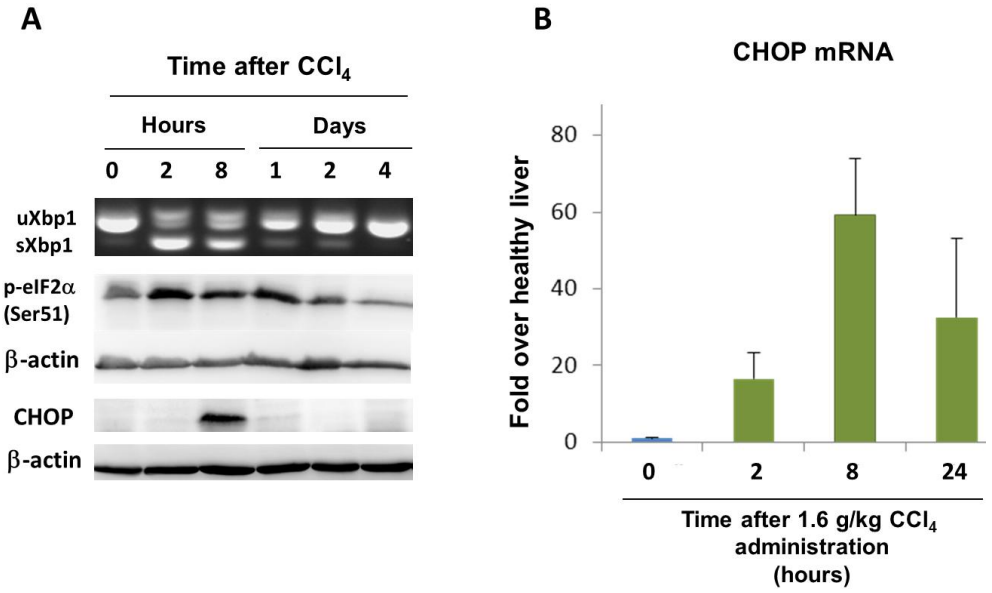

Figure 36: CCl_4 induces activation of ER-Stress pathways. A) Several molecular markers of ER-stress were used to assess activation of ER-stress pathways in liver tissue after CCl_4 administration. First, splicing of the Xbp1 mRNA was clearly detected by PCR analysis at 2 and 8 hours after CCl_4 injection. Second, phosphorylation of eIF2α and induction of the transcription factor CHOP were clearly observed by western blot analysis. β-Actin was used as loading control for western blot. The results are representative of at least 4 mice per time point and condition. **B)** The transcriptional induction of CHOP mRNA was detected by qRT-PCR analysis in mouse liver tissue after CCl_4 administration. The fold change was determined using healthy liver tissue as control (0 hours of CCl_4) and normalized to the levels of GAPDH. Bars correspond to the average of 5 independent biological replicas. Error bars indicate standard error.

6.10 The CCl_4-induced ER-stress response occurs in pericentral hepatocytes

The previous analyses demonstrated the activation of ER-stress in liver tissue after CCl_4 intoxication. Depending on the intensity and duration of ER-stress, these pathways may induce paradoxical responses, whereby in some situations they can restore homeostasis, while in certain conditions they can lead to cell death [36]. In the model of CCl_4-induced liver damage, the initial biochemical reactions leading to cell death occur in pericentral hepatocytes, suggesting that ER-stress pathways may also occur in this specific cell population. However, since the PCR, qRT-PCR and western blot analyses described above were performed with liver homogenates, the results did not provide information about the areas in the lobules were they occur. Therefore, to gain information about the zonal distribution of ER-stress, immunohistochemical (IHC) analyses of CHOP were performed. To

increase confidence of our IHC results, mice treated with the ER-stress inducer tunicamycin (Tm) were used as a positive control. As expected, Tm treatment (8h time point) presented a strong nuclear staining of CHOP in hepatocytes (Fig 37), while CHOP expression was undetectable in control (healthy) mice (Fig 37). The expression of CHOP was observed throughout the whole liver parenchyma, indicating that Tm did not induce a particular zonal-dependent ER-stress (Fig 37). Remarkably, only hepatocytes were positive for CHOP expression, while no detectable CHOP was observed in non-parenchymal cells (Fig 37). However, analysis of CHOP expression in livers after CCl_4 revealed a clear zonal distribution, whereby only pericental hepatocytes were stained positive for CHOP (Fig 37). This was evidenced by the absence of CHOP staining in hepatocytes near portal veins or bile ducts (Fig 37, closeup). The staining was strongest at 8h after CCl_4 administration, and returned to basal levels at day 4, consistent with the previous western blot and qRT-PCR results (Fig 36). These results indicated that ER-stress is part of the initial mechanisms triggered upon CCl_4 intoxication in hepatocytes.

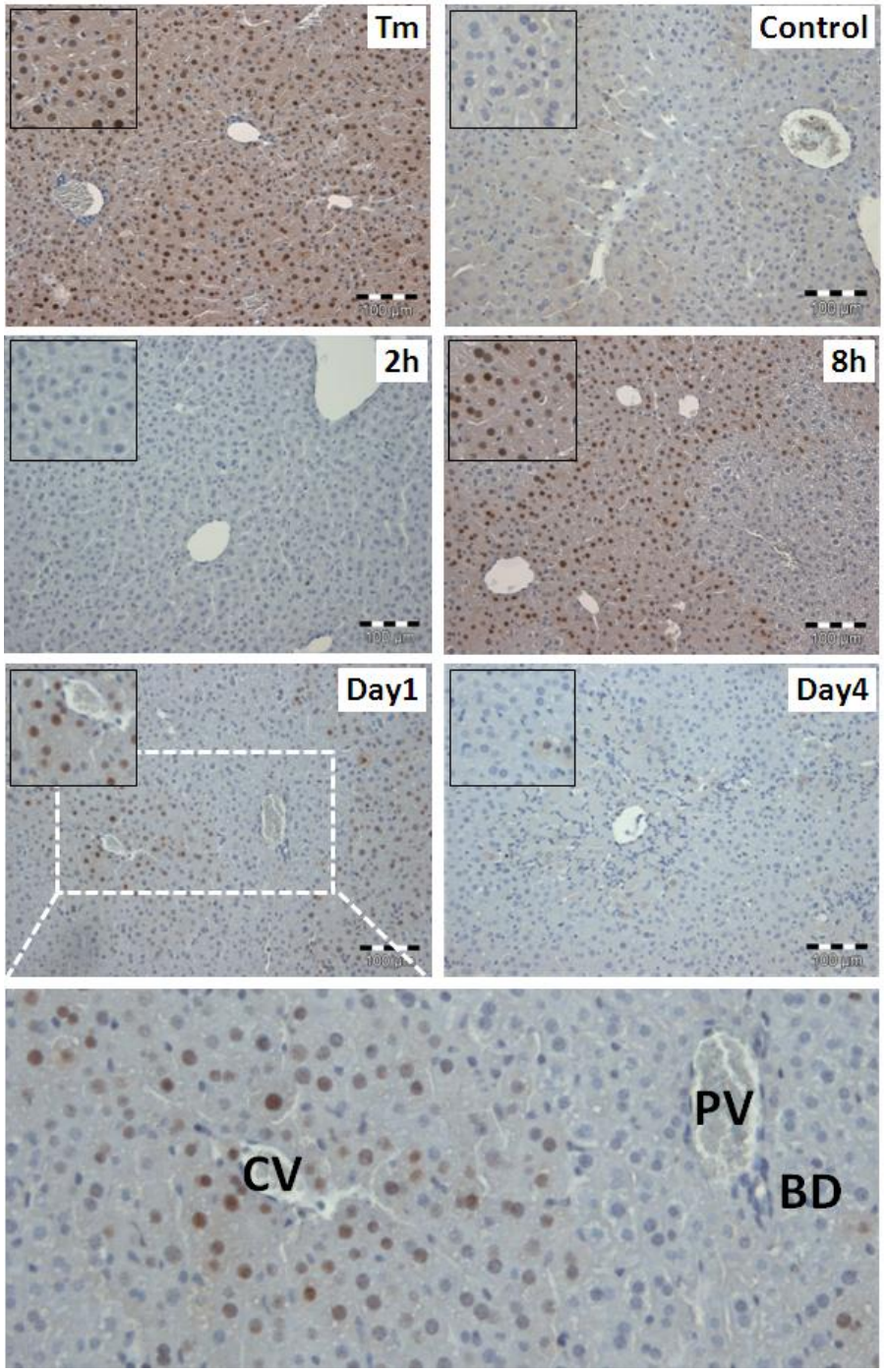

Figure 37: Immunohistochemical analysis of CHOP in mouse liver reveals a transient induction in pericentral hepatocytes after induction of damage by CCl_4. The expression and localization of the transcription factor CHOP was assessed in paraffin embedded liver sections. Liver sections from mice treated for 8h with tunicamycin (Tm, 5 mg/kg) were used as for positive control. In healthy livers, no detectable expression of CHOP was observed. However, both Tm and CCl_4 induced a strong nuclear expression of CHOP in hepatocytes. However, while Tm induces CHOP throughout the whole liver parenchyma, CCl_4 intoxication induces only a pericentral expression of CHOP. The photographs correspond to representative analyses of at least 3 independent mice per time point and condition. Scale bars represent 100 µm, Tm= Tunicamycin, CV=Central vein, PV=portal vein. BD=bile duct.

6.11 Genes associated with CHOP include well established pro-apoptotic factors such as Trb3, GADD34 and Ero1l

The ER-stress transcription factor CHOP has been extensively associated with ER-stress-induced cell killing [36, 38, 44]. Therefore, the observation that ER-stress (i.e CHOP expression) occurs in pericentral hepatocytes upon CCl_4 injection, suggested that ER-stress-dependent responses may be involved in hepatocyte killing. CHOP itself is not a direct cell death mediator, but it drives transcriptional upregulation of genes with demonstrated roles in cell death, such as Trb3, GADD34 and Ero1l [36, 41, 45, 79]. A closer examination on genes with overrepresentation of CHOP binding sites showed that these genes were included in clusters 5 and 6, which were characterized by a gene expression pattern with increased values between 2h and 8h, followed by a return to control values between day 1 and 4 (Fig 38). The timing of expression of those genes, which included Trb3 and GADD34, correlated very well with the observed induction of CHOP protein (Fig 38).

Histological examination of Trb3 expression showed an initial pericentral upregulation in hepatocytes 2h after CCl_4 administration (Fig 39). However, at later time points (8h and day 1) Trb3 expression was reduced in pericentral and increased in periportal hepatocytes (Fig 39). Nevertheless, the expression of Trb3 in pericentral hepatocytes at early time points after CCl_4 injection suggested that CHOP-dependent pro-apoptotic factors may be involved in the killing of hepatocytes by CCl_4.

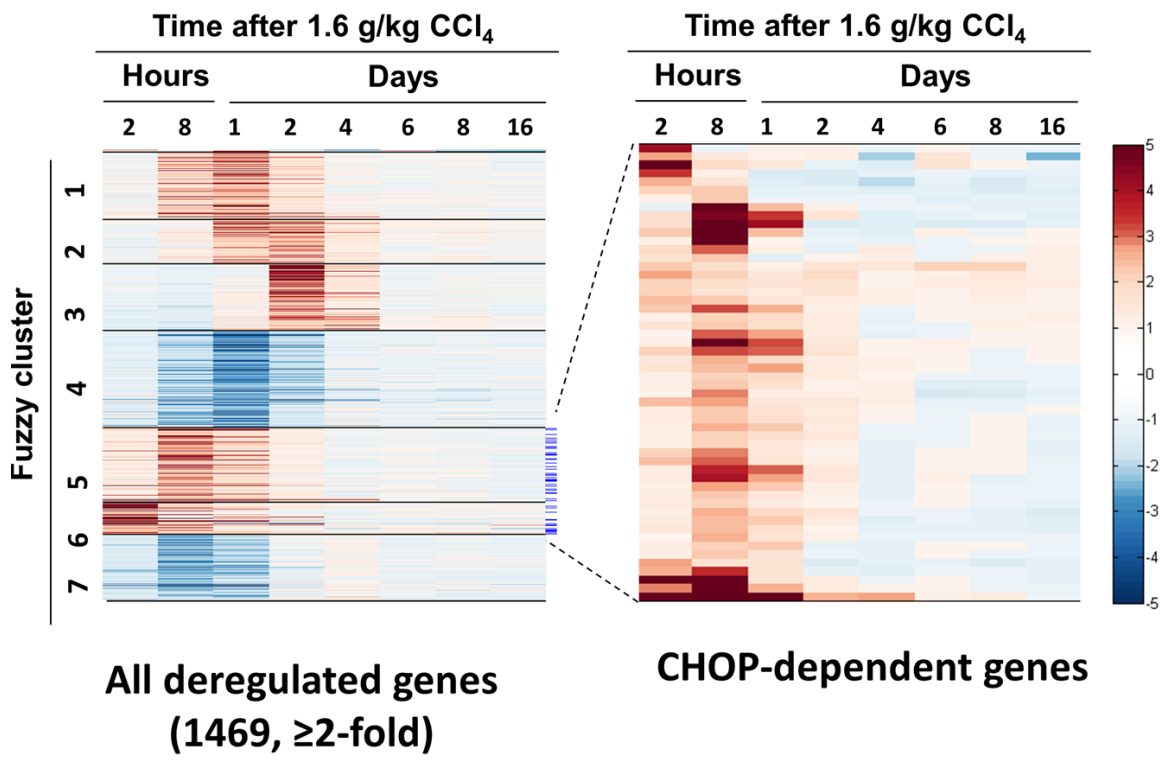

Figure 38: CHOP binding sites are overrepresented in genes upregulated early upon CCl_4 administration. CHOP binding sites were enriched in genes belonging to the clusters 5 and 6, which are upregulated early upon CCl_4 injection. A close-up examination showed that CHOP-associated genes were strongly upregulated between 2h and day 1 after CCl_4 administration.

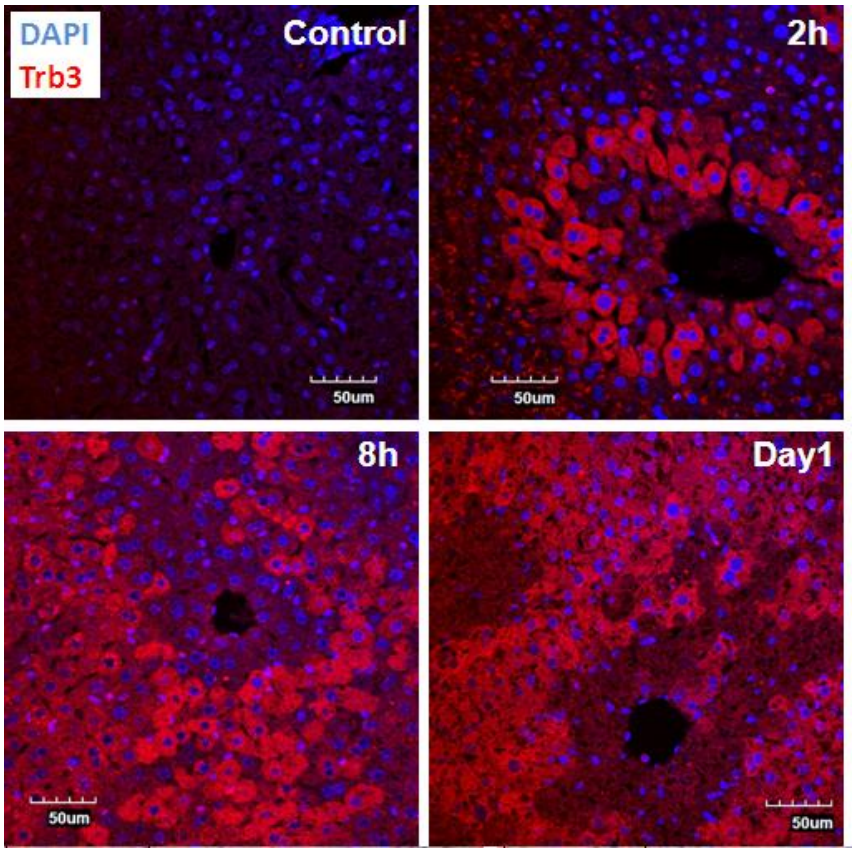

Figure 39: Immunofluorescence analysis of Trb3 expression in mouse liver reveals a sequential induction in pericentral and periportal hepatocytes after induction of damage by CCl_4. The expression and localization of the CHOP-associated gene Trb3 was assessed in paraffin embedded liver sections. In healthy livers, Trb3 expression was not detected. At 2h after CCl_4 injection, an induction in Trb3 expression was observed in pericentral hepatocytes. At later time points (8h and day 1), the expression of Trb3 was observed in periportal hepatocytes. Pictures are representative of at least 3 mice per time point and condition. DAPI was used as a nuclear staining (blue). Scale bars represent 50 µm.

6.12 **CHOP knockout mice challenge with 1.6 g/kg CCl_4**

The restricted expression of CHOP and Trb3 in hepatocytes on pericentral regions suggested that CHOP and its downstream targets genes may contribute to hepatocyte killing upon CCl_4 administration. This led to the hypothesis that deletion of the transcription factor CHOP would protect the mice against CCl_4-induced damage, which should be reflected by decreased serum transaminases and smaller dead cell areas compared to wild type mice after CCl_4 challenge. To answer this question, a challenge with 1.6 g/kg CCl_4 (intraperitoneal) for 8, 24 and 72h was performed in CHOP knockout mice ($Ddit3^{-/-}$) [44], and compared to wild type

C57BL/6J mice, which share the same genetic background. Four to five mice were analyzed for per group and time point.

The efficiency of the CHOP knockdown was controlled by qRT-PCR (Fig 40). Basal and CCl_4-induced CHOP expression were detected in wild type C57B6/J mice, which were comparable to the levels and timing observed in the previous analysis on C57B6/N mice (Fig 36), whereas no CHOP mRNA expression was detected in the CHOP knockout mice (Fig 40).

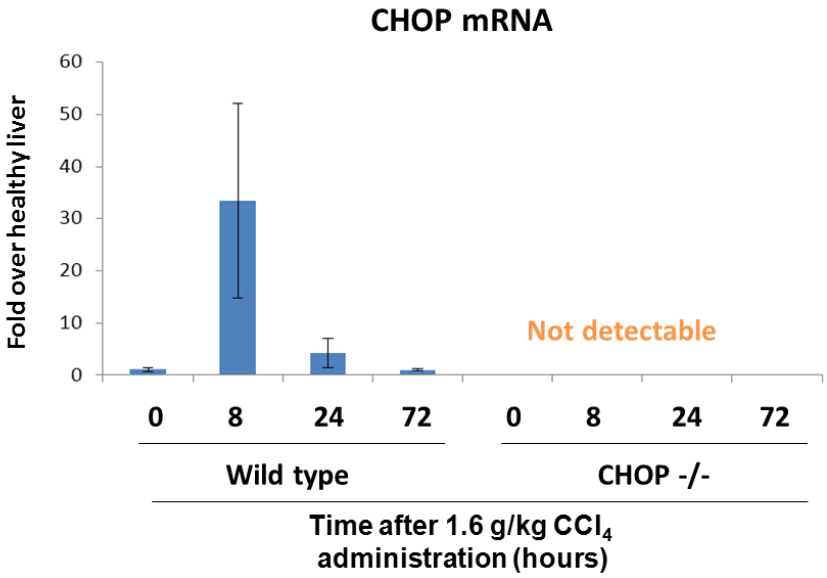

Figure 40: Validation of CHOP knockout mice. The transcriptional induction of CHOP mRNA was detected by qRT-PCR analysis in liver tissue from wild type C57B6/J mice after CCl_4 administration. CHOP mRNA expression was clearly induced upon CCl_4 injection, following a similar expression kinetic as in C57B6/N mice. No CHOP mRNA was detected in CHOP knockout mouse liver. The fold change was determined using healthy liver tissue as control (0 hours of CCl_4), and normalized to the levels of GAPDH. Bars correspond to average of 5 independent biological replicas. Error bars indicate standard error.

In both wild type and CHOP knockout mice, CCl_4 injection induced severe liver damage, as indicated by the sharp increase in serum transaminases, reaching a maximum 24h after CCl_4 administration (Fig 41). Surprisingly, no significant differences for GOT and GPT were observed for wild type and CHOP knockout mice at any of the time points analyzed.

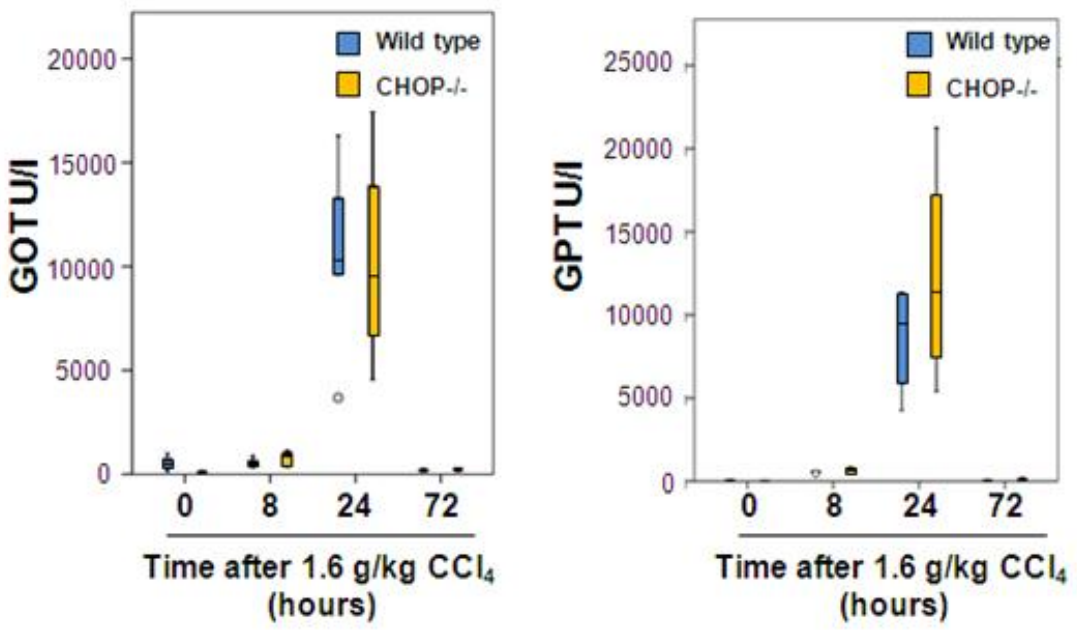

Figure 41: Plasma transaminases of wild type and CHOP knockout mice after 1.6 g/kg CCl_4 administration. A marked increase in GOT and GPT activities was observed in plasma of both wild type (blue) and CHOP knockout mice (yellow) after CCl_4 intoxication. No significant differences were observed between wild type and knockout mice. The horizontal line in the middle of a box shows the median of the sample. The edges of a box mark the 25th and 75th percentiles. The whiskers show the range of values that fall within 1.5 box-lengths. Values >1.5 box-lengths from the 25th or 75th percentiles are marked by a dot. Data was generated using four CHOP knockout and 5 wild type mice per time point.

Histological analysis with H&E stained tissues confirmed the well-reported pericentral dead cell areas induced by CCl_4 intoxication in both wild type and CHOP knockout mice (Fig 42). As with C57B6/N, these dead cell areas were visible by 24 and 72h after CCl_4 administration. Quantification of the dead cell areas also showed no a slightly increased tissue damage in CHOP knockout mice compared to wild type (Fig. 43).

The CCl_4 dose of 1.6 g/kg used for the previous experiment was very high. Since administration of too high doses might compromise differentiation between knockout and wild-type mice, the experiment was repeated using a smaller dose of CCl_4 that induces a measurable pericentral dead cell area [30]. For this experiment, a dose of 0.132 g/kg was chosen. Again, CHOP knockout did not protect from CCl_4-induced liver damage as evidenced by GOT, GPT (Fig 44) as well as dead cell area quantification (Fig 45 and 46). In contrast, a trend towards more damage was obtained for the CHOP knockout mice. However, this should be interpreted with caution, because the difference depends on a single outlier.

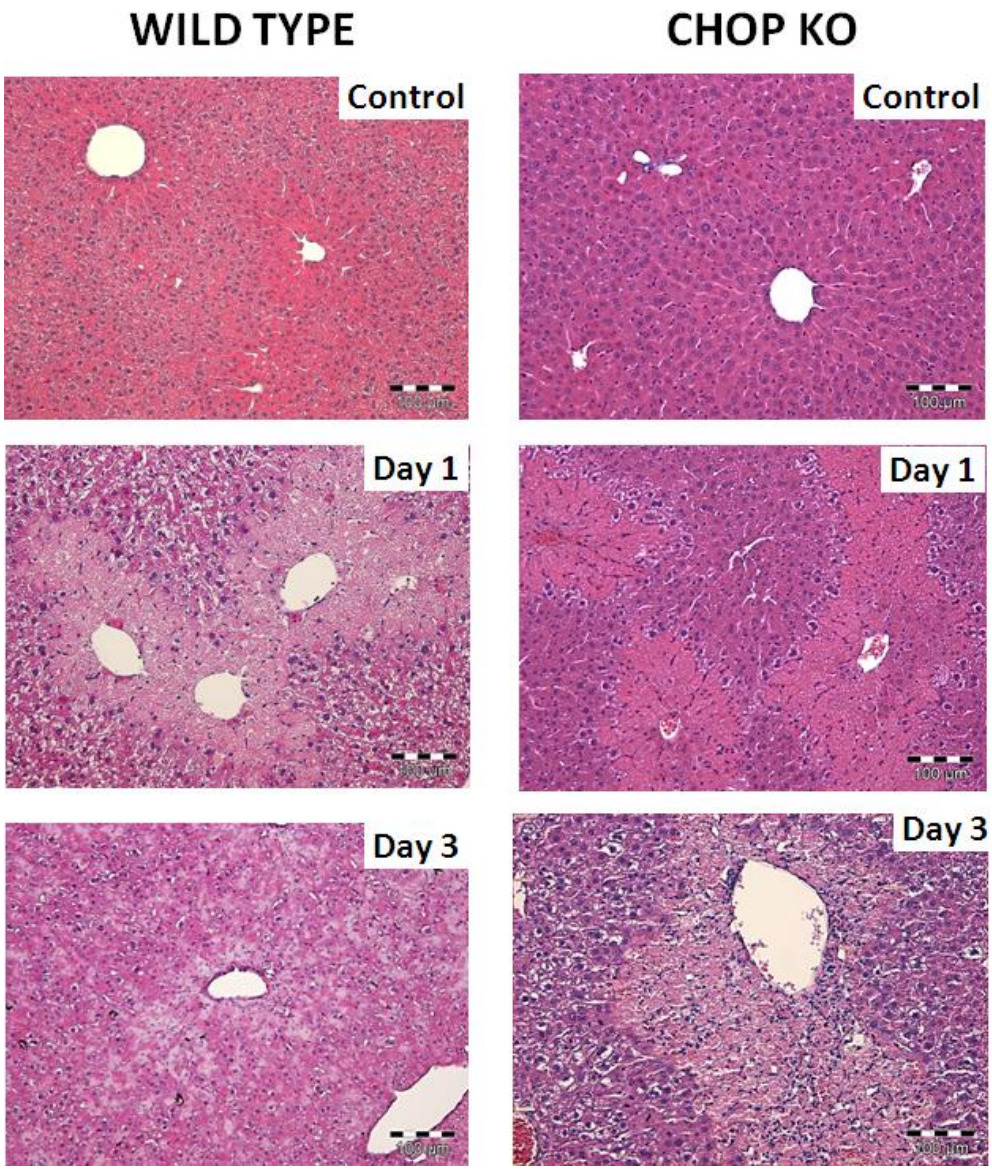

Figure 42: Histological examination of liver damage by H&E staining in wild type and CHOP knockout mice after intraperitoneal injection of 1.6 g/kg CCl_4. Paraffin embedded liver sections stained with H&E were examined under bright light microscopy (100X magnification). The centrilobular dead cell areas were clearly identified at day 1 and day 3 after CCl_4 administration. Scale bars represent 100 µm.

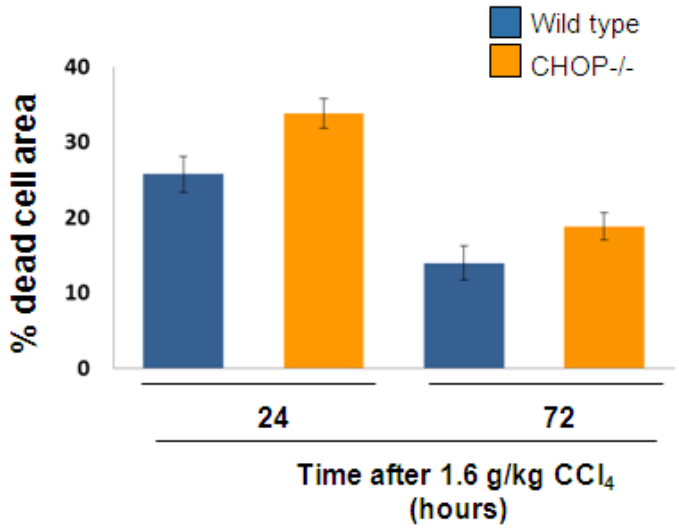

Figure 43: Quantification of dead cell areas in mouse liver after CCl_4 administration. The extent of tissue damage in wild type and CHOP knockout mice was assessed by quantification of the dead cell areas as described in methods. The quantification revealed a slightly larger tissue injury in CHOP knockout mice compared to wild type on day 1 and day 3 after CCl_4 administration. The bars are the mean values of three mice per time point. Error bars indicate standard error.

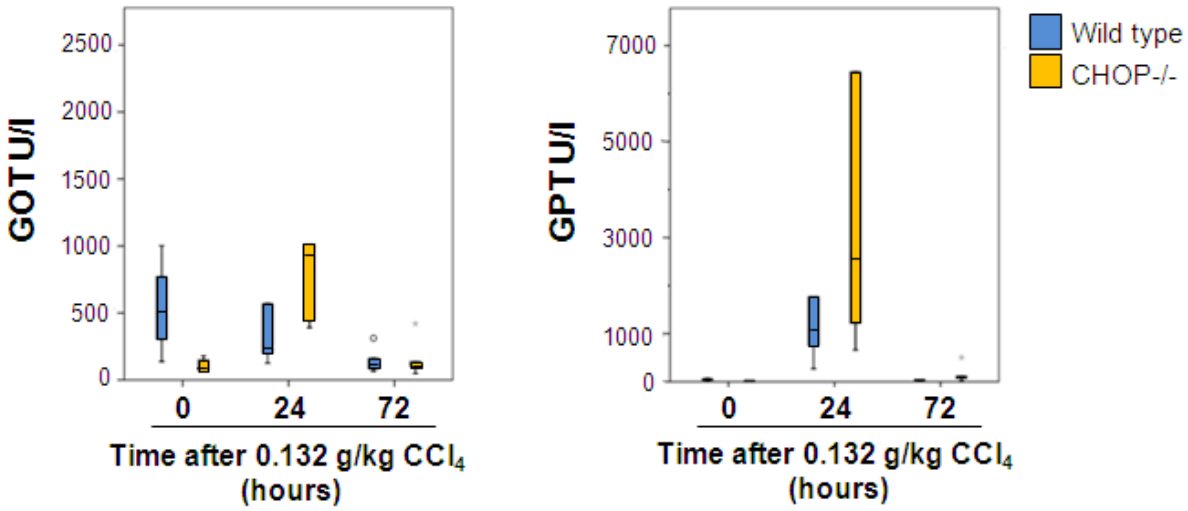

Figure 44: Plasma transaminases of wild type and CHOP knockout mice after 0.132 g/kg CCl_4 administration. A marked increase in GPT activity was observed in plasma of both wild type (blue) and CHOP knockout mice (yellow) 24h after CCl_4 intoxication. No significant differences were observed between wild type and knockout mice. The horizontal line in the middle of a box shows the median of the sample. The edges of a box mark the 25th and 75th percentiles. The whiskers show the range of values that fall within 1.5 box-lengths. Values >1.5 box-lengths from the 25th or 75th percentiles are marked by a dot. Data was generated using four CHOP knockout and 5 wild type mice per time point.

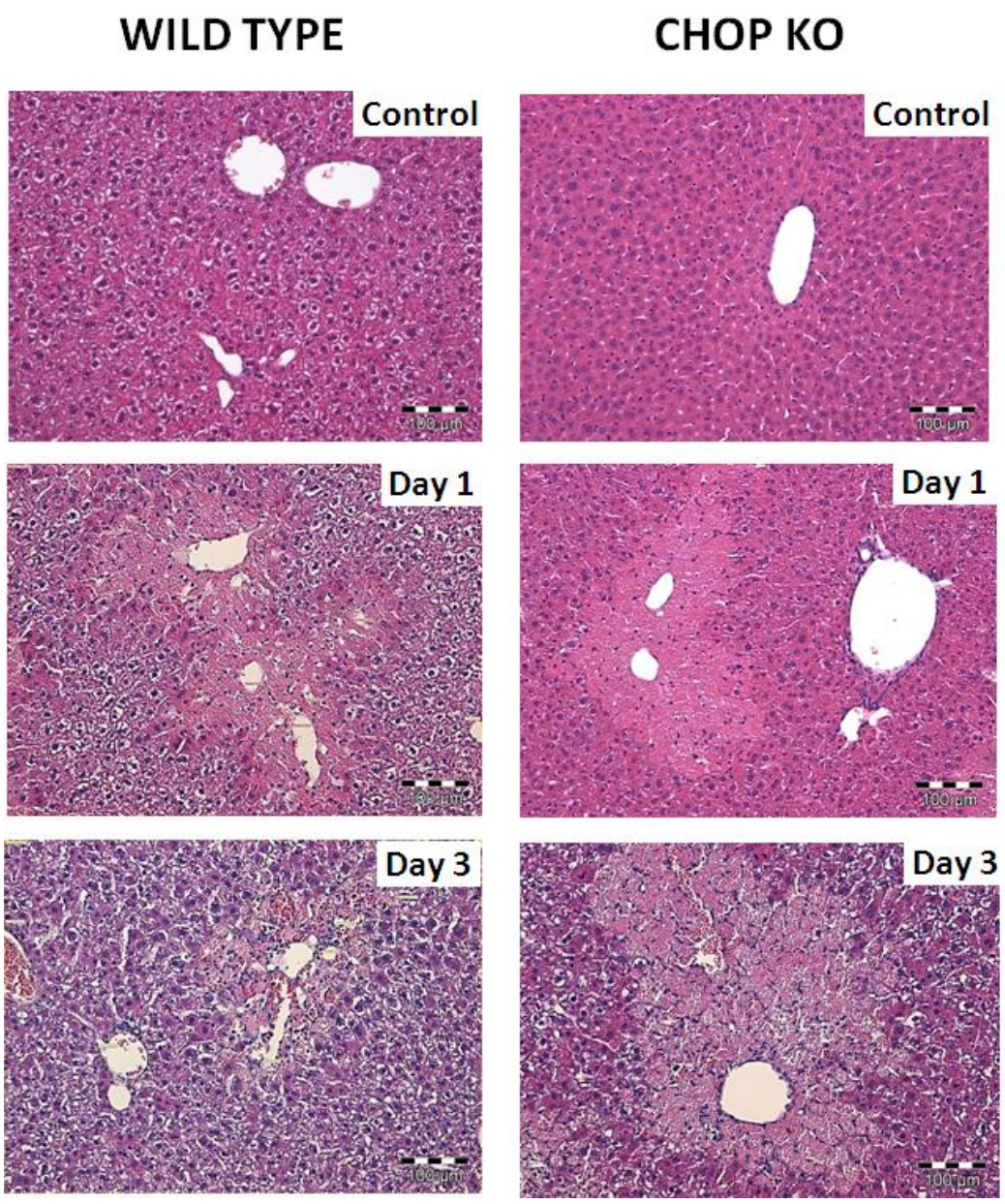

Figure 45: Histological examination of liver damage by H&E staining in wild type and CHOP knockout mice after intraperitoneal injection of 0.132 g/kg CCl_4. Paraffin embedded liver sections stained with H&E were examined under bright light microscopy (100X magnification). The well-documented centrilobular dead cell areas were clearly identified at day 1 in both wild type and CHOP knockout mice. On day 3 after CCl_4 administration, significantly larger dead cell areas were observed in CHOP knockout mice compared to wild type. The H&E staining shows larger necrotic areas at day 1 and day 3 in CHOP KO mice compared to wild type. Scale bars represent 100 µm.

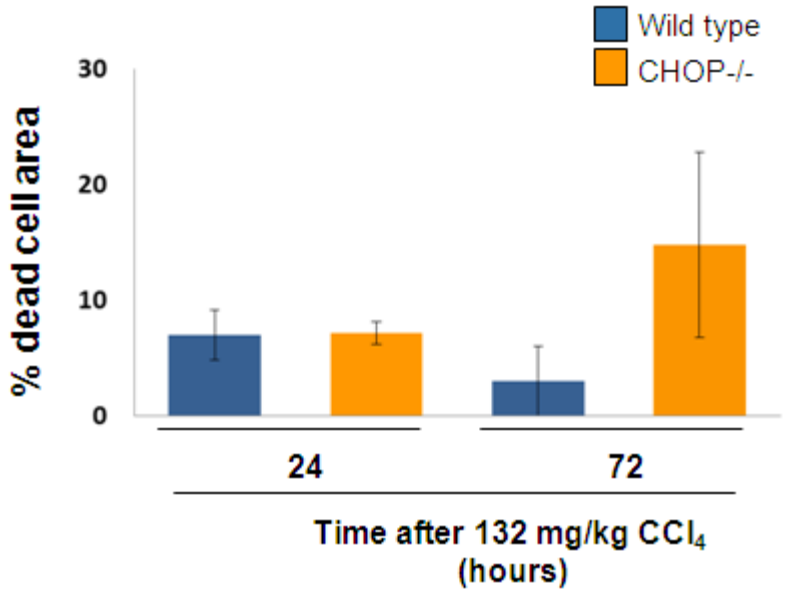

Figure 46: Quantification of dead cell areas in mouse liver after 0.132 g/kg CCl_4 administration. The extent of tissue damage in wild type and CHOP knockout mice was assessed by quantification of the dead cell areas as described in methods. The quantification revealed a slightly larger tissue injury in CHOP knockout mice compared to wild type on day 3 after CCl_4 administration. The bars are the mean values of three mice per time point. Error bars indicate standard error.

Taken together, the data shows that deletion of CHOP does not confer any protection against CCl_4 induced liver damage. Contrary to our predictions, CHOP KO mice challenged with 1.6 g/Kg CCl_4 displayed slightly larger necrotic areas concomitantly with delayed wound healing compared to wild type mice under the same treatment.

6.13 **Potential compensatory mechanisms in CHOP knockout mice**

The surprising absence of a protective role in CHOP knockout mice suggested that compensatory mechanisms may account for the regulation on genes involved in cell killing. Therefore, qRT-CPR analyses were performed to determine the effect of CHOP knockout on downstream cell-death associated genes [36]. For Trb3, a reduced expression was observed in CHOP knockout 8h after CCl_4 administration (Fig 47). However, only a small reduction on the cell death-associated gene GADD34 was observed in CHOP knockout compared to wild type mice (Fig 47). Conversely, the induction of Bim and Ero1l were stronger in CHOP knockout than in wild type (Fig 47). Therefore, it is likely that the expression of GADD34, Bim and Ero1l is not uniquely controlled by CHOP in mouse liver, and suggests that other ER-stress induced transcription factors, such as ATF4 may act in a compensatory fashion to upregulate the expression of these genes. However, in the current study, only small differences were observed for Bcl-2 expression upon CCl_4 injection, suggesting that the expression of this antiapoptotic gene is not involved in the cell death processes induced by CCl_4.

Inflammation has also been reported to contribute to hepatotoxic-induced liver damage [22, 63, 80, 81]. In the current model with CCl_4 intoxication, it was shown that several potent chemokines were strongly induced upon CCl_4 injection (Fig 47). Surprisingly, expression of Ccl2 was markedly stronger in CHOP knockout compared to wild type (Fig 47). This result suggested that the inflammatory component of the responses induced in liver upon CCl_4 intoxication was also affected in the absence of CHOP.

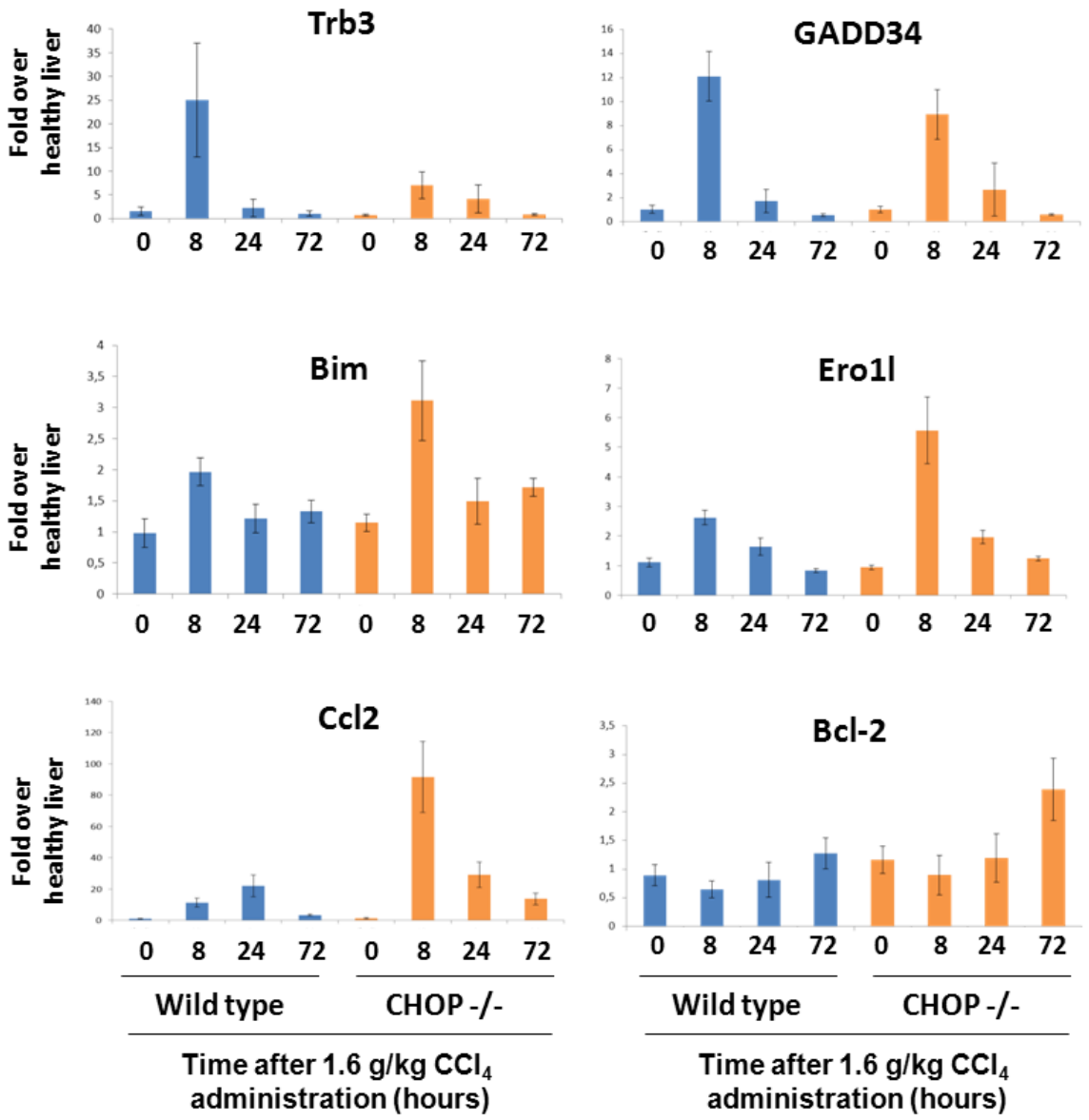

Figure 47: Evidence for compensatory mechanisms in CHOP knockout mice upon CCl_4 intoxication. Analysis of several CHOP-associated target genes was performed by qRT-PCR in liver tissue from wild type C57B6/J mice and CHOP knockout mice after CCl_4 administration. Genetic depletion of CHOP resulted in a weaker induction of Trb3, however all other CHOP-associated genes were not affected. The fold change was determined using healthy liver tissue as control (0 hours of CCl_4), and normalized to the levels of GAPDH. Bars correspond to average of 5 independent biological replicas. Error bars indicate standard error.

These results indicate that genetic deletion of CHOP causes a complex set of transcriptional mechanisms that compensate for its absence in the induction of ER-stress dependent genes. Furthermore, a novel role for ER-stress and CHOP was revealed by the

markedly stronger induction of the chemokine Ccl2 in CHOP knockout mouse liver after CCl_4 injection.

6.14 **CHOP KO mice show lower protein levels of the proliferation marker PCNA**

The larger dead cell areas in CHOP knockout livers may reflect a compromised proliferative response. To assess the extent of liver regeneration, the cell proliferation marker PCNA was analysed by western blot in mouse liver after a single CCl_4 intraperitoneal injection (1.6 g/kg). Protein extracts from 4 independent mice per time point were probed with PCNA antibodies, and β-actin was used as loading control. Consistent with this hypothesis, PCNA expression was markedly weaker in CHOP knockout livers compared to wild type (Fig 48).

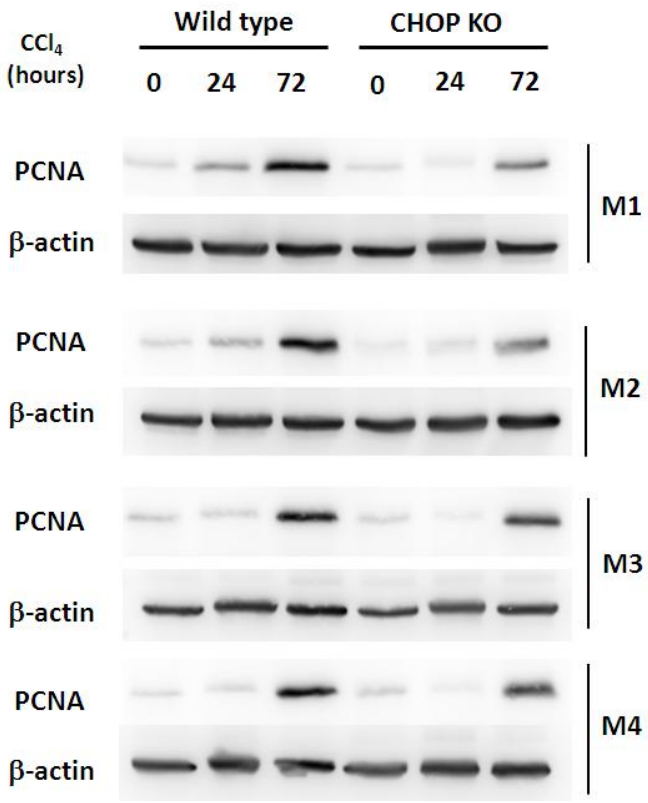

Figure 48: Genetic depletion of CHOP affects the regenerative response in liver after CCl_4-induced injury. The regenerative response in mouse liver after CCl_4 was assessed by western blot analysis of the cell proliferation marker PCNA. β-Actin was used as loading control. The results are representative of 4 mice per time point and condition.

These results suggest that CHOP contributes to several aspects of the molecular responses induced in liver injury after intoxication with CCl_4. The details of this contribution remain to be further investigated.

6.15 The activation of ER-stress pathways differentiate between the toxic mechanisms of paracetamol and CCl_4

The strong activation of ER-stress dependent pathways upon CCl_4 intoxication suggested that these mechanisms may also participate in other models of drug-induced liver injury. The antipyretic and analgesic drug Paracetamol or APAP (n-acetyl-p-aminophen) is a well reported hepatotoxicant [22, 82]. APAP toxicity occurs via similar mechanisms as CCl_4, whereby APAP is also metabolically activated through Cyp2E1 into a highly reactive oxidative intermediary (NAPQI), which generates protein adducts that lead to the activation of stress signalling such as JNK [15, 30]. Therefore, C57BL/6N mice were challenged with a single intraperitoneal injection of 500 mg/kg APAP dissolved in sterile PBS. Blood and liver tissue were collected at 2, 8 and 24h after APAP administration for further analyses as described for CCl_4. Five mice were analysed per time point.

Liver damage was clearly induced by APAP as determined by serum transaminase activity (Fig 49), although the extent of injury was less compared with the 1.6 g/kg dose of CCl_4 (Fig 49). Also, the time course of liver damage was different than in the CCl_4 model, whereby the peak of transaminase release was observed at 8h after APAP whereas for CCl_4 this peak was reached at day 1 (Fig 49).

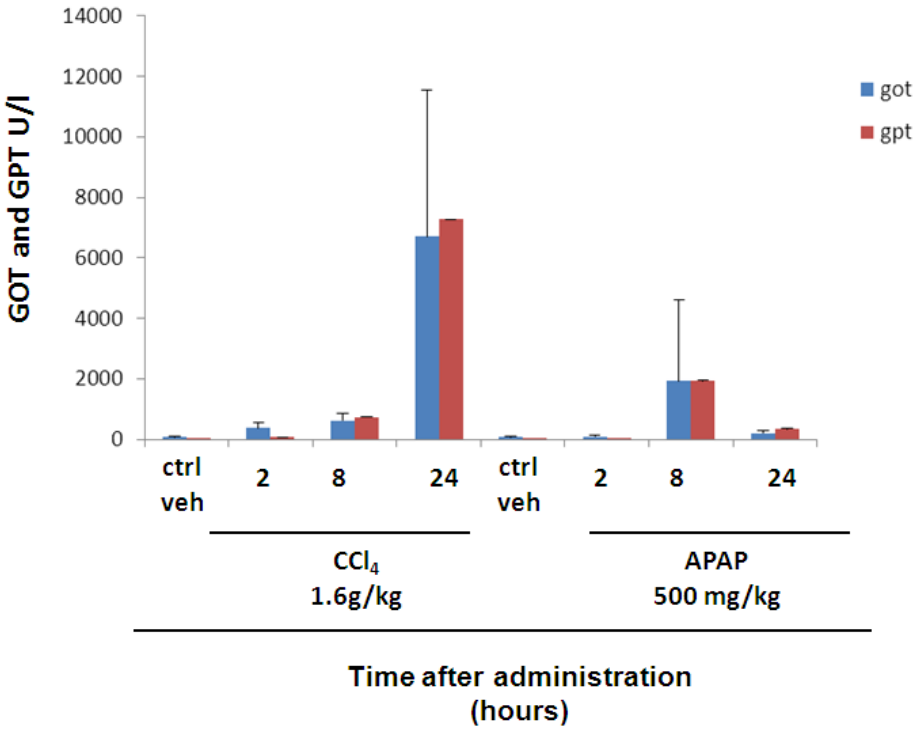

Figure 49: Comparison of plasma transaminase activities in mice after a single intraperitoneal injection of CCl_4 (1.6 g/kg) or APAP (500 mg/kg). A marked increase in GOT (blue) and GPT (red) activities was observed in plasma of mice after CCl_4 or APAP administration. However, differences were observed in the kinetics and extent of tissue damage. While the maximum damage with CCl_4 was reached 24h after injection, this occurred at 8h after APAP administration. Also, CCl_4 intoxication resulted in more extensive tissue damage, with maximal GOT and GPT levels twice as high compared to those observed after APAP intoxication. The bars are the mean values of four mice per time point ± Standard deviation.

In contrast with the CCl_4 model, histological examination of APAP treated livers did not reveal an extensive dead cell area (Fig 50). Only a marked differential eosin staining was observed around central veins, which may be associated with the hepatotoxic reaction in hepatocytes. On day 1 after APAP administration the livers looked normal. These results were consistent with the serum transaminase activity measurements (Fig 49).

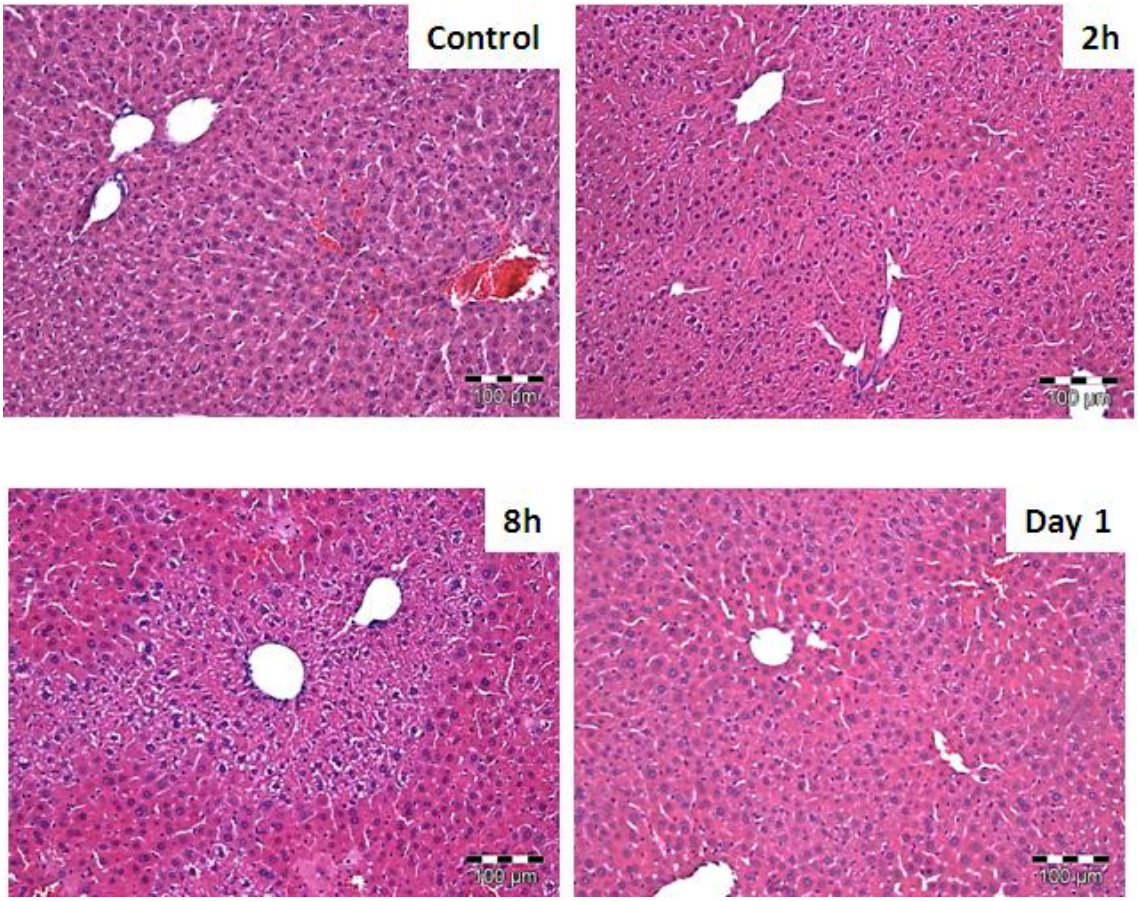

Figure 50: Histological examination of APAP-induced liver damage by H&E staining. Paraffin embedded liver sections stained with H&E were examined under bright light microscopy (100X magnification). Microscopic examination revealed a differential staining in pericentral hepatocytes at 8h after APAP administration (500 mg/kg), which correlated well with the maximum GOT and GPT activities in serum, suggesting that the observed staining pattern corresponded to hepatocyte injury. However, the tissue damage was different from that observed after CCl_4 intoxication. Five mice per time point were analyzed with similar results. Scale bars represent 100 µm.

Similar as CCl_4, APAP-induced hepatotoxicity also induced expression of CHOP mRNA (Fig 51) starting at 2h and reaching a maximum at 8h, comparable to the kinetics observed in the CCl_4 model (Fig 51). However, in the APAP model, CHOP mRNA reached levels comparable to control conditions at 24h while in the CCl_4 model the expression of CHOP remained at high levels at this time point (Fig 51).

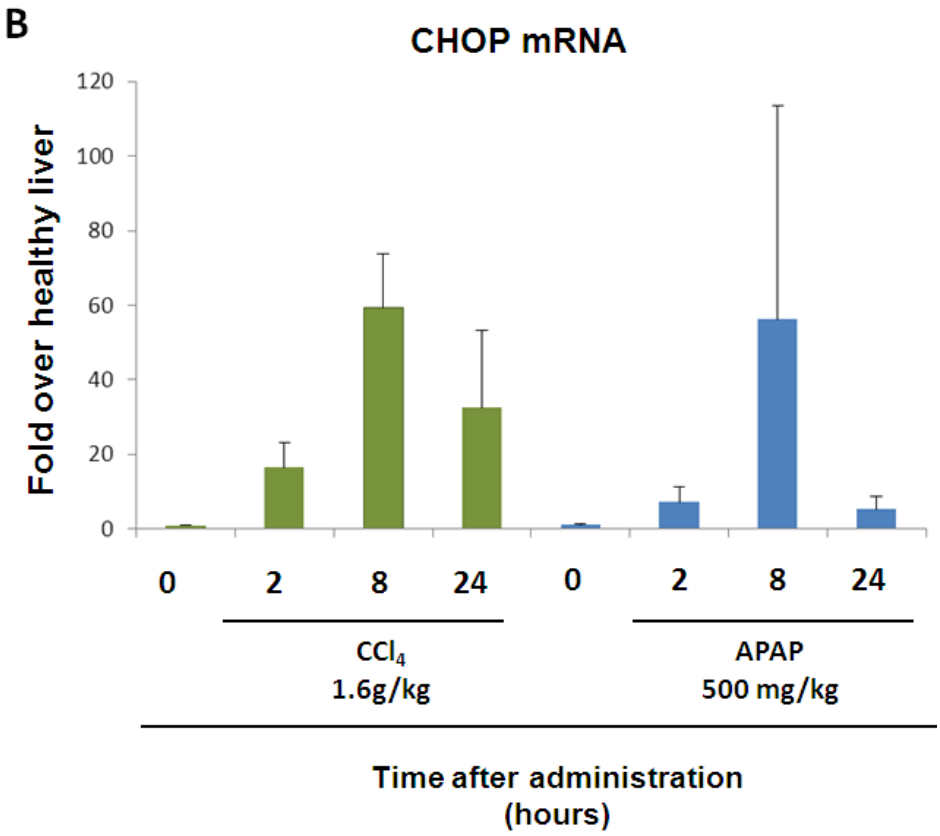

Figure 51: A comparable induction of CHOP mRNA was induced in mouse liver after CCl_4 and APAP administration. The transcriptional induction of CHOP mRNA was detected by qRT-PCR analysis in liver tissue from mice after CCl_4 (1.6 g/kg) or APAP (500 mg/kg). The maximal induction of CHOP mRNA was observed at 8h after administration of each compound. The fold change was determined using healthy liver tissue as control (0 hours of CCl_4), and normalized to the levels of GAPDH. Bars correspond to average of 5 independent biological replicas. Error bars indicate standard error.

Interestingly, APAP-induced liver damage did not result in splicing of Xbp1 (Fig 52) and expression of CHOP protein (Fig 52), indicating that the toxic response of APAP differs from that of CCl_4.

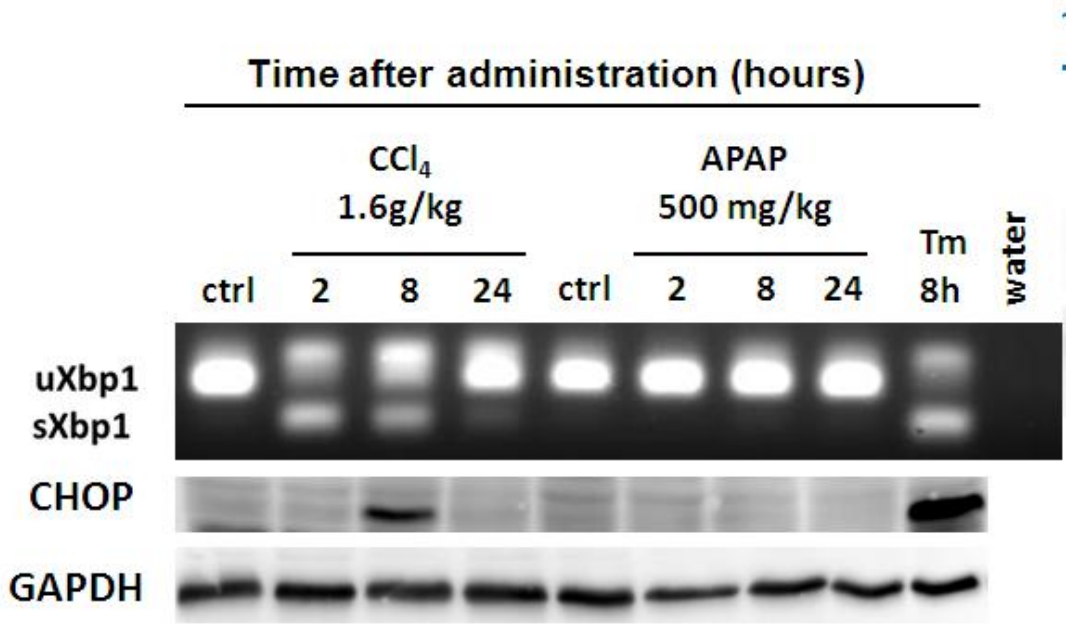

Figure 52: Activation of ER-stress pathways differs between the mechanisms induced by CCl_4 and APAP. The splicing of Xbp1 mRNA in mouse liver, which depends on the activation of the ER-stress sensor IRE1α, was observed only after CCl_4 but not after APAP-induced liver damage, as evidenced by PCR analysis of Xbp1 mRNA using primer pairs flanking the spliced region. Similarly, induction of CHOP protein was detected only after CCl_4 but not after APAP-induced liver damage. β-Actin was used as loading control. The results are representative of at least 4 mice per time point and condition. As positive control for both Xbp1 splicing and for CHOP protein expression, liver extracts from mice treated for 8h with 5 mg/kg tunicamycin were used.

Histological analysis of CHOP protein in mouse liver after APAP administration revealed an induction in hepatocyte nuclei that peaked at 8h after APAP injection (Fig 53). However, the expression levels were markedly lower than in CCl_4 exposed livers (Fig 53), which was consistent with the results obtained by western blot (Fig 52). These results suggested that APAP induces a weaker ER-stress response compared to CCl_4 in mouse liver.

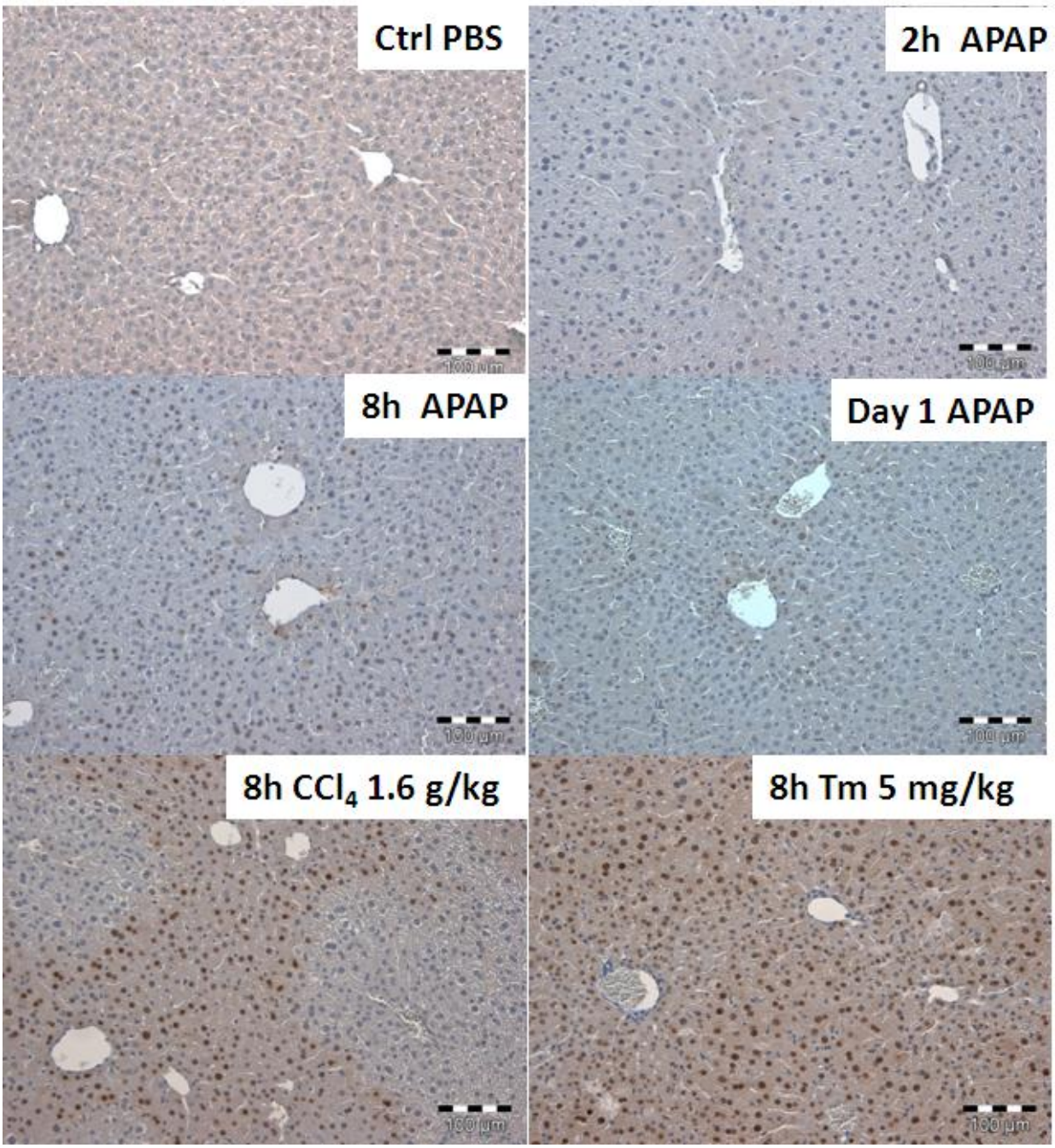

Figure 53: Immunohistochemical analysis of CHOP in mouse liver after APAP, CCl_4 and tunicamycin administration. The expression and localization of the transcription factor CHOP was assessed in paraffin embedded liver sections. In control (PBS treated) livers, no detectable expression of CHOP was observed. After 8h of APAP administration, CHOP positive nuclei were observed in hepatocytes near central veins, which was the time point when maximal CHOP expression was detected. On day 1, a weaker expression of CHOP was observed in some hepatocytes. Consistent with the previous western blot analyses, the intensity of CHOP expression 8h after APAP administration was significantly weaker compared to livers of mice treated for 8h with CCl_4 (1.6 g/kg) or tunicamycin (Tm, 5 mg/kg). Scale bars represent 100 µm.

Finally, the expression of CHOP-associated target genes was analyzed by qRT-PCR in APAP-exposed mouse livers, and compared to the expression induced by CCl_4. Consistent with the weaker expression of CHOP in the APAP model, the induction of target genes Trb3 and Ero1l were weaker in APAP compared to CCl_4 treated mouse liver (Fig 54). However, the induction of GADD34 was almost identical in both models of hepatotoxicity (Fig 54). Considering the weaker induction of CHOP in the APAP model, these results are in line with the observations in CHOP knockout mice challenged with CCl_4, where only Trb3 was severely affected by the absence of CHOP while other ER-stress dependent genes such as Ero1l and GADD34 seemed to be controlled by compensatory mechanisms (Fig 54).

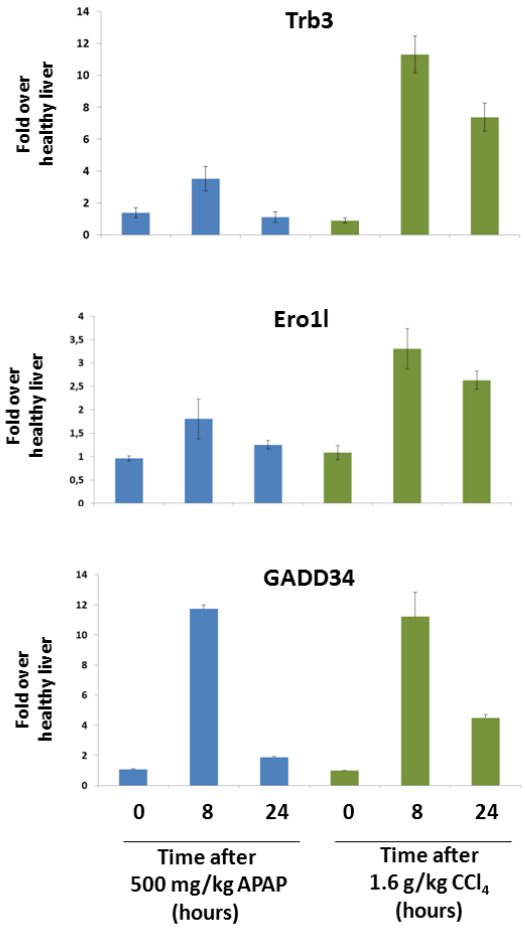

Figure 54: Differential induction of ER-stress dependent genes by APAP and CCl_4 in mouse liver. The transcriptional induction of Trb3, Ero1l and GADD34 mRNA was detected by qRT-PCR analysis in liver tissue from mice after APAP (500 mg/kg) or CCl_4 (1.6 g/kg). The maximal induction of these genes was detected after 8h of APAP or CCl_4 administration. The expression of Trb3 and Ero1l was markedly stronger in CCl_4 treated liver compared to APAP, while expression of GADD34 was comparable in both models of liver damage. The fold change was determined using healthy liver tissue as a control, and normalized to the levels of GAPDH. Bars correspond to the average of 5 independent biological replicas. Error bars indicate standard error.

7 Discussion

The liver reacts to hepatotoxic injuries by triggering a myriad of cellular and molecular mechanisms. However, the precise mechanisms controlling the response to toxicants in vivo are poorly understood. By combining a robust in vivo model of CCl_4-induced liver damage and regeneration with gene array analysis, bioinformatics and molecular biology techniques, my work unraveled detailed features of the transcriptional regulatory networks activated in response to acute liver injury, which I summarize in Fig 55. During the first 2h after intoxication, a strong transcriptional response was induced, together with activation of MAPK and inflammation-associated pathways such as ERK, JNK and STAT3, respectively. This response was followed by a second wave of gene expression between 8h and day 2, which involved two main features: 1) a potent induction of inflammation including the transcription factor CEBP/δ and chemokines such as Ccl2 and Cxcl1, and 2) activation of ER-stress dependent pathways, including splicing of Xbp1 and upregulation of the transcription factor CHOP. A third wave of gene expression between day 1 and day 4 included a massive downregulation of metabolism-associated genes, including P450 enzymes, and an upregulation of genes involved in cell proliferation (Fig 55). This analysis provides a detailed description of fundamental biological events occurring in a time-dependent fashion upon exposure to a hepatotoxic compound.

Perhaps the best understood aspect of this response has to do with the activation of a regeneration program [47]. The mechanisms involved in this process include the concerted activity of several growth factors and cytokines, such as TNFα, HGF, EGF and IL-6 [83-85]. These factors have been extensively studied in surgical models of liver regeneration such as partial hepatectomy [84, 85], and also in models of acute liver damage with hepatotoxins [86-88]. In the current study, the extent of tissue damage and the timing of regeneration were perfectly consistent with several previous reports [47, 64]. The current gene array analysis did not detect expression of TNFα, HGF, EGF or IL-6. However, the phosphorylations of ERK1/2 and STAT3 during the first 2h after CCl_4 administration are consistent with the previously described activation timing of these pathways upon CCl_4 challenge [63-65], suggesting that these factors were also induced in the current study.

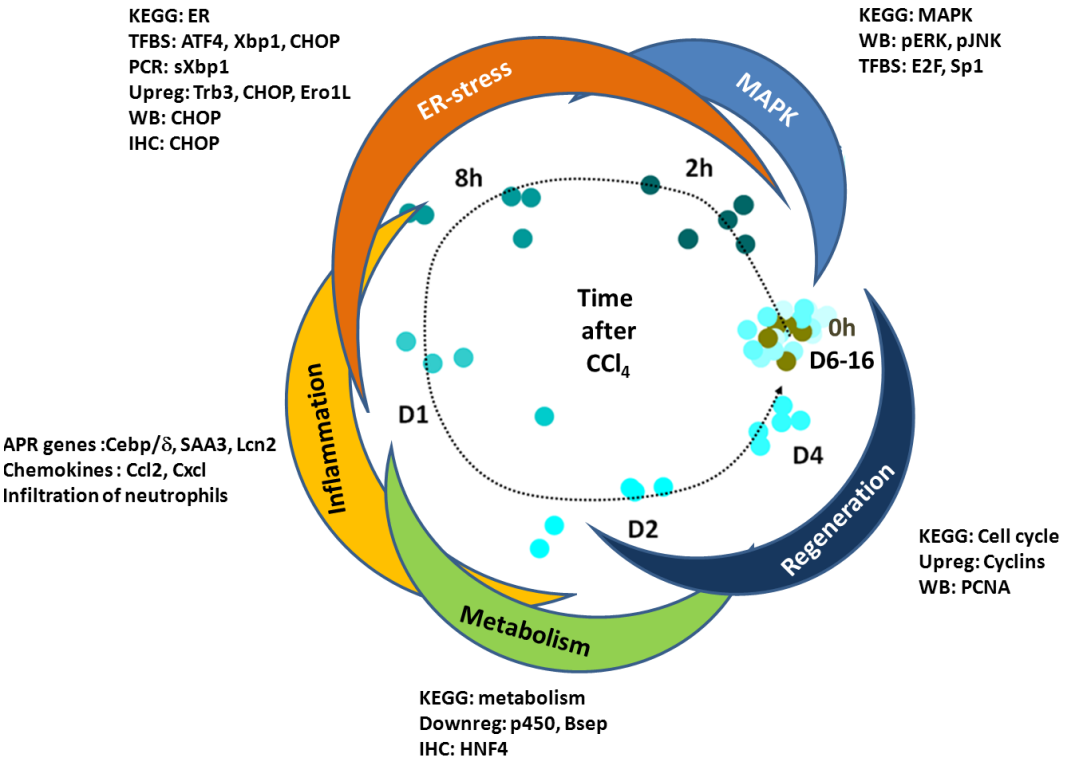

Figure 55. Transcriptional regulatory networks induced upon acute liver damage by CCl_4. A combination of bioinformatics, histological molecular biology techniques allowed the identification of time-dependent biological motifs during liver damage and regeneration. The figure shows in the middle the principal component analysis of gene expression in liver after intoxication with CCl_4, and the biological motifs identified by bioinformatics, histological and molecular biology techniques. First, intracellular alterations induced by CCl_4 metabolism cause activation of stress pathways including JNK, ERK and ER-stress. These pathways cause a strong transcriptional response which includes expression of ER-stress associated genes such as CHOP, Ero1l and Trb3. Afterwards, an inflammation response occurs, characterized by the nuclear translocation of CEBP/δ and induction of chemokines such as Ccl2, and recruitment of leukocytes (i.e. neutrophils). These events are followed by a massive repression of metabolism-associated genes, including bile salt pumps and P450 enzymes. Finally, a regeneration response takes place, whereby the loss liver parenchyma is replaced by proliferating hepatocytes.

However, an important aspect of these signal transduction events which was not resolved in the current study is the precise localization where signaling takes place in the liver lobule, i.e. in pericentral or periportal zones. Furthermore, the western blot analyses in this study were performed using whole liver protein extracts. Thus, it is not possible to identify the cell types in the liver where these signaling pathways become activated. This becomes important for systems biology approaches where mathematical modelling of time-resolved damage and regeneration still require space-temporal data of the signaling pathways that determine cellular responses such as cell death or cell proliferation [47]. The current models

can accurately predict time-dependent proliferation events upon loss of liver mass [47]. However they have not yet incorporated signal transduction or gene expression patterns as decision-making parameters in hepatocytes to engage proliferation. Hence, the results obtained in this thesis will provide a robust platform to identify time-resolved gene expression conducing to hepatocyte proliferation.

A central result in this study was the massive downregulation of metabolism-associated genes, which correlated with the regenerative phase induced between day 2 and day 4. This response may be caused by the activation of MAPK (i.e. ERK and JNK) in early time points after CCl_4 administration. This hypothesis is supported by in vitro studies, where it was shown that the expression of the P450 enzyme Cyp7a1 was strongly downregulated by HGF-induced ERK activation in primary human hepatocytes [89], and by TNFα-induced JNK activation in primary rat hepatocytes [90]. In the current study, Cyp7a1 was among the strongest metabolism-associated downregulated genes. In addition, ERK and JNK were strongly activated 2h after CCl_4 administration. Therefore, it is likely that ERK and JNK may lead to similar effects in vivo as in isolated primary hepatocytes. However, it remains to be determined whether all metabolism-associated genes are controlled via the same pathways, or if additional signaling events are necessary to explain the overall repression of metabolism-associated genes.

A remarkable aspect linked to the repression of metabolism-associated genes was the marked downregulation of HNF4α on day 1 after CCl_4 administration. Since the constitutive expression of HNF4α controls the expression of many genes involved in liver metabolism [91], it is likely that the massive downregulation of metabolism-associated genes is related to the loss of HNF4α expression. This is supported by the observation that many binding sites for HNF4α were overrepresented in a large number of downregulated, metabolism-associated genes. How these signal transduction pathways repress HNF4α expression remains unclear. A possible mechanism involved in HNF4α downregulation is the activation of ERK. In HepG2 hepatoma cells, activation of ERK induced a transient repression of HNF4α mRNA and protein expression, whereas exposure to a MAPK inhibitor PD98059 induced upregulation of HNF4α mRNA and protein [92]. Since ERK was activated as early as 2h after CCl_4 administration, it is likely that it contributes to the repression of HNF4α expression observed on day 1. However, it is not clear whether the intensity of ERK activation observed in the

current study is sufficient to generate the same effect observed in vitro [92]. Furthermore, ERK was also activated at late time points (i.e. day 2) after CCl_4 administration, and HNF4α expression was not repressed at this time point. Therefore, the precise signaling constellations regulating the expression of HNF4α in mouse liver remain to be further investigated. It is tempting to speculate that the massive repression of metabolism is necessary to ensure effective regeneration. This hypothesis is supported by the observation that overexpression of Cyp7a1 by adenovirus-mediated delivery in mouse liver caused enhanced liver injury after partial hepatectomy [93]. Similar to the observations in the current study with CCl_4 intoxication, Zhang et al demonstrated that Cyp7a1 was downregulated during liver regeneration after partial hepatectomy. Overexpression of Cyp7a1 via adenovirus delivery previous to hepatectomy resulted in enhanced serum transaminase activity and increased hepatocyte apoptosis [93]. These effects were not observed in mice treated with an empty vector [93], indicating that the enhanced damage in the liver was due to Cyp7a1 overexpression and not because of adenovirus infection. Although partial hepatectomy differs in critical aspects from intoxication with CCl_4, the study by Zhang et al [93] suggests that the repression of metabolism-associated genes during liver regeneration is necessary to prevent cellular damage.

An important aspect revealed during my thesis is the strong activation of inflammation in early stages after CCl_4 injection. This was evidenced by the induction of cytokines and chemokines such as Cxcl1 and Ccl2, and the upregulation and nuclear translocation of the inflammation-associated transcription factor CEBP/δ [75], followed by upregulation of acute phase response genes such as SAA3 and Lcn2. Although it was not surprising to observe a strong inflammation response at day 1, considering the extensive liver damage induced by CCl_4 intoxication, some inflammation markers were induced within the first 2h after CCl_4 administration, when extensive cellular damage has not yet occurred. These results suggest that early cues, most likely by intracellular signals in hepatocytes where CCl_4 is metabolized and begins to cause macromolecule alterations, may promote the subsequent wave of inflammation. One mechanism by which intracellular alterations cause inflammation is the inflammasome, a multi-protein complex that promotes activation of interleukin-1 via caspase-1 [94]. One component of the inflammasome is NALP3 (NACHT, LRR and pyrin domain-containing protein-3) a protein that recognizes endogenous signals such as monosodium urate (MSU), ATP and calcium pyrophosphate dehydrate [95]. These molecules induce

oligomerization of NALP3, which triggers the recruitment of ASC and pro-caspase-1, leading to proteolytic activation of caspase-1. Active caspase-1 cleaves inactive IL-1 and IL-18 into their active forms [94]. A recent report described a potential role for the NALP3-inflammasome in APAP-induced liver injury [26]. However, the authors suggest that the inflammasome activation occurs in non-parenchymal cells rather than in hepatocytes [26]. The results in my thesis do not allow a precise identification of the initial mechanisms inducing inflammation. However, the fact that CCl_4-induced damage occurs first in hepatocytes suggests that either the inflammasome is activated in these cells or that signals derived from stressed hepatocytes can activate the inflammasome in neighboring non-parenchymal cells such as sinusoidal endothelial cells or Kupffer cells.

The role of inflammation in drug-induced liver injury is still controversial. To date, most studies in this area have been conducted using APAP as a model hepatotoxic compound. Initial reports using antibodies to deplete leukocytes such as neutrophils [81] or natural killer cells [80] suggested that these cells exacerbated tissue injury caused by APAP. However, careful considerations must be taken in the interpretation of those studies. It has been demonstrated that the antibodies used to deplete leukocytes induce the expression of metallothionein 1 and 2 in hepatocytes [96]. These proteins act as potent scavengers of reactive oxygen or nitrogen species which are critical for APAP-induced cell killing [96] which could account for the protective effect observed in the studies where antibodies were used to deplete leukocytes [80, 81, 97]. A better documented role of inflammation is the recruitment of macrophages, which occurs during the progression of tissue damage on days 1 and 2.

The extensive tissue injury induced by CCl_4 or APAP causes the release of danger associated molecular pattern (DAMPs) such as heat shock proteins and DNA [98]. These molecules can activate toll-like receptors in sinusoidal endothelial cells and in resident macrophages (Kupffer cells) [26], triggering the secretion of chemokines that recruit circulating monocytes [98]. Depletion of circulating monocytes by irradiation, or depletion of resident liver macrophages (Kupffer cells) by administration of clodronate liposomes induced a delayed regeneration response after APAP-induced liver damage [24]. These cells have been well documented to mediate removal of cell debris, thus contributing to the regeneration process [22]. In conclusion, my thesis identified a strong inflammatory component in the

transcriptional response induced by CCl_4 intoxication. This can be subdivided into an early, stress-related response, which includes expression of chemokines, cytokines and activation of the transcription factor CEBP/δ, and a late response whereby macrophages are recruited to remove cell debris which is necessary for proper tissue regeneration.

An interesting connection between inflammation and metabolism comes from studies where endotoxemia-induced inflammation caused a repression of metabolism-associated genes in the liver [99-101]. It is likely that the sterile inflammation caused by DAMPs released during CCl_4-induced liver damage also influence expression of metabolism genes. This suggested that inflammation and repression of metabolism may be a general feature of liver stress responses. Therefore, a comparison of the transcriptional responses induced in profoundly different stress conditions, namely CCl_4 intoxication, partial hepatectomy, LPS exposure and hepatocyte isolation and cultivation was performed. This analysis revealed a high overlap in the transcriptional responses on all perturbations tested, suggesting that inflammation and repression of metabolism constitutes a stereotypic stress response in hepatocytes. A detailed examination of representative genes of inflammation and metabolism showed that not all metabolism-associated genes were equally affected in each model. This indicates that although inflammation and metabolism gene clusters are similarly affected in all models of liver stress, the specific genes which are modulated on each response may differ. Therefore, further studies may reveal precise gene expression signatures for specific types of liver stress.

Stress responses, in particular stress-associated signal transduction pathways, have been recently demonstrated to play crucial roles in drug-induced hepatotoxicity [14, 15, 30]. Therefore, a closer examination on CCl_4-induced stress signaling was taken, which showed that stress pathways such as JNK were activated within the first 2h after CCl_4 administration. Considering that tissue damage at this time point was minimal, the activation of JNK suggested that stress signaling events may occur within hepatocytes exposed to CCl_4. Bioinformatics analysis showed an overrepresentation of endoplasmic reticulum associated genes induced within this time frame, suggesting that ER-stress pathways may have been activated during the early time points after CCl_4 administration. This was confirmed by several markers: i) Xbp1 splicing, which occurs as a consequence of the RNAse activity of the ER sensor IRE1α [37], ii) phosphorylation of eIF2α, which depends on the activation of

the ER sensor PERK [35] and iii) induction of CHOP expression at mRNA and protein, which depends on the activation of several ER-stress sensors, including PERK [38]. The hypothesis that these pathways were induced in hepatocytes by CCl_4 was confirmed by histological examination of CHOP, which was found only in hepatocyte nuclei, and more precisely, on hepatocytes near central veins, which corresponds to the area where CCl_4 is metabolized to its highly reactive intermediaries by Cyp2E1 [62].

ER-stress pathways have been well documented to generate a strong transcriptional response [36, 37]. However, their precise influence on cell behavior is still not fully understood. The current view on ER-stress pathways indicates that short, mild ER-stress activates mechanisms aimed to restore homeostasis to the ER, including a general attenuation of mRNA translation by phosphorylation of eIF2α, and induction of ER-chaperones such as Bip [37]. Conversely, long or intense ER-stress has been shown to cause cell death [36, 38]. A central mediator of ER-stress induced cell killing is the transcription factor CHOP [36, 38]. Therefore, the observation that CHOP expression was induced in hepatocytes in pericentral areas, which correspond to the areas where tissue injury takes place, suggested that ER-stress may contribute to the cell killing induced by CCl_4. To test this hypothesis, CHOP knockout mice were challenged with CCl_4 and compared to wild type mice of the same genetic background. Surprisingly, CHOP knockout mice were not protected against CCl_4-induced liver damage. Rather, larger tissue damage was observed in those mice, even when challenged with a minimal CCl_4 dose. These negative results are in contrast to a recent publication using the same CHOP knockout mice strain [102]. The authors used identical readouts as in the present study, namely liver transaminases and quantification of the dead cell area. They report a large protective effect of the CHOP knockout leading to a 10-fold lower dead cell area compared to wild type [102]. The obvious discrepancy to the present study remains difficult to explain. Possibly APAP as applied by Uzi et al [102] and CCl_4 as used in the present study may cause different responses. This has been shown for example by the different role of JNK signaling in both models, where JNK inhibitors protected against APAP but not CCl_4-induced liver damage [30]. Nevertheless, it should be considered that in the present study CCl_4 also caused ER-stress, with induction of CHOP and CHOP-dependent genes. In the current study, a stronger Xbp1 splicing induced by CCl_4 was observed compared to the effect induced by APAP [102]. Therefore, the discrepancy between APAP and CCl_4 require further investigation.

Similar to APAP [22] also CCl_4 has been shown to induce apoptosis in hepatocytes [103, 104], although CCl_4 may also activate non-apoptotic pathways of cell death. Considering the huge amount of literature linking CHOP to apoptosis [36, 38, 41, 44, 105], the present negative result is unexpected. A possible explanation may be compensatory mechanisms mediated by other transcription factors. Therefore, the expression of Trb3, Ero1l, GADD34, Bim and Bcl-2 was analyzed, genes which have been reported to be CHOP dependent [36, 106]. In those studies, ER-stress was induced in fibroblasts which led to induction of GADD34, Ero1l and Trb3 expression. This induction was clearly reduced in CHOP knockout fibroblasts [106]. In the present study, using CCl_4 and liver tissue, ER-stress associated genes Trb3, Ero1l, GADD34 and Bim were also induced in wild type mice. However, I did not observe reduced expression of Ero1l, GADD34 and Bim in CHOP knockout compared to wild type mice. Ero1l was even higher in CHOP knockout compared to wild type mice. Only the decrease of Trb3 as a consequence of the CHOP knockout could be confirmed, although the degree of reduction was much milder compared to the effect reported by Han et al [106]. The liver is well known for its enormous repertoire of compensatory mechanisms [23]. Therefore, the lack of protection against CCl_4-induced hepatotoxicity in CHOP knockout mice, suggests that in hepatocytes, CHOP can be compensated by alternative factors.

A surprising result of this study was the absence of a protective effect in the CHOP knockout mice, but rather an increased level of tissue damage (Fig 41 and 42). Transaminases, as well as the dead cell area after CCl_4 intoxication were slightly higher in CHOP knockout compared to wild type mice. However, since the difference observed was small, it still should be interpreted with caution unless reproduced in a larger cohort of mice. However, it should be considered that besides CHOP, CCl_4 also induced the IRE1α pathway which may cause cell death by alternative pathways. In conclusion, the role of CHOP in hepatotoxicity may be more complex than hitherto expected and may not strictly be linked to apoptosis. The present study demonstrates that CHOP as a biomarker for ER-stress-induced hepatotoxicity should be treated with caution, because at least in the case of CCl_4 it is not linked to cell death.

8 Literature

1. Tredger, J.M., *DRUG METABOLISM AND HEPATOTOXICITY*. The liver in biology and disease, ed. E. Bittar. 2004, London, UK: Elsevier.

2. Bataller, R. and D.A. Brenner, *Liver fibrosis.* Journal of Clinical Investigation, 2005. **115**(2): p. 209-218.

3. Benhamouche, S., et al., *Apc tumor suppressor gene is the "zonation-keeper" of mouse liver.* Dev Cell, 2006. **10**(6): p. 759-70.

4. Colnot, S. and C. Perret, *Liver Zonation.* 2011. **5**: p. 7-16.

5. Groves, J.T., *Models and Mechanisms of Cytochrome P450 Action*. Third ed. Cytochrome p450. Structure, mechanism and biochemistry, ed. P.R.O.d. Montellano. 2005, New York: KluwerAcadennic/Plenum Publishers.

6. Wilke, R.A., et al., *Identifying genetic risk factors for serious adverse drug reactions: current progress and challenges.* Nat Rev Drug Discov, 2007. **6**(11): p. 904-16.

7. Park, B.K., et al., *The role of metabolic activation in drug-induced hepatotoxicity.* Annu Rev Pharmacol Toxicol, 2005. **45**: p. 177-202.

8. Jaeschke, H., et al., *Models of drug-induced liver injury for evaluation of phytotherapeutics and other natural products.* Food Chem Toxicol, 2013. **55**: p. 279-89.

9. Kaufman, D.W., et al., *Recent patterns of medication use in the ambulatory adult population of the United States: the Slone survey.* JAMA, 2002. **287**(3): p. 337-44.

10. Zaher, H., et al., *Protection against acetaminophen toxicity in CYP1A2 and CYP2E1 double-null mice.* Toxicol Appl Pharmacol, 1998. **152**(1): p. 193-9.

11. Tonge, R.P., et al., *Role of CYP1A2 in the hepatotoxicity of acetaminophen: investigations using Cyp1a2 null mice.* Toxicol Appl Pharmacol, 1998. **153**(1): p. 102-8.

12. Matthews, A.M., et al., *Acetaminophen-induced hepatotoxicity. Analysis of total covalent binding vs. specific binding to cysteine.* Drug Metab Dispos, 1996. **24**(11): p. 1192-6.

13. Mitchell, J.R., et al., *Acetaminophen-induced hepatic necrosis. IV. Protective role of glutathione.* J Pharmacol Exp Ther, 1973. **187**(1): p. 211-7.

14. Han, D., et al., *Regulation of drug-induced liver injury by signal transduction pathways: critical role of mitochondria.* Trends Pharmacol Sci, 2013. **34**(4): p. 243-53.

15. Hanawa, N., et al., *Role of JNK translocation to mitochondria leading to inhibition of mitochondria bioenergetics in acetaminophen-induced liver injury.* J Biol Chem, 2008. **283**(20): p. 13565-77.

16. Dara, L., C. Ji, and N. Kaplowitz, *The contribution of endoplasmic reticulum stress to liver diseases.* Hepatology, 2011. **53**(5): p. 1752-63.

17. Weber, L.W., M. Boll, and A. Stampfl, *Hepatotoxicity and mechanism of action of haloalkanes: carbon tetrachloride as a toxicological model.* Crit Rev Toxicol, 2003. **33**(2): p. 105-36.

18. Raucy, J.L., J.C. Kraner, and J.M. Lasker, *Bioactivation of halogenated hydrocarbons by cytochrome P4502E1.* Crit Rev Toxicol, 1993. **23**(1): p. 1-20.

19. Dianzani, *Lipid peroxidation and haloalkylation: two distinct mechanism for CCl4-induced liver damage.* Liver and Lipid Metabolism, Elsevier Exerpta Medica, Amsterdam 1984: p. 39-50.

20. Yuan, L. and N. Kaplowitz, *Mechanisms of drug-induced liver injury.* Clin Liver Dis, 2013. **17**(4): p. 507-18, vii.

21. Saberi, B., et al., *Protein kinase C (PKC) participates in acetaminophen hepatotoxicity through c-jun-N-terminal kinase (JNK)-dependent and -independent signaling pathways.* Hepatology, 2013.

22. Jaeschke, H., et al., *Acetaminophen hepatotoxicity and repair: the role of sterile inflammation and innate immunity.* Liver Int, 2012. **32**(1): p. 8-20.

23. Godoy P, H.N., Albrecht U, Andersen ME, Ansari N, Bhattacharya S, Bode JG, et al., *Recent advances in 2D and 3D in vitro systems using primary hepatocytes, alternative hepatocyte sources and non-parenchymal liver cells and their use in investigating mechanisms of hepatotoxicity, cell signaling and ADME. .* Arch Toxicol 2013, 2013. **87:1315-1530**.

24. Campion, S.N., et al., *Hepatic Mrp4 induction following acetaminophen exposure is dependent on Kupffer cell function.* Am J Physiol Gastrointest Liver Physiol, 2008. **295**(2): p. G294-304.

25. Holt, M.P., L. Cheng, and C. Ju, *Identification and characterization of infiltrating macrophages in acetaminophen-induced liver injury.* J Leukoc Biol, 2008. **84**(6): p. 1410-21.

26. Imaeda, A.B., et al., *Acetaminophen-induced hepatotoxicity in mice is dependent on Tlr9 and the Nalp3 inflammasome.* J Clin Invest, 2009. **119**(2): p. 305-14.

27. James, L.P., et al., *Interleukin 6 and hepatocyte regeneration in acetaminophen toxicity in the mouse.* Biochem Biophys Res Commun, 2003. **309**(4): p. 857-63.

28. Gardner, C.R., et al., *Exaggerated hepatotoxicity of acetaminophen in mice lacking tumor necrosis factor receptor-1. Potential role of inflammatory mediators.* Toxicol Appl Pharmacol, 2003. **192**(2): p. 119-30.

29. Ishida, Y., et al., *A pivotal involvement of IFN-gamma in the pathogenesis of acetaminophen-induced acute liver injury.* FASEB J, 2002. **16**(10): p. 1227-36.

30. Gunawan, B.K., et al., *c-Jun N-terminal kinase plays a major role in murine acetaminophen hepatotoxicity.* Gastroenterology, 2006. **131**(1): p. 165-78.

31. Saito, C., J.J. Lemasters, and H. Jaeschke, *c-Jun N-terminal kinase modulates oxidant stress and peroxynitrite formation independent of inducible nitric oxide synthase in acetaminophen hepatotoxicity.* Toxicol Appl Pharmacol, 2010. **246**(1-2): p. 8-17.

32. Nakagawa, H., et al., *Deletion of apoptosis signal-regulating kinase 1 attenuates acetaminophen-induced liver injury by inhibiting c-Jun N-terminal kinase activation.* Gastroenterology, 2008. **135**(4): p. 1311-21.

33. Malhi, H. and R.J. Kaufman, *Endoplasmic reticulum stress in liver disease.* J Hepatol, 2011. **54**(4): p. 795-809.

34. Schroder, M. and R.J. Kaufman, *ER stress and the unfolded protein response.* Mutat Res, 2005. **569**(1-2): p. 29-63.

35. Hetz, C., *The unfolded protein response: controlling cell fate decisions under ER stress and beyond.* Nat Rev Mol Cell Biol, 2012. **13**(2): p. 89-102.

36. Tabas, I.a.R., David, *Integrating the mechanisms of apoptosis induced by endoplasmic reticulum stress.* Nat Cell Biol 2011. **13, 3**

37. Ron, D. and P. Walter, *Signal integration in the endoplasmic reticulum unfolded protein response.* Nat Rev Mol Cell Biol, 2007. **8**(7): p. 519-29.

38. Oyadomari, S. and M. Mori, *Roles of CHOP/GADD153 in endoplasmic reticulum stress.* Cell Death Differ, 2004. **11**(4): p. 381-9.

39. Puthalakath, H., et al., *ER stress triggers apoptosis by activating BH3-only protein Bim.* Cell, 2007. **129**(7): p. 1337-49.

40. McCullough, K.D., et al., *Gadd153 sensitizes cells to endoplasmic reticulum stress by down-regulating Bcl2 and perturbing the cellular redox state.* Mol Cell Biol, 2001. **21**(4): p. 1249-59.

41. Li, G., et al., *Role of ERO1-alpha-mediated stimulation of inositol 1,4,5-triphosphate receptor activity in endoplasmic reticulum stress-induced apoptosis.* J Cell Biol, 2009. **186**(6): p. 783-92.

42. Timmins, J.M., et al., *Calcium/calmodulin-dependent protein kinase II links ER stress with Fas and mitochondrial apoptosis pathways.* J Clin Invest, 2009. **119**(10): p. 2925-41.

43. Marciniak, S.J., et al., *CHOP induces death by promoting protein synthesis and oxidation in the stressed endoplasmic reticulum.* Genes Dev, 2004. **18**(24): p. 3066-77.

44. Zinszner, H., et al., *CHOP is implicated in programmed cell death in response to impaired function of the endoplasmic reticulum.* Genes Dev, 1998. **12**(7): p. 982-95.

45. Ohoka, Y., Hattori, Onozaki, Hayashi, *TRB3, a novel ER stress-inducible gene, is induced via ATF4–CHOP pathway and is involved in cell death.* The EMBO Journal, 2005. **24**: p. 1234-1255.

46. Du, K., et al., *TRB3: a tribbles homolog that inhibits Akt/PKB activation by insulin in liver.* Science, 2003. **300**(5625): p. 1574-7.

47. Hoehme S, B.M., Bauer A, Bedawy E, Schormann W, Hermes M, Puppe V, et al., *Prediction and validation of cell alignment along microvessels as order principle to restore tissue architecture in liver regeneration.* Proc Natl Acad Sci U S A 2010;107:10371-10376.

48. Granberg, R.A. and Å.C. Rasmuson, *Solubility of Paracetamol in Pure Solvents.* Journal of Chemical & Engineering Data, 1999. **44**(6): p. 1391-1395.

49. Hewitt, N.J., et al., *Primary hepatocytes: current understanding of the regulation of metabolic enzymes and transporter proteins, and pharmaceutical practice for the use of hepatocytes in metabolism, enzyme induction, transporter, clearance, and hepatotoxicity studies.* Drug Metab Rev, 2007. **39**(1): p. 159-234.

50. Madrahimov N, D.O., Broelsch C, Dahmen U. , *Marginal hepatectomy in the rat: from anatomy to surgery. .* Ann Surg 2006;244:89-98.

51. Uygun, B.E., et al., *Organ reengineering through development of a transplantable recellularized liver graft using decellularized liver matrix.* Nat Med, 2010. **16**(7): p. 814-20.

52. NG., A., *The mass isolation of whole cells from rat liver. .* Science 1953(117 .): p. 627-628.

53. Dunn JC, Y.M., Koebe HG, Tompkins RG., *Hepatocyte function and extracellular matrix geometry: long-term culture in a sandwich configuration. .* Faseb J 1989(3:174-177.).

54. Livak KJ, S.T.A.o.r.g.e.d.u.r.-t.q.P.a.t.-D.D.C.T.M.M.-. *Analysis of relative gene expression data using real-time quantitative PCR and the 2(-Delta Delta C(T)) Method. .* Methods Cell Biol, 2001;25:402-408.

55. Godoy P, H.J., Ilkavets I, Meyer C, Bachmann A, Muller A, Tuschl G, et al. , *Extracellular matrix modulates sensitivity of hepatocytes to fibroblastoid dedifferentiation and transforming growth factor beta-induced apoptosis.* Hepatology 2009;49:2031-2043.

56. BM., B., *Low Level Analysis of High-density OligonucleotideArray Data: Background, Normalization and Summarization. Berkeley: University of California; 2004.* Berkeley: University of California; 2004.

57. Gentleman RC, C.V., Bates DM, Bolstad B, Dettling M, Dudoit S, Ellis B, et al. , *Bioconductor: open software development for computational biology and bioinformatics.* . Genome Biol 2004;5:R80.

58. Gentleman R, C., V., Dudoit, S., Irizarry, R., Huber, W. , *Smyth GK: Limma: linear models for microarray data.* . 'Bioinformatics and Computational Biology Solutions using R and Bioconductor'. .

59. Dai M, W.P., Boyd AD, Kostov G, Athey B, Jones EG, Bunney WE, et al., *Evolving gene/transcript definitions significantly alter the interpretation of GeneChip data.* . Nucleic Acids Res 2005;33:e175.

60. Bezdek JC, H.R., *Numerical convergence and interpretation of the fuzzy c-shells clustering algorithm.* . IEEE Trans Neural Netw 1992;3:787-793.

61. Ulitsky I, M.-K.A., Shavit S, Sagir D, Linhart C, Elkon R, Tanay A, et al. . *Expander: from expression microarrays to networks and functions.* . Nat Protoc 2010;5:303-322.

62. Sekine, S., R. Ogawa, and Y. Kanai, *Hepatomas with activating Ctnnb1 mutations in 'Ctnnb1-deficient' livers: a tricky aspect of a conditional knockout mouse model.* Carcinogenesis, 2011. **32**(4): p. 622-8.

63. Horiguchi, N., et al., *Dissociation between liver inflammation and hepatocellular damage induced by carbon tetrachloride in myeloid cell-specific signal transducer and activator of transcription 3 gene knockout mice.* Hepatology, 2010. **51**(5): p. 1724-34.

64. Kwon, Y.H., et al., *The Cdk inhibitor p21 is required for necrosis, but it inhibits apoptosis following toxin-induced liver injury.* J Biol Chem, 2003. **278**(32): p. 30348-55.

65. Meng, Z., et al., *FXR regulates liver repair after CCl4-induced toxic injury.* Mol Endocrinol, 2010. **24**(5): p. 886-97.

66. Bezdek, J.C. and R.J. Hathaway, *Numerical convergence and interpretation of the fuzzy c-shells clustering algorithm.* IEEE Trans Neural Netw, 1992. **3**(5): p. 787-93.

67. Werner, T., *Bioinformatics applications for pathway analysis of microarray data.* Curr Opin Biotechnol, 2008. **19**(1): p. 50-4.

68. Kanehisa, M., et al., *The KEGG resource for deciphering the genome.* Nucleic Acids Res, 2004. **32**(Database issue): p. D277-80.

69. Vaquerizas, J.M., et al., *A census of human transcription factors: function, expression and evolution.* Nat Rev Genet, 2009. **10**(4): p. 252-63.

70. Wasserman, W.W. and A. Sandelin, *Applied bioinformatics for the identification of regulatory elements.* Nat Rev Genet, 2004. **5**(4): p. 276-87.

71. Elkon, R., et al., *Genome-wide in silico identification of transcriptional regulators controlling the cell cycle in human cells.* Genome Res, 2003. **13**(5): p. 773-80.

72. Claire Attwooll, E.L.D.a.K.H., *The E2F family specific functions and overlapping interests.* The EMBO Journal, 2004.

73. Chen, H.Z., S.Y. Tsai, and G. Leone, *Emerging roles of E2Fs in cancer: an exit from cell cycle control.* Nat Rev Cancer, 2009. **9**(11): p. 785-97.

74. Li, J., G. Ning, and S.A. Duncan, *Mammalian hepatocyte differentiation requires the transcription factor HNF-4alpha.* Genes Dev, 2000. **14**(4): p. 464-74.

75. Balamurugan, K. and E. Sterneck, *The many faces of C/EBPdelta and their relevance for inflammation and cancer.* Int J Biol Sci, 2013. **9**(9): p. 917-33.

76. Cantwell, C.A., E. Sterneck, and P.F. Johnson, *Interleukin-6-specific activation of the C/EBPdelta gene in hepatocytes is mediated by Stat3 and Sp1.* Mol Cell Biol, 1998. **18**(4): p. 2108-17.

77. Rossi, D. and A. Zlotnik, *The biology of chemokines and their receptors.* Annu Rev Immunol, 2000. **18**: p. 217-42.

78. Flo, T.H., et al., *Lipocalin 2 mediates an innate immune response to bacterial infection by sequestrating iron.* Nature, 2004. **432**(7019): p. 917-21.

79. Ma, Y. and L.M. Hendershot, *Delineation of a negative feedback regulatory loop that controls protein translation during endoplasmic reticulum stress.* J Biol Chem, 2003. **278**(37): p. 34864-73.

80. Liu, Z.X., S. Govindarajan, and N. Kaplowitz, *Innate immune system plays a critical role in determining the progression and severity of acetaminophen hepatotoxicity.* Gastroenterology, 2004. **127**(6): p. 1760-74.

81. Liu, Z.X., et al., *Neutrophil depletion protects against murine acetaminophen hepatotoxicity.* Hepatology, 2006. **43**(6): p. 1220-30.

82. Jaeschke, H., et al., *Current issues with acetaminophen hepatotoxicity--a clinically relevant model to test the efficacy of natural products.* Life Sci, 2011. **88**(17-18): p. 737-45.

83. Taub, R., *Liver regeneration: from myth to mechanism.* Nat Rev Mol Cell Biol, 2004. **5**(10): p. 836-47.

84. Fausto, N., J.S. Campbell, and K.J. Riehle, *Liver regeneration.* Hepatology, 2006. **43**(2 Suppl 1): p. S45-53.

85. Michalopoulos, G.K., *Liver regeneration.* J Cell Physiol, 2007. **213**(2): p. 286-300.

86. Yamada, Y. and N. Fausto, *Deficient liver regeneration after carbon tetrachloride injury in mice lacking type 1 but not type 2 tumor necrosis factor receptor.* Am J Pathol, 1998. **152**(6): p. 1577-89.

87. Huh, C.G., et al., *Hepatocyte growth factor/c-met signaling pathway is required for efficient liver regeneration and repair.* Proc Natl Acad Sci U S A, 2004. **101**(13): p. 4477-82.

88. Wang, H., et al., *Interplay of hepatic and myeloid signal transducer and activator of transcription 3 in facilitating liver regeneration via tempering innate immunity.* Hepatology, 2010. **51**(4): p. 1354-62.

89. Song, K.H., et al., *Hepatocyte growth factor signaling pathway inhibits cholesterol 7alpha-hydroxylase and bile acid synthesis in human hepatocytes.* Hepatology, 2007. **46**(6): p. 1993-2002.

90. Gupta, S., et al., *Down-regulation of cholesterol 7alpha-hydroxylase (CYP7A1) gene expression by bile acids in primary rat hepatocytes is mediated by the c-Jun N-terminal kinase pathway.* J Biol Chem, 2001. **276**(19): p. 15816-22.

91. Schrem, H., J. Klempnauer, and J. Borlak, *Liver-enriched transcription factors in liver function and development. Part I: the hepatocyte nuclear factor network and liver-specific gene expression.* Pharmacol Rev, 2002. **54**(1): p. 129-58.

92. Hatzis, P., I. Kyrmizi, and I. Talianidis, *Mitogen-activated protein kinase-mediated disruption of enhancer-promoter communication inhibits hepatocyte nuclear factor 4alpha expression.* Mol Cell Biol, 2006. **26**(19): p. 7017-29.

93. Zhang, L., et al., *Significance and mechanism of CYP7a1 gene regulation during the acute phase of liver regeneration.* Mol Endocrinol, 2009. **23**(2): p. 137-45.

94. Ogura, Y., F.S. Sutterwala, and R.A. Flavell, *The inflammasome: first line of the immune response to cell stress.* Cell, 2006. **126**(4): p. 659-62.

95. Mariathasan, S. and D.M. Monack, *Inflammasome adaptors and sensors: intracellular regulators of infection and inflammation.* Nat Rev Immunol, 2007. **7**(1): p. 31-40.

96. Jaeschke, H. and J. Liu, *Neutrophil depletion protects against murine acetaminophen hepatotoxicity: another perspective.* Hepatology, 2007. **45**(6): p. 1588-9; author reply 1589.

97. Minagawa, M., et al., *Activated natural killer T cells induce liver injury by Fas and tumor necrosis factor-alpha during alcohol consumption.* Gastroenterology, 2004. **126**(5): p. 1387-99.

98. Bianchi, M.E., *DAMPs, PAMPs and alarmins: all we need to know about danger.* J Leukoc Biol, 2007. **81**(1): p. 1-5.

99. Hartmann, G., A.K. Cheung, and M. Piquette-Miller, *Inflammatory cytokines, but not bile acids, regulate expression of murine hepatic anion transporters in endotoxemia.* J Pharmacol Exp Ther, 2002. **303**(1): p. 273-81.

100. Geier, A., et al., *Effects of proinflammatory cytokines on rat organic anion transporters during toxic liver injury and cholestasis.* Hepatology, 2003. **38**(2): p. 345-54.

101. Geier, A., et al., *Cytokine-dependent regulation of hepatic organic anion transporter gene transactivators in mouse liver.* Am J Physiol Gastrointest Liver Physiol, 2005. **289**(5): p. G831-41.

102. Uzi, D., et al., *CHOP is a critical regulator of acetaminophen-induced hepatotoxicity.* J Hepatol, 2013. **59**(3): p. 495-503.

103. Shi, J., et al., *Evidence of hepatocyte apoptosis in rat liver after the administration of carbon tetrachloride.* Am J Pathol, 1998. **153**(2): p. 515-25.

104. Bansal, M.B., et al., *Interleukin-6 protects hepatocytes from CCl4-mediated necrosis and apoptosis in mice by reducing MMP-2 expression.* J Hepatol, 2005. **42**(4): p. 548-56.

105. Silva, R.M., et al., *CHOP/GADD153 is a mediator of apoptotic death in substantia nigra dopamine neurons in an in vivo neurotoxin model of parkinsonism.* J Neurochem, 2005. **95**(4): p. 974-86.

106. Han, J., et al., *ER-stress-induced transcriptional regulation increases protein synthesis leading to cell death.* Nat Cell Biol, 2013. **15**(5): p. 481-90.